Advanced Modulation Techniques for Power Converters

by

Ali Mehrizi-Sani

A Thesis submitted to the Faculty of Graduate Studies of

The University of Manitoba

in partial fulfilment of the requirements of the degree of

Master of Science

Department of Electrical and Computer Engineering

University of Manitoba

Winnipeg, Manitoba

Acknowledgement

Submission of this thesis marks a milestone in my academic career. After 18 years of schooling, there are lots of people who have helped me, either directly or indirectly, in my achievements in life. It is a pleasure to acknowledge such people.

My deepest thankfulness goes to my thesis advisor, Dr. Shaahin Filizadeh. During the course of my Master's program, beside being my academic supervisor, he was a great friend, an insightful mentor, an open-minded supporter, and an encouraging person. I cannot imagine a more pleasurable Master's. We had countless hours of laughter, discussion on many topics, and of course, technical conversation. He also was an incredibly fast (and precise) thesis-reader. I do consider myself privileged to have had the opportunity to work with him.

I wish to express my sincere appreciation for my committee members who took the time to go through my thesis: Dr. Ani Golé, my internal examiner, who although was not directly involved with my research, remained a supportive person; and Mr. Randy Wachal, my external examiner, who kindly agreed to be on my committee and provided me with his extensive technical insight and experience.

Partial financial support from the Manitoba HVDC Research Center, the Natural Sciences and Engineering Research Council (NSERC) of Canada, and the Mathematics of Information Technology and Complex Systems (MITACS) Internship Program is greatly acknowledged.

I also want to thank all the people at the Power Tower, and the great people I came across during my program: Dr. Udaya Annakkage (for the new things I learned in his challenging course on Power System Analysis), Dr. Athula Rajapakse (for allowing me to use the loss estimation components he had developed in PSCAD), Dr. Dharshana Muthumuni (for hours of discussion on electric machine models of PSCAD and also for presenting my paper at the IPST07), and Mr. Behzad Qahraman (for being a living Encyclopedia Winnipegia). And also, Maziar (for letting me use his nicely-done STATCOM component), the Balatarin community website (for providing a fun place to read news and find more about the world, and establishing a venue to hang out virtually and to know a whole lot more about people), and LaTeX (for making the whole process of thesis writing more adventurous).

I would also like to thank my best friend, Aziz, who although was physically far from me, never stopped encouraging and inspiring me. Not only had he a great impact on my academic career, but he also helped me with other aspects of life and remained a precious confidant of mine. Thanks for your believing in my capabilities, for your sense of humor, and for your big heart, Aziz.

And most importantly, I owe a lot to my marvelous mother and to my unflinching father, who were on my side whenever I needed them. To them I dedicate this thesis.

to

my loving Parents

Abstract

Pulse-width modulation methods are widely used for the synthesis of ac voltages at the terminals of a voltage-sourced converter (VSC). Traditionally sinusoidal pulse-width modulation (SPWM) has been used. A powerful alternative for this purpose is space-vector modulation (SVM), in which the converter is placed in a finite number of states in order to best approximate the reference voltage. This method offers better utilization of the dc bus voltage and provides several degrees of freedom for enhancement of the harmonic spectrum as well as switching losses.

This thesis studies the SVM method for two- and three-level VSCs. A model for implementation of SVM in the electromagnetic transients simulation program PSCAD/EMTDC is developed. The model is able to generate firing pulses in linear as well as overmodulation range and is used to study the performance of different SVM strategies in terms of their harmonic spectra and associated converter and harmonic losses. The model is also used to demonstrate the suitability of the method for network applications. The thesis also employs genetic algorithms to find an optimized SVM sequence for improved harmonic performance. An objective function is defined that seeks to minimize the most significant harmonic components of the generated waveform, while keeping the other harmonic components within the acceptable range outlined in the available standards. The obtained sequence shows great improvement over the conventionally-used SVM sequence.

Table of Contents

List of Figures

List of Tables

List of Algorithms

Nomenclature

α_i	ith switching angle in SHE modulation scheme
A_i	Origin vertex of the ith triangle in three-level SVM
$\mathbf{A}_1$	Adjacent active space-vector to the right of the current sampled reference vector
$\mathbf{A}_2$	Adjacent active space-vector to the left of the current sampled reference vector
$\triangle_i$	Index of the smaller triangle in three-level SVM
E	Half of the dc link voltage, $V_{\mathrm{dc}}/2$
f	Fundamental frequency
F_s	Sampling frequency
F_{sn}	Normalized sampling frequency, F_s/f
k_1, k_2	Auxiliary variables used in three-level SVM to determine the triangle index
m	Modulation index, $V_{\mathrm{ref(max)}}/(V_{\mathrm{dc}}/2)$
θ	Phase of the sampled reference voltage space-vector
T_0	Time share of the zero space-vector $\mathbf{Z}_0$
T_1	Time share of the lower-numbered space-vector, $\mathbf{A}_1$
T_2	Time share of the higher-numbered space-vector, $\mathbf{A}_2$
T_7	Time share of the zero space-vector $\mathbf{Z}_7$

T_a	Duration of the space-vector aligned with the α-axis
T_b	Duration of the space-vector at 60° from the α-axis
T_s	Sampling period, $1/F_s$
V_α, V_β	xy-coordinates of the tip of the reference vector in three-level SVM
$V_{\alpha i}$, $V_{\beta i}$	xy-coordinates of the tip of the shifted reference vector in three-level SVM
V_{dc}	DC link voltage
$\mathbf{V}_i$	Each of the eight space vectors in two level SVM
$V_{\text{ref(max)}}$	Magnitude of fundamental component of the phase voltage
$\mathbf{Z}_0$	Zero space-vector corresponding to the state 000 in a two-level converter
$\mathbf{Z}_7$	Zero space-vector corresponding to the state 111 in a two-level converter

List of Abbreviations

3PS	Three-Phase Symmetry
CBPWM	Carrier-Based Pulse-Width Modulation
FACTS	Flexible AC Transmission System
GA	Genetic Algorithm
HVDC	High Voltage DC
HWS	Half-Wave Symmetry
OPWM	Optimal Pulse-Width Modulation
PWM	Pulse-Width Modulation
QWS	Quarter-Wave Symmetry
RMS	Root Mean Square (also rms)
SHE	Selective Harmonic Elimination
SPWM	Sinusoidal Pulse-Width Modulation
STATCOM	Static Compensator
SVM	Space-Vector Modulation
THD	Total Harmonic Distortion
VSC	Voltage-Sourced Converter
WTHD	Weighted Total Harmonic Distortion

Chapter 1

Introduction

Contents

Proper operation of power systems is essential to modern life, in which electricity is the most versatile type of energy. A major goal of power electronics is to find new solutions for existing problems to enable better utilization of equipment and to invent more efficient methods to control and facilitate flow of electric power, while meeting stringent operating conditions of today's heavily-loaded networks. One such application is conversion and shaping of voltage waveforms, which is generally referred to as *modulation*.

Electric power systems heavily depend on power electronic apparatus, which enhance the operation of the system. The ability of high-power electronic apparatus in controlling the flow of real and reactive power through designated electrical paths,

improvement of dynamic and transient performance of the system, and support of voltage profile has led to their widespread use in modern power networks.

Among the most employed high-power electronic apparatus are *voltage-sourced converters* (VSCs), which are able to convert an essentially constant dc voltage to an ac voltage of controllable magnitude, frequency, and phase. The basic function of a VSC in the context of power systems is to act as a controlled voltage source. Based on the direction of the flow of energy, such a converter can be called either an inverter (when power is transferred from the dc side to ac side) or a rectifier (when power is transferred from the ac side to dc side).

The output voltage of a VSC comprises a number of voltage pulses. *Pulse-width modulation* (PWM) techniques are used to design the width of such pulse sequences so that a fundamental component voltage with specified magnitude and phase emerges, and harmonics are shifted towards higher frequency bands.

The scope of this thesis is the converter-level modulation techniques and strategies that enhance the operation parameters of the VSC. Therefore, methods such as lowering of the harmonics by using multiple converters connected through special transformer configurations, e.g., 12-pulse configuration, are out of the area of interest of this thesis.

1.1 Motivation

VSCs are building blocks of high-power electronic equipment used in power networks. Therefore, devising apposite control schemes that conform to the industry standards is essential for their reliable operation. These control schemes should lead to output waveforms that, while not exceeding circuit components' voltage, current, and frequency limitations, possess minimal harmonic content.

Control of harmonics in a power system is particulary important, because while harmonics occupy the current-carrying capacity of transmission lines, they do not contribute to transmitting real power in fundamental frequency. This leads to overheating and overloading of equipment and adversely affects their operation. In order to assess such effects, study of harmonic spectrum of switching control schemes is of primary importance.

One other consideration is the loss that is associated with the converter. The repetitive switching of power electronic devices leads to losses that result in temperature increase in switches and load. Moreover, rapid switchings subject power electronic devices to voltage stresses. These can damage the device and hence, it is important to estimate such losses.

Because of the nature of power systems, their initial studies are done using simulation software. Study of system harmonics and losses, which are characterized by frequencies much higher that the fundamental, requires tools capable of handling electromagnetic transients. Therefore, a model implemented in such a software and capable of providing such information could facilitate system studies and planning.

1.2 Problem Definition

There is a wealth of methods suggested in the literature for control of VSCs. These methods range from traditional, carrier-based, *sinusoidal PWM* (SPWM) to mathematically-involved *space-vector modulation* (SVM) and *selective harmonic elimination* (SHE). They differ in factors such as the typical range of switching frequency, nature of implementation (digital or analog), and harmonic spectrum of the generated waveforms.

The sinusoidal PWM technique has been traditionally used for control of VSCs. While the underlying idea of SPWM is uncomplicated and its analog implementation is straightforward, it needs extra effort for realization in a digital system. Moreover, it has a relatively robust harmonic spectrum, i.e., the harmonic spectrum of the resulting waveform is tied to the selected switching frequency. Also, it suffers from a low utilization of the dc bus voltage.

Space-vector modulation technique, in contrast, enjoys a higher dc bus utilization. That is, for a certain dc voltage, the maximum fundamental-component ac voltage that an SVM-controlled VSC can generate linearly is higher than that of an SPWM-controlled converter. Furthermore, the SVM is inherently suitable for digital implementation, which due to the current inclination towards using microcontrollers, is a desired feature. Another notable characteristic of SVM is the fact that it provides more means to manipulate the switching pulses and hence, optimize harmonic spectrum of the output waveform. These degrees of freedom have caused SVM to receive a great deal of popularity in recent years.

As with other studies, investigation of properties of the SVM method requires availability of appropriate models. Since rapid switchings in power electronic circuits generates rapidly-changing waveforms, the model should be capable of handling such transients and hence, be developed in a electromagnetic transients simulation program. As a VSC is normally used in the context of a power network, the model also needs to be easily adoptable to different power system applications. Possibility of performing parametric studies is another desired property of a suitable model.

1.3 Research Objectives

The primary objective of this thesis is to provide a solid framework for advanced modulation techniques for high-power applications. The thesis' focus is space-vector modulation.

A thorough scrutiny of SVM requires investigation of its various realizations, which demonstrates flexibility of SVM in arrangement of switching pulses through exploitation of available degrees of freedom. An extensive harmonic and loss analysis, pertaining to harmonic spectrum of each realization is also desired. Therefore, one goal in this research is to perform comparative studies involving SVM and other modulation schemes to reveal the suitability and applicability of each method for certain applications.

Another objective of this work is to develop a comprehensive model that is capable of performing parametric studies to facilitate observing the impact of changing SVM variables. As mentioned, the model should be developed in a reliable, accurate, and robust transient simulation platform. This thesis uses the PSCAD/EMTDC program as one such electromagnetic transients simulation program.

The third objective of this research is to determine optimum SVM sequences that enhance certain performance parameters, such as harmonic distortion. Due to the extremely nonlinear nature of problem and inadmissibility of traditional, analytical methods, genetic algorithms are used to face the challenge.

1.4 Organization of the Thesis

As mentioned earlier, the SVM technique is an alternative method to control high-power VSCs. In this thesis, the performance parameters of SVM are studied and compared to other control schemes. In order to render the study more effectively,

background information conveying other modulation schemes is presented. The thesis structure is as follows.

Following this introductory chapter, Chapter 2 presents background concepts related to pulse-width modulation techniques and also basics of waveform generation.

Chapter 3 presents in-depth information about various modulation schemes. It studies three major groups of pulse-width modulation schemes. The first section in this chapter talks about sinusoidal pulse-width modulation. In addition to the conventional, sinusoidal PWM, its alternative methods are also reviewed. Each of these methods are invented to enhance the performance of the conventional SPWM. For example, trapezoidal modulation and harmonic-injection modulation are devised to decrease the switching rate (and hence, the switching losses) and increase the maximum obtainable ac voltage, respectively.

This chapter then introduces selective harmonic elimination methods along with their benefits and shortcomings. Both two- and three-level SHE are presented. This section also derives equations governing the operation of the SHE scheme. The last section of Chapter 3 delivers information about the space-vector modulation. SVM is further studied in more details in the next chapter.

Chapter 4 is devoted to the space-vector modulation. This chapter commences with presenting the underlying idea of space-vectors. After establishing this concept, it presents two-level SVM. As multilevel SVM schemes can be basically implemented by referencing them back to the two-level SVM, this section elaborates on two-level modulators. Three-level SVM is also described and its implementation algorithm is explained.

Case studies regarding application of SVM-controlled VSCs in power networks are presented in Chapter 5. The operation of a two-level, SVM-controlled VSC in the context of a three-phase inductive load constitutes the first part of this chapter. The

second part of this chapter assesses the performance of a three-level, SVM-controlled VSC used in a three-level STATCOM application. Harmonic performance of generated output waveforms as well as switching losses are evaluated and compared to other modulation schemes in the same context. This provides a general assessment of suitability of the space-vector modulation for different applications.

Chapter 6 proposes a method for optimization of the harmonic spectrum of converters under space-vector modulation control using genetic algorithms. An objective function is defined that seeks to minimize the most significant harmonic components of the generated waveform, while keeping the other components within the acceptable range outlined in the available standards.

Finally, Chapter 7 provides concluding remarks and summarizes thesis contributions. It also suggests future work and possible expansion of the thesis.

Three appendices and the list of references close the thesis. Appendix A defines harmonics indices used in this thesis. Appendix B contains derivation of formulae. Appendix C details least pth interior point penalty functions.

Chapter 2

Background

Contents

High-power electronic converters are known to provide convenient means for regulation of real and reactive power flow, voltage support, and improvement of dynamic performance of power networks. Use of such converters, in particular voltage-sourced converters (VSCs), within the context of modern power systems has been accelerated with the advent of fast switching devices with higher ratings as well as development of advanced techniques for their control.

There are a number of methods suggested in the literature to control generation of firing pulses for a VSC [1]-[3]. The basic difference between these methods lies in the employed switching frequency and also the nature of the approach to determine

switching instants. That is, whether it is done through *comparison* of a reference waveform with a carrier waveform, or by performing online or offline *calculations* to find the duration of voltage pulses.

In this chapter, a brief explanation of such methods and an overview of different VSC layouts are presented.

2.1 Categories of Modulation Schemes

In a broad categorization, modulation methods can be grouped based on their operating frequency [4]. High-frequency modulation schemes use a switching frequency that is normally much larger than the fundamental frequency. Conventional, *sinusoidal pulse-width modulation* (SPWM) method, which compares one (or more, when the number of available dc voltage levels is higher than two) high-frequency triangular waveform with one (or more) sinusoidal waveform is one basic method in this category. *Space-vector modulation* (SVM), which approximates the desired waveform by placing the converter in a sequence of states, is another method.

On the other hand, low-frequency modulation schemes are those for which the switching frequency is close to the fundamental frequency. These methods include *selective harmonic elimination* (SHE),[1] in which the switching instants are precalculated so that certain harmonic components are eliminated, and *space-vector control* (SVC) [5], in which a high number of converter levels is used to approximate the desired output waveform using only one converter state in each sampling period (in contrast to the SVM method in which at least three converter states are employed in each sampling period).

[1] In the literature, the term *optimal PWM* (OPWM) is sometimes used to refer to SHE.

2.2 Basics of Waveform Generation

Quality of the generated three-phase sinusoidal waveform depends upon two factors. As all the mentioned modulation schemes essentially generate approximate sinusoidal waveforms, a higher sampling frequency provides more samples of the target waveform and hence, provides a more accurate approximation. In other words, a higher sampling frequency F_s provides a higher resolution for the time axis. Higher accuracy along the amplitude axis is obtained by employing a VSC that is capable of producing a larger number of voltage levels from the provided dc voltage source(s).

While a two-level converter can only generate two voltage levels of $\pm V_{\rm dc}/2$,[2] a three-level converter is capable of generating voltage levels of $+V_{\rm dc}/2$, $-V_{\rm dc}/2$, and 0. A higher number of voltage levels provides a closer approximation to the target sinusoidal waveform. A general multilevel converter with m levels (m is odd), produces voltage levels from $-V_{\rm dc}/2$ to $+V_{\rm dc}/2$ in steps of $V_{\rm dc}/(m-1)$ [6].

Because of the increasing number of switch combinations, as the number of voltage levels increases, control of the converter becomes more complicated . Although this thesis considers multilevel converters, it is mainly aimed at studying two- and three-level converters and does not go into details on control strategies devised for higher-level converters.

Quality of a waveform is normally stated based on its harmonic content. The goal of switching pulse-generation methods is to produce a waveform as harmonic-free as possible. Therefore, as a means to determine, compare, and contrast the ability of a switching method to produce quality waveforms some indices have been defined, which are summarized in Appendix A. *Total harmonic distortion* (THD) and *weighted THD* (WTHD) are two of the most used indices. THD provides a measure

[2]The voltage levels of $\pm V_{\rm dc}/2$ are for the case that the total dc link voltage is $V_{\rm dc}$ and the voltage is measured with respect to a fictitious zero voltage at the middle of the dc leg.

to compare the energy of the fundamental component of the synthesized waveform with the total energy of the waveform. WTHD is based on the same philosophy as THD, but it also considers the harmonic order to account for the attenuation of higher-order harmonics because of the inductive nature of power systems [7]. The IEEE Standard 519 [8] states the criteria of an acceptable waveform.

2.2.1 Waveform Synthesis

In order to keep harmonics minimal, to improve harmonic indices, and to meet the power system requirements, in addition to *periodicity* (or synchronization), it is desired that synthesized waveforms possess *three-phase symmetry* (3PS), *half-wave symmetry* (HWS), and *quarter-wave symmetry* (QWS) [9].

Periodicity of waveforms ensures that they have a discrete spectrum. This is guaranteed if the sampling frequency F_s is an integer multiple of fundamental frequency f of the reference waveform. Therefore, the switching pattern of the inverter remains identical in all periods; as such, constructed voltages are also periodic.

For balanced operation of the load, it is required that the converter output waveforms possess three-phase symmetry. In this case, all harmonics are also balanced. In the particular case of triple-n harmonics in a three-phase system, this leads to their elimination from the line voltages. The necessary and sufficient condition for 3PS of three-phase voltages is that they are displaced by 120°. For positive sequence voltages, this implies that the following conditions should hold.

$$v_a(\theta + 2\pi/3) = v_c(\theta) \tag{2.1a}$$

$$v_b(\theta + 2\pi/3) = v_a(\theta) \tag{2.1b}$$

$$v_c(\theta + 2\pi/3) = v_b(\theta) \tag{2.1c}$$

While 3PS is targeted at eliminating triple-n harmonics, half-wave symmetry eliminates even harmonics. Absence of even harmonics is particularly important as otherwise they may lead to resonance in power networks. Moreover, the dc component, because of changing the operating point of electrical apparatus, is harmful. A waveform possesses HWS if its mirror in x-axis shifted by half of the period is identical to itself. The condition for HWS is expressed mathematically as

$$v(\theta) = -v(\theta + \pi) \tag{2.2}$$

Quarter-wave symmetry, which is a subset of HWS, guarantees not only are even harmonics zeros, but also all harmonics are either in phase or anti-phase with the fundamental component. Since there are only two phase angles (0° and 180°) involved for a waveform with such a symmetry, elimination of harmonics by injection requires less effort. This is a desired feature, albeit a restrictive one. QWS is obtained if the waveform has symmetry around the midpoint of positive and negative half-cycles. This means that the waveform repeats the same pattern every quarter-cycle. Such a waveform can be expressed as

$$v(\theta) = \begin{cases} \hat{v}(\theta); & 0 \leq \theta < \pi/2 \\ \hat{v}(-\theta + \pi); & \pi/2 \leq \theta < \pi \\ -\hat{v}(\theta - \pi); & \pi \leq \theta < 3\pi/2 \\ -\hat{v}(-\theta + \pi); & 3\pi/2 \leq \theta < 2\pi \end{cases} \tag{2.3}$$

Conditions for periodicity, HWS, and 3PS, which impose certain constraints on the switching strategy, are summarized in Table 2.1.

TABLE 2.1
DESIRED TYPES OF SYMMETRY IN THE OUTPUT WAVEFORM

	Periodicity	HWS	3PS
θ	$\theta + 2\pi$	$\theta + \pi$	$\theta + 2\pi/3$
v_a	v_a	$-v_a$	v_c
v_b	v_b	$-v_b$	v_a
v_c	v_c	$-v_c$	v_b

2.3 Voltage-Sourced Converter Topologies

The purpose of a *voltage-sourced converter* (VSC) is to synthesize a nearly sinusoidal output voltage from two or more levels of dc voltage. By proper coordination of switches of a VSC, electrical energy from one form can be converted to another, e.g., from dc to an ac voltage with desired magnitude and frequency. The switches in a VSC are of controlled type, so that they can be turned ON or OFF, as the control scheme determines.

Over time, the power industry has developed different topologies of VSCs, each used in a certain application depending on its power rating, voltage level, and the type of the available switching device. For example, in order to obtain a high-quality waveform with a two-level inverter with minimal harmonics, one option is to use a higher switching frequency. An alternative to this, especially in high-power applications, is to use a multilevel inverter that instead of using only $\pm V_{\text{dc}}/2$ pulses, uses voltage levels in steps of $V_{\text{dc}}/(m-1)$ (m is the number of levels) [10]. The harmonic content and filtering requirements of the output voltage waveform reduces as the number of levels increases. However, the control scheme for multilevel converters is more complex.

Fig. 2.1 shows one leg of a two-level VSC. Upper and lower switches cannot have the same state at the same time. Turning both S_1 and $\overline{S_1}$ ON at the same time

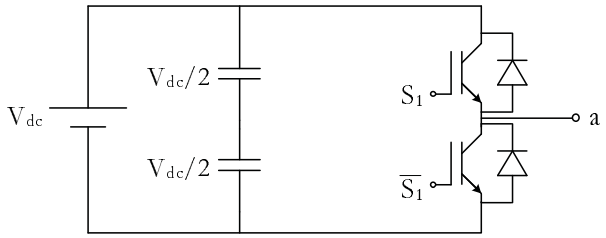

Fig. 2.1. Structure of one leg of a diode-clamped, two-level VSC.

TABLE 2.2
FIRING PULSES FOR A THREE-LEVEL VSC FOR THREE POSSIBLE POLE VOLTAGES

Pole Voltage	S_1	S_2
$+V_{dc}/2$	ON	OFF
0	OFF	ON
$-V_{dc}/2$	OFF	OFF

causes a short circuit of the source voltage, and turning them both OFF leads to an open circuit, which produces high voltages because of the inductive nature of power systems. If S_1 is ON ($\overline{S_1}$ is OFF), the voltage at a with respect to the midpoint is $+V_{dc}/2$. If it is OFF, the voltage is $-V_{dc}/2$.

Multilevel converters are used in high-power applications. Fig. 2.2 shows one leg of a diode-clamped, three-level VSC, and Fig. 2.3 shows one leg of a capacitor-clamped, three-level VSC. As mentioned earlier, a three-level VSC is capable of producing 0 and $\pm V_{dc}/2$ voltage levels. When all switches in the upper part of a leg are ON, the output voltage is $+V_{dc}/2$ and when they are OFF, the output voltage is $-V_{dc}/2$. A momentarily zero output voltage is obtained by turning the upper-most switch OFF.[3] Note that similar to the two-level VSC, in order to avoid short-circuit and open-circuit, the states of the switches of the lower half are always complementary to those of the upper half. These states are summarized in Table 2.2.

A simplified diode-clamped, three-phase, three-level VSC is depicted in Fig. 2.4.

[3]In general, by turning each of the upper switches (starting from top) OFF, the output voltage decreases by $V_{dc}/(m-1)$, where m is the number of levels.

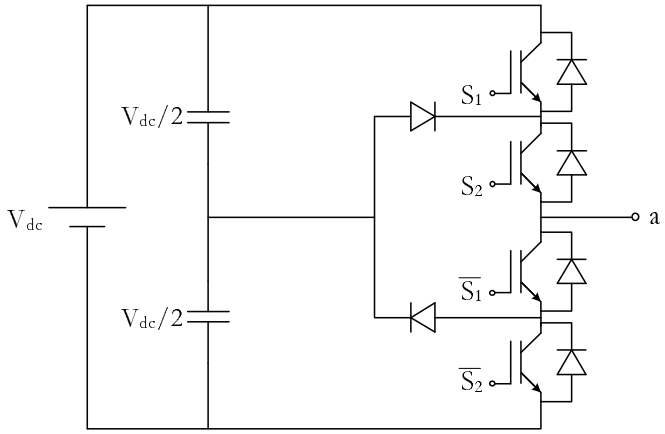

Fig. 2.2. Structure of one leg of a diode-clamped, three-level VSC.

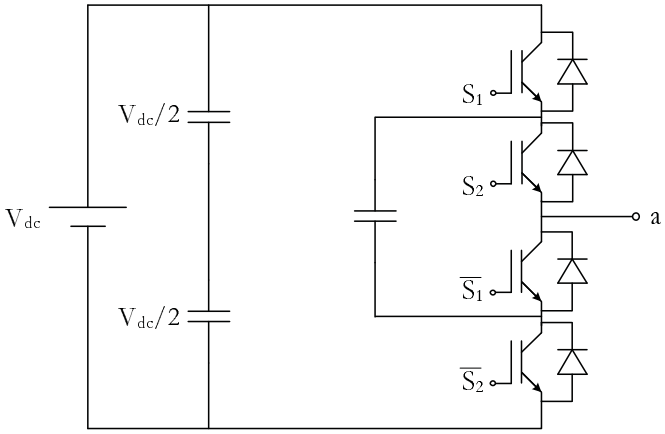

Fig. 2.3. Structure of one leg of a capacitor-clamped, three-level VSC.

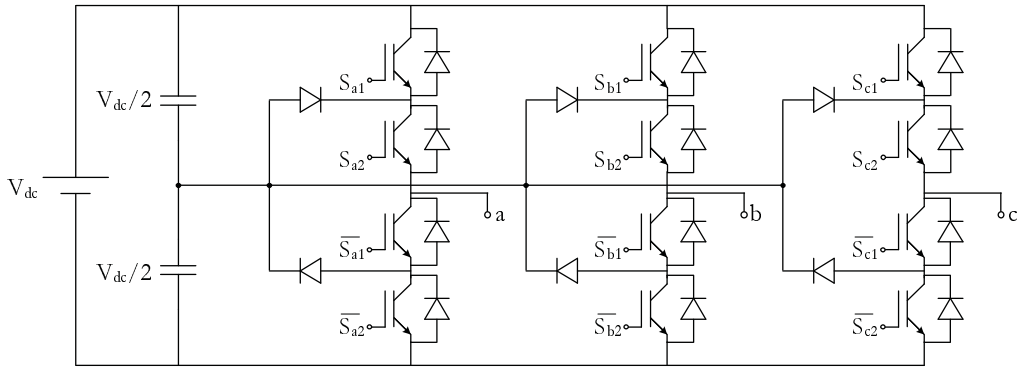

Fig. 2.4. Schematic diagram of a diode-clamped, three-level VSC.

2.4 Overview of Modulation Schemes

In PWM methods, a certain sampled voltage level is approximated by ON and OFF pulses whose shares are determined so that the average voltage over the sampling period is equal to the sampled voltage. The pulse level is determined from comparison of the carrier and target waveforms. Conventional *sinusoidal pulse-width modulation* (SPWM) compares a low-frequency sinusoidal waveform (or a set of three waveforms phase-shifted by 120° for applications in power networks) with a higher frequency triangular or saw-tooth carrier and decides whether to turn switches ON or OFF. The underlying philosophy of SPWM is simple and easily comprehendible.

While analog implementation of SPWM is straight-forward and can be realized using a set of signal generators and comparators that generate the required firing pulses, its digital implementation could be cumbersome. It requires digitization of the signals involved, which introduces errors. Also, analytical determination of switching instants requires solving a transcendental equations. Moreover, as a drawback to both analog and digital SPWM, a SPWM-controlled VSC has limited dc bus voltage utilization and linear range of operation. In order to relax such limitations, a number of alternative methods have been suggested, which are reviewed in the next two chapters.

In a three-phase system, line voltages, rather than phase voltages, are of primary importance. As in such a system waveforms are separated by 120° and as a result, there are no triple-n harmonics present in line voltages, existence of such harmonic components in the phase voltages does not adversely affect the system performance. Therefore, harmonic injection methods, mostly third-harmonic injection, are used to flatten the top of the output waveforms to increase the dc bus utilization of the modulation scheme.

If switching instants can be calculated beforehand, lower order harmonics can be eliminated by computing the necessary switching instants. The number of harmonics that can be eliminated in this method is equal to the number of voltage pulses available to manipulate. This approach is called *selective harmonic elimination* (SHE), and requires finding the solution to a nonlinear, transcendental, implicit system of equations expressed in the switching angles. Due to the nature of calculations, it is not possible to compute the solution on-the-fly. Aside from the complexity of solving such a system, one problem with SHE is that existence of a solution is not always guaranteed [11]. There are cases that switching angles cannot be found, unless alternative states of the converter are used. This can add to the complexity of this method.

Both SPWM and SHE can be applied to single phase as well as three-phase systems. In fact, they generate the necessary firing pulses for each phase independently of other phases. An alternative method, which has attracted a great deal of attention since its introduction, is *space-vector modulation* (SVM). In SVM, which is developed primarily for three-phase converters, the converter is deemed and controlled as one entity. The converter is placed in a set of states that are determined by the ON and OFF status of switches. Each set of states produces a certain line voltage and hence the desired voltage can be approximated by successively placing the converter in a sequence of states.

In addition to two-level VSCs, all of the mentioned modulation strategies, with minor modifications, can be applied to multilevel VSCs as well. As stated earlier, multilevel VSCs generate waveforms that are generally less contaminated with harmonics content than the respective two-level VSC.

The subsequent two chapters provide more details about modulation techniques and in particular, space-vector modulation.

Chapter 3

Conventional Modulation Techniques

Contents

The output voltage of a voltage-sourced converter comprises a number of voltage pulses. The number of such voltage pulses and their duration are determined by the specific modulation technique employed. These *pulse-width modulation* (PWM)

techniques generate pulse sequences in such a way that a waveform with a fundamental component having the specified magnitude and phase is synthesized.

In the first part of this chapter carrier-based PWM methods are portrayed, their characteristics are explained, and a number of variations to enhance some operating characteristics are studied. The second part of the chapter reviews another modulation scheme, *selective harmonic elimination* (SHE). The *space-vector modulation* (SVM) is studied in the next chapter.

3.1 Carrier-Based PWM

Carrier-based PWM (CBPWM)[1] methods compare a reference waveform with a triangular or saw-tooth carrier at a higher frequency F_s (sampling frequency) and decide whether to turn a switch ON or OFF. Based on the method of determining the switch ON-times, there are two types of CBPWM, which are as follows [12].

1. Analog, or *naturally-sampled* CBPWM, in which switching is done at the intersection of the two waveforms.

2. Digital, or *regularly-sampled* CBPWM, in which switching is done at the intersection of the sampled reference waveform and the high frequency carrier. Further, if one sample is used per carrier period, the regular method is *symmetric*, while in case of two samples it is called *asymmetric*.

The conventional carrier-based method to control a voltage-sourced converter is *sinusoidal PWM* (SPWM), for which the reference waveform is a sinusoidal waveform. SPWM controls each leg of the VSC independently of other legs. Hence,

[1]Because of the popularity of sinusoidal PWM, the term PWM alone is also sometimes used to refer to it. Since in general sense the term PWM can be used for all methods that control a VSC and to avoid confusion in this thesis the term PWM is always used with a modifier to clarify the meaning.

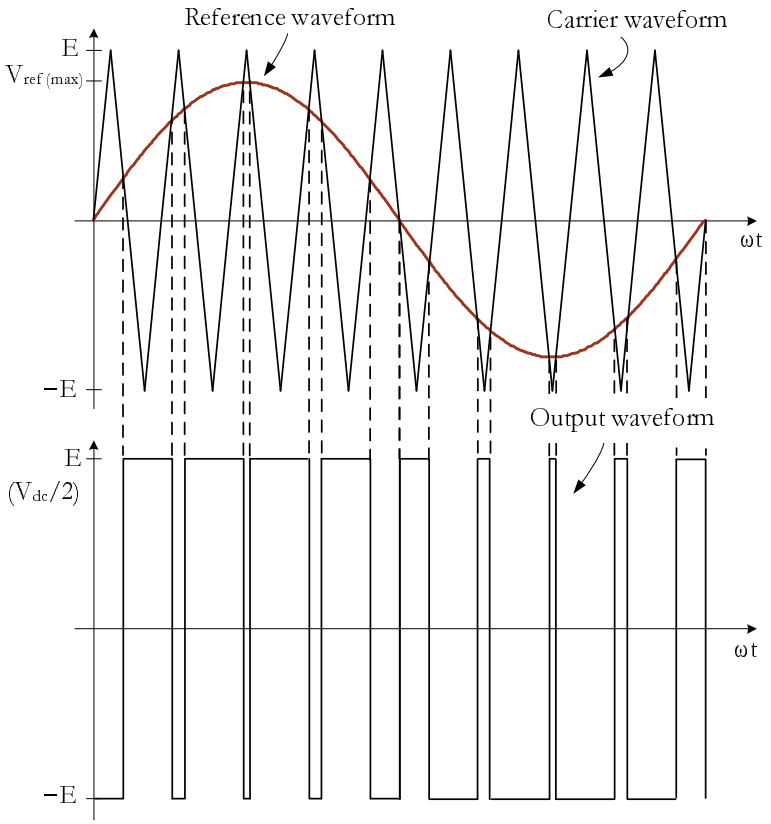

Fig. 3.1. Output voltage generated by two-level SPWM.

a three-phase SPWM controller essentially consists of three separate SPWM controllers with reference waveforms that are 120° out of phase. Moreover, SPWM can be used control a VSC with two, three, or higher number of levels. Using the same carrier frequency, the larger the number of voltage levels, the higher the quality of the output waveform. The number of used carrier waveforms and the number of switches in each leg, depend on the number of VSC voltage levels.

Since in SPWM only the value of the reference waveform at its intersection with the carrier is used to determine voltage pulses, this method essentially uses an approximation of the reference waveform. Fig. 3.1 shows an example of an SPWM-approximated waveform for a two-level reconstruction.

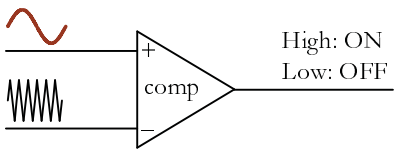

Fig. 3.2. Schematic diagram of analog implementation of SPWM.

The ratio of the magnitude of the reference phase voltage to the amplitude of the carrier waveform (which is equal to half of the available dc bus voltage), is called *modulation index* m, as defined in (3.1).

$$m = \frac{V_{\text{ref(max)}}}{V_{\text{dc}}/2} \tag{3.1}$$

When m is less than one, the fundamental component of the output voltage increases linearly with m. For higher m values, increase in the fundamental component is not linear, and the modulator operates in non-linear (overmodulation) mode. Hence, the maximum modulation index for linear operation of SPWM is 1.0. This reflects how effective the modulation method is in exploiting the full capacity of the available dc voltage.

Despite the simplicity of SPWM method, it suffers from a number of drawbacks. While it can be easily implemented in analog form using a number of comparators and waveform generators (Fig. 3.2), in today's microcontroller-dominated world, it is more favorable to implement it in digital domain. But due to complexities involved in calculations, achieving a digital realization of SPWM with the same performance as its analog counterpart is hard. Furthermore, since the positions of voltage pulses are solely determined by two sets of waveforms, SPWM does not allow any direct control over the harmonic content of the output waveform. Finally, SPWM offers a limited dc bus utilization, which is represented by a maximum linear-range m of 1.0.

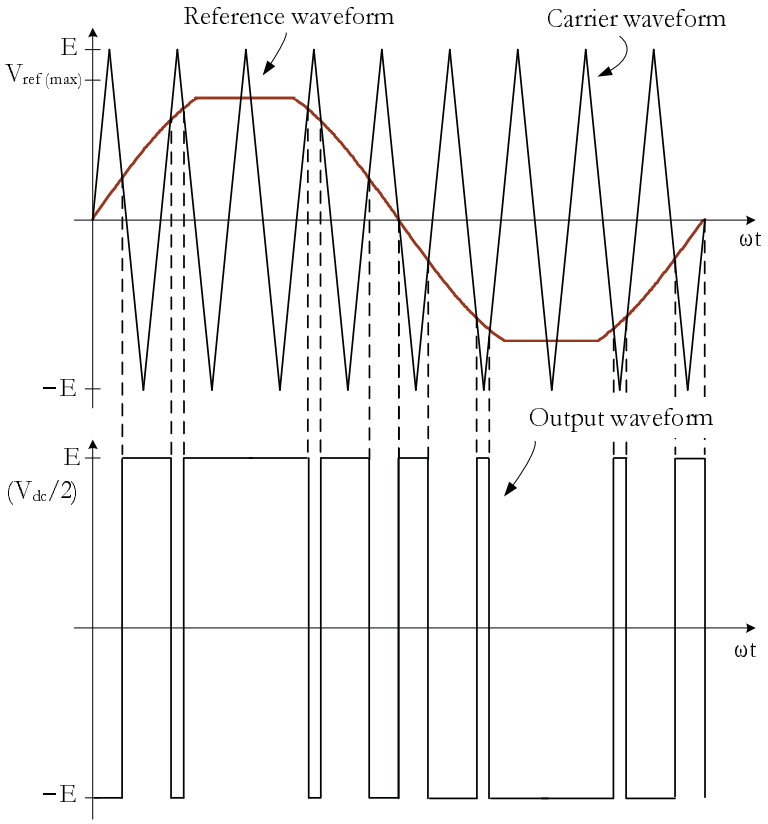

Fig. 3.3. 60-degree modulation.

Variations of SPWM are suggested to overcome some of these limitations. For example, harmonic injection method is used to flatten the top of the waveform and extend the linear region. The 60-degree method is used to decrease the number of switchings in each period. These methods [7], for two-level CBPWM, are briefly presented.

3.1.1 60-Degree Modulation

The idea behind 60° PWM is to reduce the switching losses by reducing the number of switchings in each period. In this strategy, the state of switches in each leg does not change from 60° to 120° in the first half-cycle and from 240° to 300° in the second half-cycle. Fig. 3.3 illustrates this type of modulation.

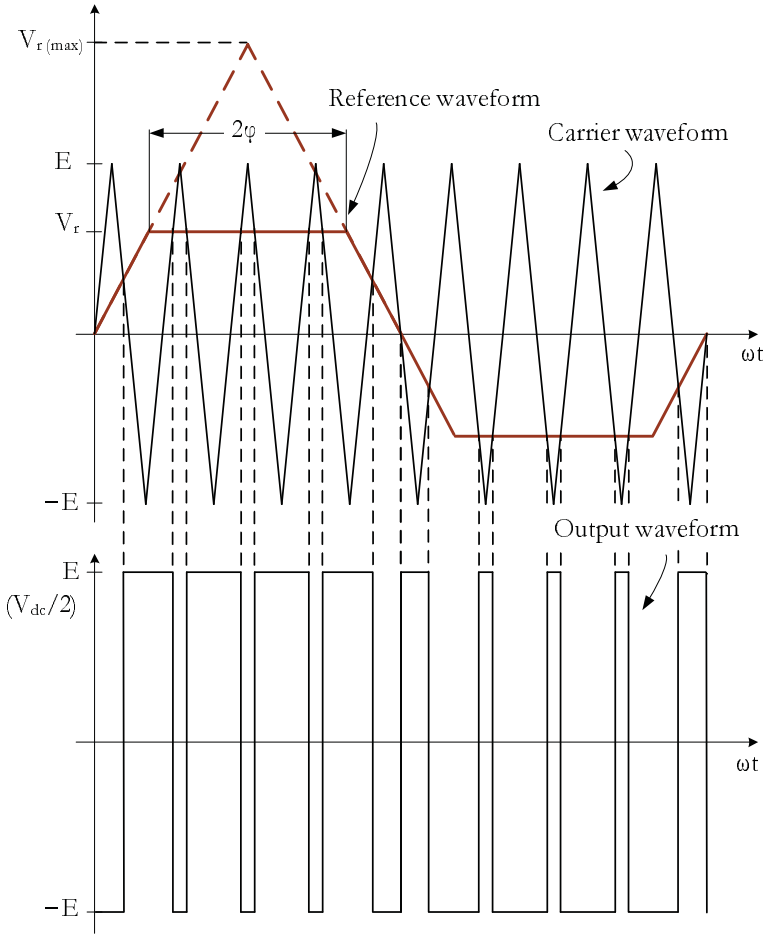

Fig. 3.4. Trapezoidal PWM.

3.1.2 Trapezoidal Modulation

In this method, a triangular waveform (with a peak of $V_{r(\max)}$) is hard-limited to produce a trapezoidal waveform (with a limiting level of $V_r = \sigma V_{r(\max)}$, where σ is called the *triangular factor*). The resulting waveform is then compared with a triangular carrier, as shown in Fig. 3.4. The portion of the flat part of the trapezoidal is equal to $2\phi = (1 - \sigma)\pi$ in each half-cycle. In this method, low order harmonics are larger than the SPWM, but the maximum modulation index m in the linear range increases from 1 to 1.05, which happens for $\sigma = 1/3$ [13].

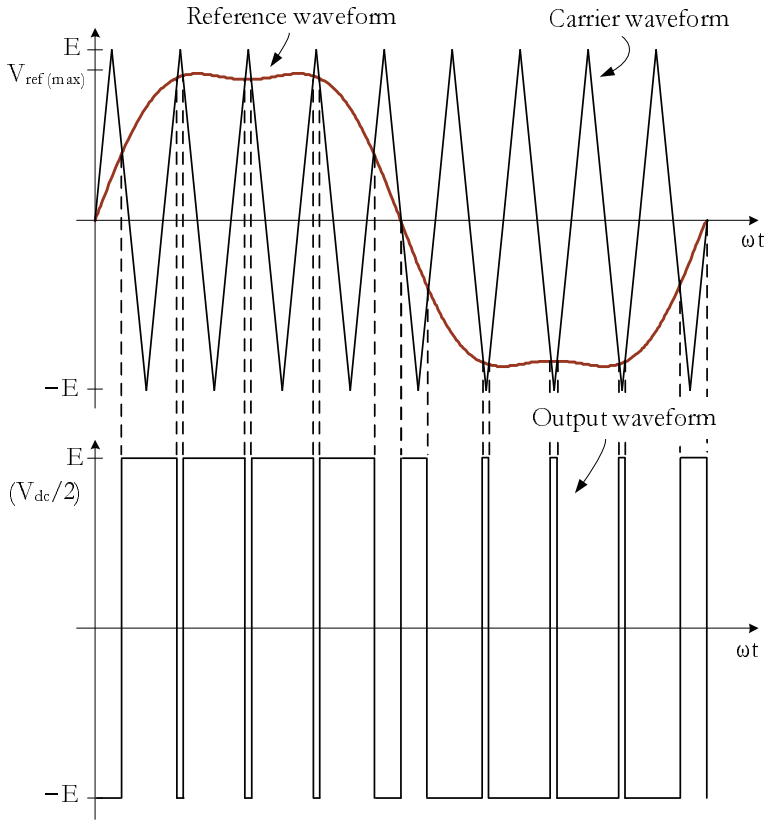

Fig. 3.5. Third-harmonic injection PWM.

3.1.3 Harmonic Injection Modulation

Another method to extend the linear modulation range is to flatten the top of the modulation waveform by adding one or more harmonics to it. In a three-phase system, injection of triple-n harmonics to phase voltages does not affect line voltages and hence, third harmonic can be added to the reference waveform without downgrading the quality of the output waveform. It can be shown that a ratio of 1/6 for the magnitude of the third harmonic to the fundamental of the reference vector provides maximum reduction of the peak of the resulting waveform and therefore, maximum extension of the linear range [14], [15]. This corresponds to a maximum linear-range modulation index of 1.15. Fig. 3.5 shows an example waveform obtained using this method.

3.2 Selective Harmonic Elimination

In contrast to carrier-based PWM methods, in which switching instants are determined by direct comparison of reference and carrier waveforms, in *selective harmonic elimination* (SHE) method the exact moments of switching are calculated according to the desired fundamental component and the harmonic components to be eliminated.

Because of complexity of equations to be solved to find switching instants, the number of switchings is normally kept low to make the calculations possible. This also has the advantage of lowering the converter switching losses.

Switching instants are found by offline calculations. Different values of modulation index, different harmonic components to be eliminated, and different number of dc voltage levels all lead to different systems of equations that cannot be solved in real-time, considering the limited calculating power of a microcontroller. Therefore, for a certain VSC with known harmonic elimination criteria, solutions for a number of m values are found and stored in a look-up table. It is also worthwhile to note that it is not guaranteed that one is able to find switching times for all m values without changing the sequence and magnitude of voltage pulses [16], [17].

Similar to other modulation schemes, SHE can be used to control both two-level and higher level VSCs. A two-level SHE, in which in each half period both $+V_{\mathrm{dc}}/2$ and $-V_{\mathrm{dc}}/2$ voltage pulses are used, is sometimes called bipolar, while three-level, where in each half cycle only one of $+V_{\mathrm{dc}}/2$ or $-V_{\mathrm{dc}}/2$ is used, is known as unipolar SHE.

The output waveform of a SHE-modulated VSC is normally constructed in a way that it possesses quarter-wave symmetry (QWS); however, this is not strictly necessary [18]. The output waveform of one phase can be expressed in Fourier series

expansion as

$$v(t) = \frac{1}{2}a_0 + \sum_{n=1}^{\infty}(a_n \cos \omega_n t + b_n \sin \omega_n t) \tag{3.2}$$

where ω_n is $n\frac{2\pi}{T}$. The coefficients a_n and b_n can be found from the canonical form as

$$a_n = \frac{1}{\pi}\int_{-\pi}^{\pi} f(\theta)\cos(n\theta)\, d\theta \tag{3.3}$$

$$b_n = \frac{1}{\pi}\int_{-\pi}^{\pi} f(\theta)\sin(n\theta)\, d\theta \tag{3.4}$$

Because of the half-wave symmetry of the waveform, all a_n and even-numbered b_n coefficients are zero. The nth harmonic can be eliminated if the respective b_n coefficient is set equal to zero. Also, for a three-phase system, triple-n harmonics in the phase-voltage are canceled out in the line voltage and hence, are not important. Therefore, the low-order harmonics to be removed are odd, non–triple-n components starting as 5, 7, 11, 13, 17, ...

Fourier series expansion of waveforms for two- and three-level SHE are explained next. The resulting transcendental equations can be solved using iterative methods. A method to obtain all possible solutions is suggested in [17]. Mathematical software, such as MATHCAD [19] can be used to find the numerical solution of the resulting system of equations.

Note that the equations of the SHE method might not always lead to a valid solution [16]. This happens for some values of the modulation index m. Therefore, the SHE method possesses only a narrow range of m. For example, for a seven-level SHE, appropriate firing angles can only be found for a modulation index between 0.5 and 1.05. In order to increase the range of m for which the method works, it is necessary to alter the voltage level transitions after switching instances. Fig. 3.6

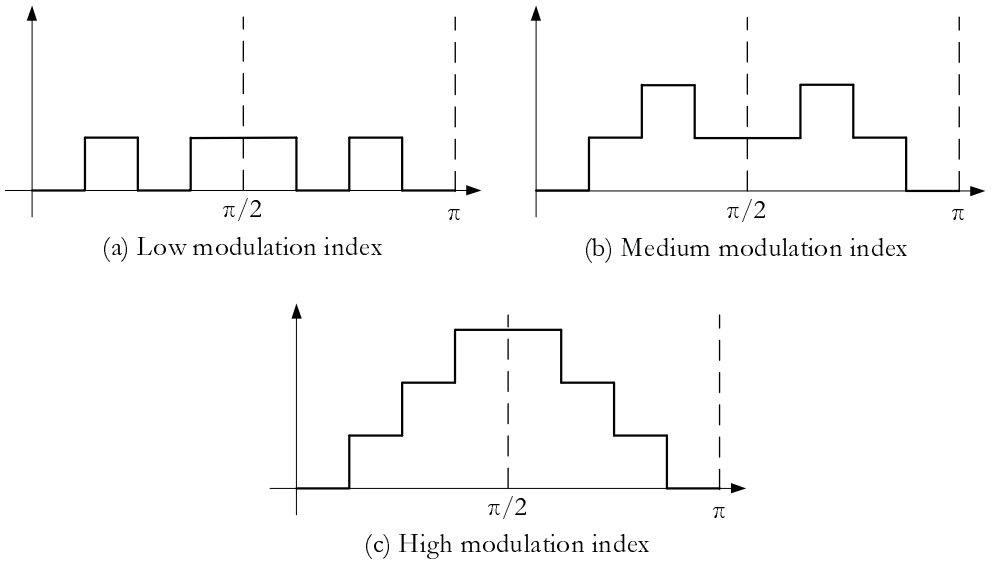

Fig. 3.6. Necessity of adjusting pulse patterns in SHE for different m values.

shows this distinction for three qualitatively-described situations corresponding to low, medium, and high modulation indices.

3.2.1 Two-Level SHE

In two-level (bipolar) SHE, voltage pulses are $\pm V_{\rm dc}/2$. Fourier series expansion of a waveform with m switchings per quarter cycle is

$$\begin{aligned} v(t) = \frac{2V_{\rm dc}}{\pi}\Big\{ & (1 - 2\cos\alpha_1 + 2\cos\alpha_2 - 2\cos\alpha_3 + \cdots)\sin\omega t \\ & + (1 - 2\cos 3\alpha_1 + 2\cos 3\alpha_2 - 2\cos 3\alpha_3 + \cdots)\frac{\sin 3\omega t}{3} \\ & + (1 - 2\cos 5\alpha_1 + 2\cos 5\alpha_2 - 2\cos 5\alpha_3 + \cdots)\frac{\sin 5\omega t}{5} + \cdots \Big\} \\ = \frac{2V_{\rm dc}}{\pi}\Bigg\{ & \sum_{n=1,3,\ldots}^{\infty} \frac{\sin n\omega t}{n}\left[1 + 2\sum_{k=1}^{m}(-1)^k \cos n\alpha_k\right]\Bigg\} \end{aligned} \tag{3.5}$$

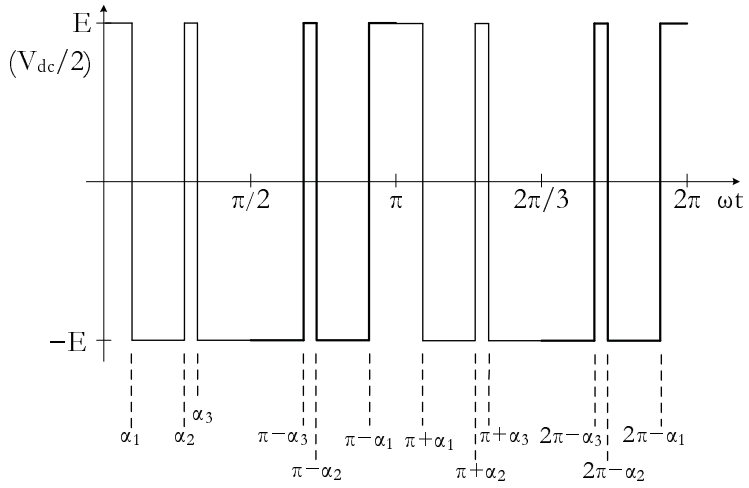

Fig. 3.7. Output voltage of a two-level, three–switching-angle SHE.

Non-zero b_n coefficients are calculated from

$$b_n = \frac{2V_{\rm dc}}{n\pi}\left(1 - 2\cos n\alpha_1 + 2\cos n\alpha_2 - 2\cos n\alpha_3 + \cdots\right) \tag{3.6}$$

where $V_{\rm dc}$ is the available dc bus voltage and $\alpha_1 < \alpha_2 < \cdots < \alpha_m < \frac{\pi}{2}$.

When there are three switchings in each quarter-cycle, three unknowns of α_1, α_2, and α_3 lead to three equations. Fig. 3.7 shows the output waveform of a two-level SHE-controlled VSC with three switching angles. One equation is used to satisfy the condition on the magnitude of the fundamental component, and the remaining two equations are used to eliminate the 5th and 7th harmonic components. This is shown in the following.

$$v_{1,\rm rms} = \frac{\sqrt{2}V_{\rm dc}}{\pi}\left(1 - 2\cos\alpha_1 + 2\cos\alpha_2 - 2\cos\alpha_3\right) \tag{3.7}$$

$$0 = \left(1 - 2\cos 5\alpha_1 + 2\cos 5\alpha_2 - 2\cos 5\alpha_3\right) \tag{3.8}$$

$$0 = \left(1 - 2\cos 7\alpha_1 + 2\cos 7\alpha_2 - 2\cos 7\alpha_3\right) \tag{3.9}$$

3.2.2 Three-Level SHE

In three-level SHE, in addition to $\pm V_{\rm dc}/2$, the output voltage can also assume a zero value. Fourier series expansion of the waveform is

$$\begin{aligned} v(t) = \frac{2V_{\rm dc}}{\pi}\Bigg\{ & (\cos\alpha_1 - \cos\alpha_2 + \cos\alpha_3 + \cdots)\sin\omega t \\ & + (\cos 3\alpha_1 - \cos 3\alpha_2 + \cos 3\alpha_3 + \cdots)\frac{\sin 3\omega t}{3} \\ & + (\cos 5\alpha_1 - \cos 5\alpha_2 + \cos 5\alpha_3 + \cdots)\frac{\sin 5\omega t}{5} + \cdots \Bigg\} \\ = \frac{2V_{\rm dc}}{\pi}\Bigg\{ & \sum_{n=1,3,\ldots}^{\infty} \frac{\sin n\omega t}{n}\left[\sum_{k=1}^{m}(-1)^{k+1}\cos n\alpha_k\right]\Bigg\} \end{aligned} \tag{3.10}$$

The b_n coefficients (for an odd n) are

$$b_n = \frac{2V_{\rm dc}}{n\pi}\left(\cos n\alpha_1 - \cos n\alpha_2 + \cos n\alpha_3 + \cdots\right) \tag{3.11}$$

where, the same as the case of two-level SHE, $V_{\rm dc}$ is the available dc bus voltage and $\alpha_1 < \alpha_2 < \cdots < \alpha_m < \frac{\pi}{2}$.

When there are three switchings in each quarter cycle as depicted in Fig. 3.8, three unknowns of α_1, α_2, and α_3 lead to three equations. Again, one of these equations is used to satisfy the condition on the magnitude of the fundamental component, and the remaining two equations are used are eliminate two lowest harmonics (5 and 7), as follows.

$$v_{1,\rm rms} = \frac{\sqrt{2}V_{\rm dc}}{\pi}\left(\cos\alpha_1 - \cos\alpha_2 + \cos\alpha_3\right) \tag{3.12}$$

$$0 = \left(\cos 5\alpha_1 - \cos 5\alpha_2 + \cos 5\alpha_3\right) \tag{3.13}$$

$$0 = \left(\cos 7\alpha_1 - \cos 7\alpha_2 + \cos 7\alpha_3\right) \tag{3.14}$$

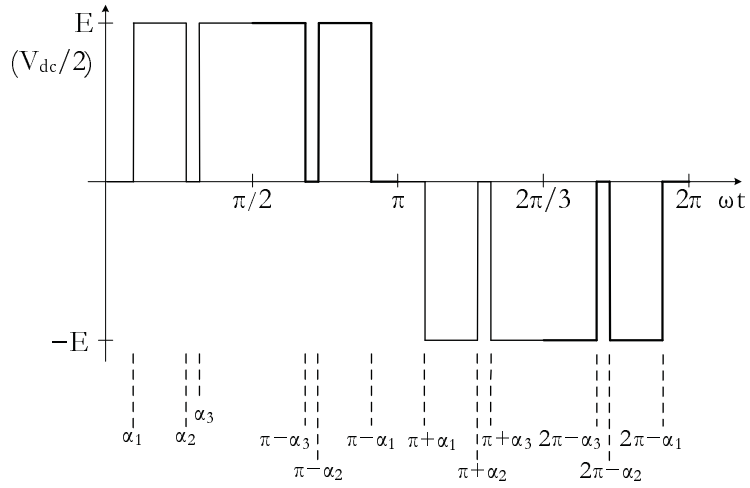

Fig. 3.8. Output voltage of a three-level, three–switching-angle SHE.

3.3 Space-Vector Modulation

Space-vector modulation (SVM), although a pulse-width modulation strategy, is quite different from CBPWM methods. CBPWM methods are based on comparison of a reference waveform with a high-frequency carrier, whereas in the SVM strategy switching instants and duration of each switching state are calculated from simple equations. Moreover, there is only one reference vector, in contrast to the three individual reference waveforms for three phases of the system. It offers more flexibility as well as a higher maximum modulation index m of 1.15. SVM is studied in detail in the next chapter.

Chapter 4

Space-Vector Modulation

Contents

In the previous chapter, two families of pulse-width modulation schemes were presented: carrier-based PWM and selective harmonic elimination. This chapter intro-

duces a relatively new modulation method for three-phase converters, which offers certain advantages over conventional PWM methods.

In conventional pulse-width modulation strategies, each leg of the VSC is controlled independently. That is, SPWM uses one sinusoidal waveform for controlling each of the three legs of the converter. Likewise, placement of the switching pulses for each leg of a converter under SHE control is determined separately. In contrast, *space-vector modulation* (SVM) is intrinsically designed for three-phase converters. It combines the three reference waveforms used in CBPWM methods in one single vector, called the reference *space vector*. In SVM, instead of modulating waveforms, a modulating reference vector is employed.

Since its introduction, space-vector modulation has been the center of a great deal of research to investigate its advantages in terms of ease of implementation in digital domain, harmonic performance, maximum modulation index, and approach towards overmodulation. SVM offers a number of degrees of freedom that can be exploited to achieve desired operation characteristics. It has found numerous applications in both power system schemes such as STATCOM [20] and HVDC converter systems [21], and electrical drive applications [22].

This chapter opens with introducing the concept of space vector and converter states, which are central to understanding how space-vector modulation functions. SVM is also capable of controlling multilevel VSCs, which can be based on the two-level scheme. Several three-level space-vector modulation approaches, which provide a higher number of degrees of freedom, have been presented in literature [23], [24].

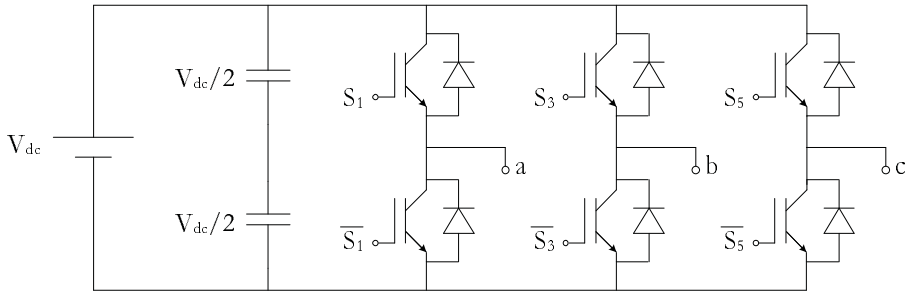

Fig. 4.1. Schematic diagram of a two-level, three-phase VSC.

4.1 Concept of Space Vector

Space vectors and their corresponding converter states are at the crux of SVM. In SVM, as mentioned earlier, the converter (Fig. 4.1) is controlled through the concept of converter states [25], [26]. Each converter state corresponds to a certain combination of switches. There are two switches in each leg of a two-level converter. As the switches in one leg cannot be both ON or OFF at the same time (the former leads to a short circuit of the associated phase, and the latter results in an open circuit), and there are three converter legs in a three-phase system, the total number of converter states is 8. States are numbered in binary (0 for OFF state of the upper switch and 1 for its ON state) from 000 to 111, where the leftmost digit shows the state of phase-c of the converter and the rightmost digit corresponds to the state of phase-a (cba).

Each of the converter states can be mapped into dq-plane by applying Park's transformation to the phase voltages as given in (4.1) [12]. Similarly, any set of balanced reference phase voltages v_a, v_b, and v_c can be represented as a corresponding reference space vector $\mathbf{V}$ in two dimensions using the same equation.

$$\mathbf{V} = \frac{2}{3}\left(v_{\mathrm{a}}(t) + v_{\mathrm{b}}(t)e^{j2\pi/3} + v_{\mathrm{c}}(t)e^{-j2\pi/3}\right) \tag{4.1}$$

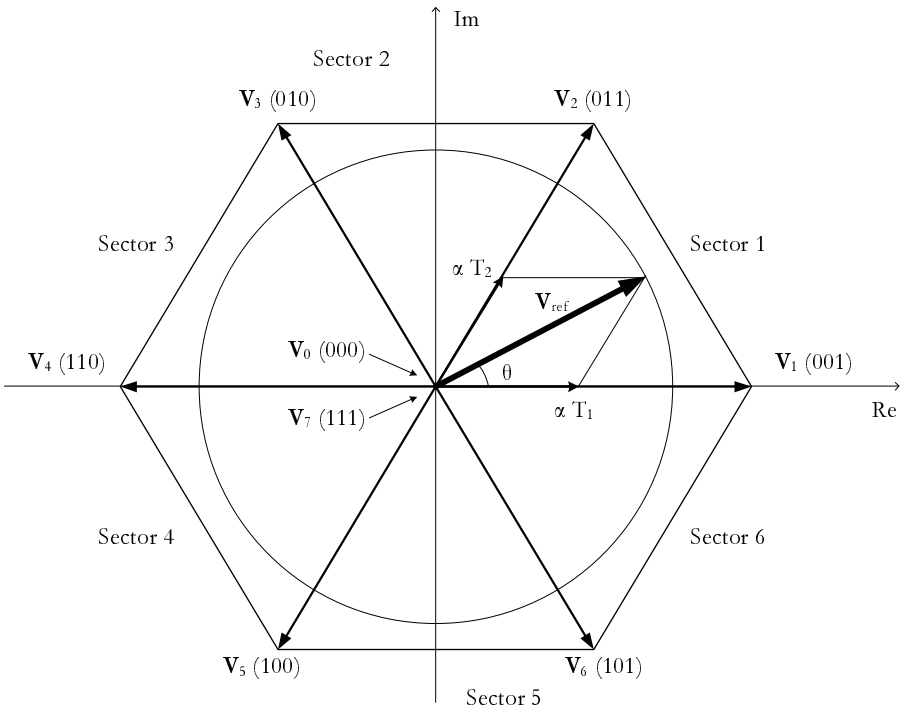

Fig. 4.2. Six active space-vectors and two zero space-vectors in two-level SVM.

The length of six active space-vectors, denoted by $\mathbf{V}_1$ to $\mathbf{V}_6$ in Fig. 4.2, is $2V_{\mathrm{dc}}/3$. They are separated by 60° in the plane, pointing to vertices of a hexagon as shown in Fig. 4.2. Two zero space-vectors, $\mathbf{V}_0$ and $\mathbf{V}_7$, lie at the origin. Table 4.1 summarizes these eight possible configurations and the resulting space vectors, along with corresponding phase- and pole-voltages. Each of six sections of the hexagon is called a *sextant* or *sector*.

In two-level SVM, $\mathbf{V}_0$ and $\mathbf{V}_7$ generate the same line voltage (which is zero), and hence are redundant states. One can choose one or both, as suited, to reduce the number of switchings or manipulate harmonics. These two vectors are the only redundant space vectors for a two-level SVM. As the number of levels of the SVM implementation increases, the number of redundant space vectors increases, which can be exploited to achieve desired performance characteristics. This is described in more detail in Chapter 6.

TABLE 4.1
EIGHT SPACE-VECTORS AND THEIR CORRESPONDING PHASE- AND LINE-VOLTAGES

State	c, b, a	**V**	Pole Voltage, multiply by $V_{\rm dc}/2$			Phase Voltage		
			V_{az}	V_{bz}	V_{cz}	V_{an}	V_{bn}	V_{cn}
0	**000**	0	-1	-1	-1	0	0	0
1	**001**	$2V_{\rm dc}/3e^{j0}$	1	-1	-1	$2V_{\rm dc}/3$	$-V_{\rm dc}/3$	$-V_{\rm dc}/3$
2	**011**	$2V_{\rm dc}/3e^{j\pi/3}$	1	1	-1	$V_{\rm dc}/3$	$V_{\rm dc}/3$	$-2V_{\rm dc}/3$
3	**010**	$2V_{\rm dc}/3e^{j2\pi/3}$	-1	1	-1	$-V_{\rm dc}/3$	$2V_{\rm dc}/3$	$-V_{\rm dc}/3$
4	**110**	$2V_{\rm dc}/3e^{j\pi}$	-1	1	1	$-2V_{\rm dc}/3$	$V_{\rm dc}/3$	$V_{\rm dc}/3$
5	**100**	$2V_{\rm dc}/3e^{j4\pi/3}$	-1	-1	1	$-V_{\rm dc}/3$	$-V_{\rm dc}/3$	$2V_{\rm dc}/3$
6	**101**	$2V_{\rm dc}/3e^{j5\pi/3}$	1	-1	1	$V_{\rm dc}/3$	$-2V_{\rm dc}/3$	$V_{\rm dc}/3$
7	**111**	0	1	1	1	0	0	0

The applied space vectors and their duration depend on the three-phase output waveform to be constructed. The following details waveform generation using the SVM method.

4.2 Generation of Waveforms

Since SVM is inherently a regularly-sampled method [27], the reference voltage vector, which rotates in the dq-plane at the frequency of the desired output voltage, is sampled evenly at the rate determined by the sampling frequency F_s, or equivalently $F_{sn} = F_s/f$ times in each period. The magnitude of the constructed three-phase voltage is proportional to the magnitude of this reference vector and the phase angle of the reference vector is equal to that of phase-a of the output voltage. In order to prevent non-characteristic harmonics, the normalized sampling frequency F_{sn} should be an integer multiple of 6, so that the same number of samples is allocated to all six sectors of the hexagon.

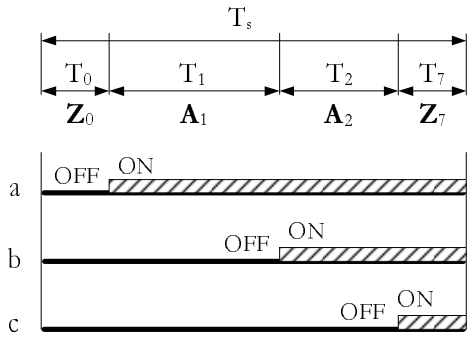

Fig. 4.3. Averaging of space vectors over time in each sampling period.

The goal of SVM is to approximate the reference vector using space vectors by placing the converter in a sequence of appropriate states for designated time shares within each sampling period. Any reference vector $\mathbf{V}_{\text{ref}}$ that lies entirely within the hexagon can be decomposed to space vectors $\mathbf{V}_0$ to $\mathbf{V}_7$ as depicted in Fig. 4.2 for a $\mathbf{V}_{\text{ref}}$ in the first sector of the hexagon. This is achieved by constructing voltages that average to the reference vector, as shown in (4.2) and illustrated in Fig. 4.3, where the two adjacent active space-vectors $\mathbf{A}_1$ and $\mathbf{A}_2$ and one or both zero space-vectors $\mathbf{Z}_0$ and $\mathbf{Z}_7$ are used.

$$\mathbf{V}_{\text{ref}} = \frac{T_0 \times \mathbf{Z}_0 + T_1 \times \mathbf{A}_1 + T_2 \times \mathbf{A}_2 + T_7 \times \mathbf{Z}_7}{T_s} \tag{4.2}$$

Note that vectors $\mathbf{A}_1$ and $\mathbf{A}_2$ correspond to vectors $\mathbf{V}_i$ depending on the sector in which the sampled space vector lies. For example, in the first sector, $\mathbf{A}_1$ is $\mathbf{V}_1$ and $\mathbf{A}_2$ is $\mathbf{V}_2$; in the second sector, $\mathbf{A}_1$ is $\mathbf{V}_2$ and $\mathbf{A}_2$ is $\mathbf{V}_3$; and in the sixth sector, $\mathbf{A}_1$ is $\mathbf{V}_6$ and $\mathbf{A}_2$ is $\mathbf{V}_1$.

Time shares of active space-vectors are proportional to the length of respective projected vectors. The rest of the sampling period is filled with zero space-vectors $\mathbf{Z}_0$ and/or $\mathbf{Z}_7$. The time share of each space vector can be calculated by decomposing the reference vector onto the two adjacent space vectors. T_1 and T_2 (time shares of

the active space-vectors adjacent to the reference vector, $\mathbf{A}_1$ and $\mathbf{A}_2$) and T_z (the remaining time of sampling period, time share of zero space vectors, $\mathbf{Z}_0$ and $\mathbf{Z}_7$) are calculated as

$$T_1 = \frac{\sqrt{3}}{2} \times T_s m \sin(\pi/3 - \theta) \tag{4.3}$$

$$T_2 = \frac{\sqrt{3}}{2} \times T_s m \sin(\theta) \tag{4.4}$$

$$T_0 + T_7 = T_z = T_s - T_1 - T_2 \tag{4.5}$$

where T_s is the sampling period and is equal to $1/F_s$, θ is the angle between the reference vector and the space vector $\mathbf{A}_1$, and m is the modulation index, which is defined as in (3.1) and repeated in (4.6)

$$m = \frac{V_{\text{ref(max)}}}{V_{\text{dc}}/2} \tag{4.6}$$

where $V_{\text{ref(max)}}$ is the amplitude of desired fundamental component of the output phase voltage. The value of m determines whether the converter is in linear or over-modulation region. Operation of the converter in overmodulation region is studied in Section 4.3.

Note that in (4.5) the individual time shares of zero vectors $\mathbf{Z}_0$ and $\mathbf{Z}_7$ are not specified and are left to be decided by the specific implementation criteria. Besides, there is no restriction on the placement of active vectors, and they can be placed in any order within the sampling period. Moreover, once a sequence format is chosen, it can be applied in two ways: either the same for consecutive sampling periods, or alternatively forward and backward. For example, if the sequence $\mathbf{Z}_0\mathbf{A}_1\mathbf{A}_2\mathbf{Z}_7$ is chosen, is can be applied as $\mathbf{Z}_0\mathbf{A}_1\mathbf{A}_2\mathbf{Z}_7|\mathbf{Z}_0\mathbf{A}_1\mathbf{A}_2\mathbf{Z}_7$ (only forward sequence) or

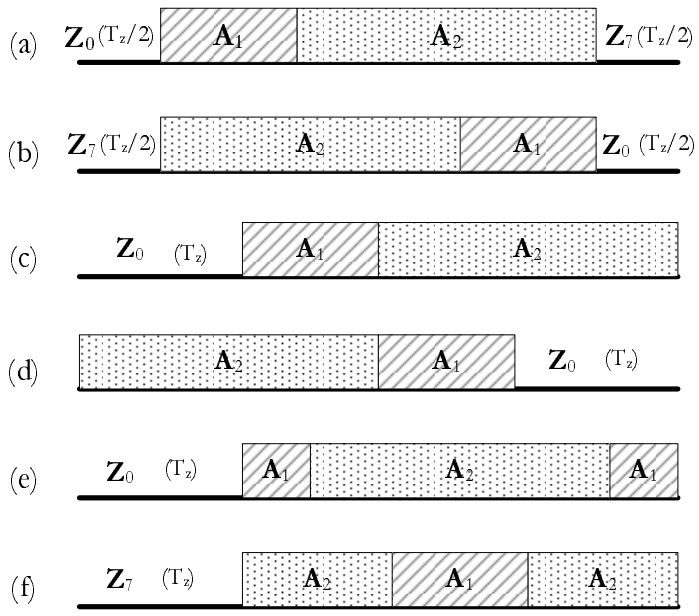

Fig. 4.4. Some of the possible switching sequences. (a), (b) conventional SVM, (c), (d) 120° bus-clamped SVM, and (e), (f) 60° bus-clamped SVM. (T_z is $T_s - T_0 - T_1$.)

forward sequence for one sampling period and backwards to the next period, i.e., $\mathbf{Z}_0\mathbf{A}_1\mathbf{A}_2\mathbf{Z}_7|\mathbf{Z}_7\mathbf{A}_2\mathbf{A}_1\mathbf{Z}_0$.

It is this freedom in positioning of space vectors that makes SVM flexible. In addition to eliminating harmonics, this can be used to decrease the number of switchings in a cycle by placing *neighbor*[1] states adjacent to each other. There are several methods suggested in the literature for arrangement of states in a sampling period [9], [28], [29]. These methods are different in the number of states used, their order, and share of zero-vectors, which further lead to difference in the number of switching actions, switching losses, and harmonic behavior of the converter. Some possible switching sequences are shown in Fig. 4.4.

The conventional SVM (Fig. 4.4a) uses successions of $\mathbf{Z}_0\mathbf{A}_1\mathbf{A}_2\mathbf{Z}_7$ and $\mathbf{Z}_7\mathbf{A}_2\mathbf{A}_1\mathbf{Z}_0$, to take advantage of the inherent symmetry in this method. Another suggested strategy is $\mathbf{Z}_0\mathbf{A}_1\mathbf{A}_2$ followed by $\mathbf{Z}_7\mathbf{A}_2\mathbf{A}_1$. Through eliminating one zero vector

[1]Neighbor states are those that differ in the state of only one switch.

in each cycle, this method ensures minimum number of switchings by alternating between states that are different only in one leg state [30], [31]. This family of methods are called discontinuous (or bus-clamped), in contrast to the conventional SVM, which is identified as a continuous method [12]. In discontinuous strategies, each phase is clamped to the top or bottom dc rail for one-third (120°), one-sixth (60°), or one-twelfth (30°) of the fundamental cycle, which eliminates the switching of that phase during the corresponding period.

Aside from freedom in arranging the converter states within a sampling period, which is absent in the conventional carrier-based PWM methods, SVM is superior to conventional PWM in that it is innately designed for digital implementation. This makes it readily available for microcomputer-based implementation as well as simulation with digital simulators. In the next chapter, implementation of SVM in one such simulator is elucidated.

A simplified version of the algorithm to implement two-level SVM is shown in Algorithm 4.1. Three-level SVM is considered in a later section, and is implemented based on SVM for two-level converters.

Algorithm 4.1 Summary of implementation of two-level SVM

1. Decide on the SVM **sequence** to be used.
2. Repeat, for each **sample** of the reference vector $\mathbf{V}_{\text{ref}}$
   - 2.1. Find the **sector** in which $\mathbf{V}_{\text{ref}}$ lies, and $\mathbf{A}_1$ and $\mathbf{A}_2$, based on θ.
   - 2.2. **Project** the reference vector to the first sector.
   - 2.3. Find **time shares** T_1, T_2, and T_z, based on m and θ.
   - 2.4. If $T_z > 0$, **share** T_z between T_0 for $\mathbf{Z}_0$ and T_7 of $\mathbf{Z}_7$, based on the sequence;
     otherwise, set $T_z = 0$ and adjust T_1 and T_2 based on the **overmodulation** strategy.
   - 2.5. **Place** the VSC in states $\mathbf{A}_1$, $\mathbf{A}_2$, $\mathbf{Z}_0$, and $\mathbf{Z}_7$ in the order determined by the chosen sequence.

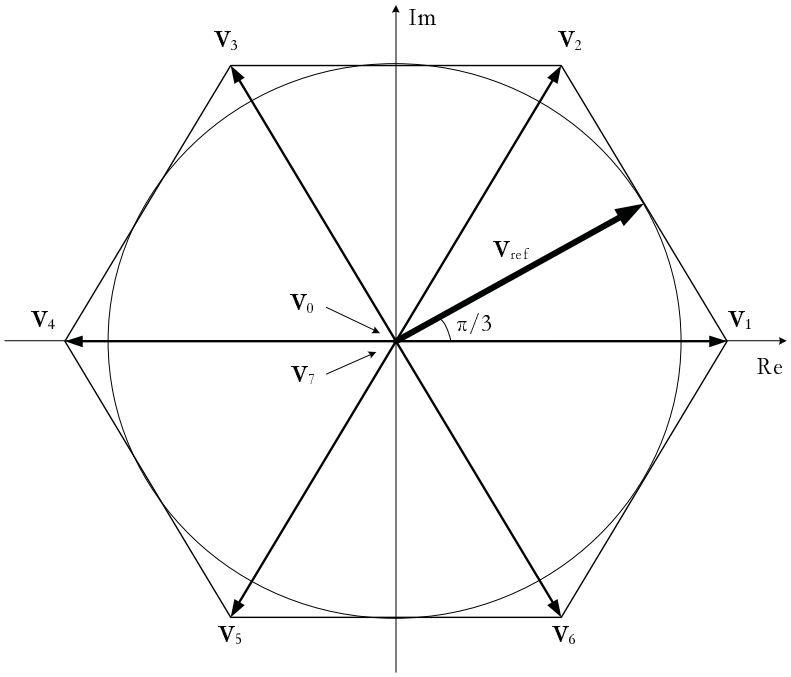

Fig. 4.5. Maximum length of the reference vector for $m = 1.15$.

4.3 Overmodulation Mode of Operation

As long as the reference vector lies inside the hexagon, it can be approximated successfully using the available space vectors $\mathbf{V}_0$ to $\mathbf{V}_7$. The maximum allowable length of the reference vector happens when it touches the boundary of hexagon, which occurs for an angle of $\theta = \pi/3$ for $m = 2/\sqrt{3} \simeq 1.15$ [32], as shown in Fig. 4.5.

Any further increase in the modulation index causes the reference vector to be partially outside the hexagon. Mathematically, this means that the cumulative time share of active vectors $(T_1 + T_2)$ becomes larger than T_s and hence, $T_z = T_0 + T_7$ becomes negative. In this case, the converter exceeds its linear region of operation and enters overmodulation region. Therefore, the synthesized waveform becomes distorted, which also disturbs the linear characteristic between m and the magnitude of fundamental component of the output voltage. In other words, in the overmodulation region, the fundamental component of the output voltage does not

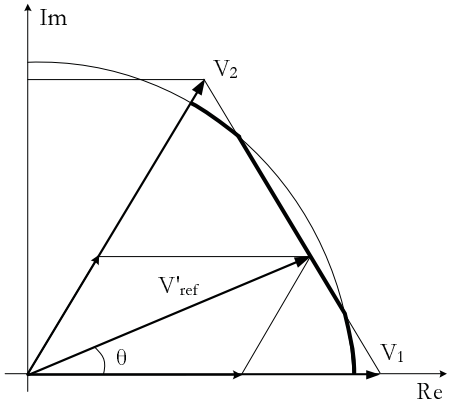

Fig. 4.6. Reference vector hard-limited to the hexagon in overmodulation region.

increase commensurately as m increases. Overmodulation is normally avoided in applications that are sensitive to distortion, such as uninterruptable power supplies (UPS).

In a simple modulator, the reference vector is hard-limited to the hexagon as shown in Fig. 4.6. This is equivalent to setting $T_0 + T_7$ equal to zero and adjusting the time shares of active vectors.

Modified time shares T_1 and T_2 can be computed as shown in (4.7) and (4.8).

$$T_1 = T_s \frac{\sqrt{3}\cos(\theta) - \sin(\theta)}{\sqrt{3}\cos(\theta) + \sin(\theta)} \tag{4.7}$$

$$\begin{aligned} T_2 &= T_s \frac{2\sin(\theta)}{\sqrt{3}\cos(\theta) + \sin(\theta)} \\ &= T_s - T_1 \end{aligned} \tag{4.8}$$

In this case, the magnitude of the reference voltage is not constant, but a function of the phase angle θ as shown in (4.9).

$$V'_{\text{ref}} = \frac{2V_{\text{dc}}/\sqrt{3}}{\sin(\theta) + \sqrt{3}\cos(\theta)} \tag{4.9}$$

The expression for V'_{ref} in (4.9) is independent of m, implying that this basic

method does not compensate for the drop in the magnitude of the reconstructed voltage. This can lead to generation of severely distorted waveforms. In Section 4.4 some methods to deal with this problem and to extend the linear region of operation are presented.

If m increases beyond 1.33, the tip of reference vector $\mathbf{V}_{\text{ref}}$ would always be outside the hexagon, and zero vectors are never used. In such a case, the modified reference voltage traces the hexagon boundary and linear formulae are no longer valid for calculation of T_1 and T_2. This mode, which is known as square-wave operation, begins when the magnitude of $\mathbf{V}_{\text{ref}}$ becomes equal to the magnitude of the space vectors, which is equal to half of the diameter of the hexagon. Hence, the modulation index is

$$m = \frac{\frac{2}{3}V_{\text{dc}}}{\frac{1}{2}V_{\text{dc}}} = \frac{4}{3} \simeq 1.33 \tag{4.10}$$

In this mode, the state of the converter is changed from $\mathbf{V}_1$ to $\mathbf{V}_2$ to $\mathbf{V}_3$ to $\mathbf{V}_4$ to $\mathbf{V}_5$ to $\mathbf{V}_6$, solely operating at the vertices of the hexagon. The converter remains in each state for one-sixth of the fundamental period. Any further increase in m has no effect on the reconstructed voltage.

Note that overmodulation is also virtually possible in CBPWM schemes such as SPWM and 3rd harmonic injection SPWM. However, these two methods cannot maintain the linear relationship between m and the desired output voltage for higher values of m. SVM, on the other hand, has an extended linear region achieved by employing compensation, which is described in the next section.

Fig. 4.7 compares the extent of the linear relationship of SPWM, 3rd harmonic injection SPWM, and SVM. It is readily observable that the mentioned CBPWM

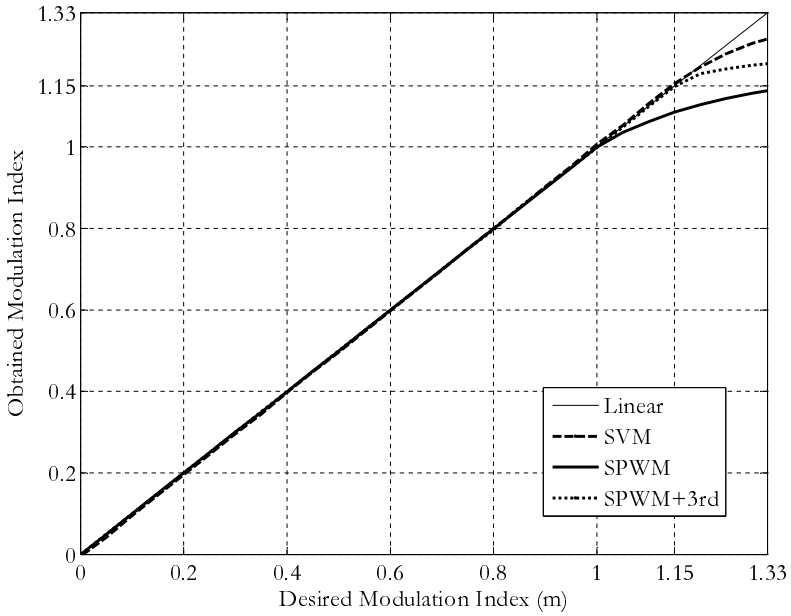

Fig. 4.7. Comparison of the degree of overmodulation in PWM methods.

methods reach saturation at a smaller m compared to SVM. This higher utilization of the dc bus voltage is one of the most distinctive features of SVM.

4.4 Compensation in Overmodulation Region

A short introduction to the behavior of SVM for higher values of modulation index was presented in the previous section. The fact that even in the overmodulation region the reference vector is inside the hexagon for some period of time has suggested compensation for the instants of time that the reference vector is outside the hexagon. This compensation can only be performed for small deviations from linear mode, and cannot be employed when the lost magnitude is excessively large. Compensation aims to increase the linear region of operation of space-vector modulators and hence, to maximize utilization of the dc link voltage [33].

Several approaches to compensation in the overmodulation region have been

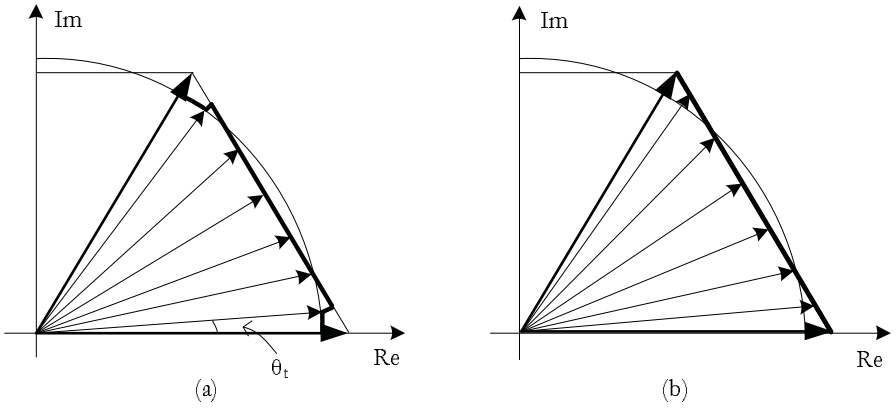

Fig. 4.8. Two-zone overmodulation approach, (a) zone I, and (b) zone II.

proposed in the literature to extend the linear region of SVM. Two of such methods are presented in this section.

4.4.1 Two-Zone Overmodulation Approach

The two-zone approach to overmodulation strategy is proposed in [34]. In zone I of this method, trajectory of the reference vector is partly circular (corresponding to the desired m, and hence no modification) and partly on boundary of the hexagon (Fig. 4.8a). Transition from circular trajectory to boundary tracking is determined by the transition angle θ_t, which is a function of the given modulation index [32]. For the boundary tracking region, the instantaneous value of m is changed with the phase angle of reference vector so that the reference vector always remains within the hexagon. The maximum value of modulation index in this zone is 1.21, which occurs for a transition angle of zero.

While only the magnitude of the reference vector is changed in zone I, both its magnitude and angle are modified in zone II to achieve a higher modulation index. In zone II (Fig. 4.8b), the reference vector is kept at a vertex of the hexagon for a particular time determined by the hold angle θ_h (a nonlinear function of m), and

then it is moved to the boundary of the hexagon. The modified phase angle of the reference vector is determined as

$$\theta' = \begin{cases} 0, & \text{if } 0 \leq \theta \leq \theta_h; \\ \dfrac{\theta - \theta_h}{\pi/6 - \theta_h}, & \text{if } \theta_h < \theta < \pi/3 - \theta_h; \\ \pi/3, & \text{if } \pi/3 - \theta_h \leq \theta \leq \pi/3. \end{cases} \tag{4.11}$$

Transition to square-wave operation completes when the reference vector is held at a vertex for half of the sector time; that is, when θ_h reaches $\pi/6$.

4.4.2 One-Zone Overmodulation Approach

A much simpler overmodulation approach is suggested in [35], called one-zone approach. In this method a single algorithm is used for the whole range of overmodulation. This is done by defining a hold angle, which is the angle at which the hexagon intersects the circular trajectory of the reference voltage (Fig. 4.9). The reference vector is produced as long as it remains inside the hexagon. When it goes beyond the hexagon boundary (which happens for $\theta > \theta_h$), a voltage vector of the same magnitude but with a modified phase is generated. The phase is kept at the hold angle until θ reaches $\pi/6$. From $\pi/6$ to $\pi/3 - \theta_h$, the phase is held at $\pi/6 - \theta_h$. The modified angle is defined below. Square-wave operation is achieved for a hold angle of zero.

$$\theta' = \begin{cases} \theta, & \text{if } 0 \leq \theta < \theta_h; \\ \theta_h, & \text{if } \theta_h \leq \theta < \pi/6; \\ \pi/3 - \theta_h, & \text{if } \pi/6 \leq \theta < \pi/3 - \theta_h; \\ \theta, & \text{if } \pi/3 - \theta_h \leq \theta \leq \pi/3. \end{cases} \tag{4.12}$$

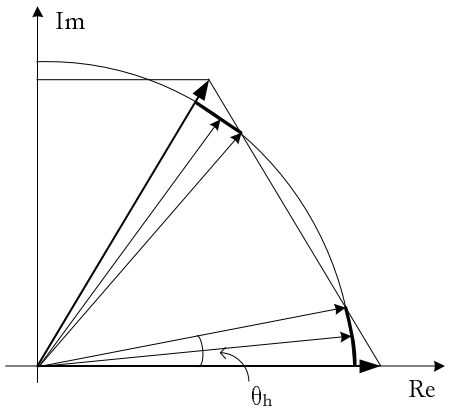

Fig. 4.9. One-zone overmodulation approach.

Hold angle θ_h is calculated from

$$\theta_h = \frac{\pi}{6} - \arccos(\frac{2}{\sqrt{3}m}) \tag{4.13}$$

Compared to the two-zone method, this method can be more conveniently implemented, but results in more severe distortion of the output waveform. It can be argued, however, that with the lower computational load, the microcontroller is able to perform more computations per cycle and increase the switching frequency, hence partially balance the adverse effects of larger harmonic components.

4.4.3 Other Approaches to Overmodulation

There are other compensation methods proposed in the literature to incorporate the overmodulation region into SVM [36]-[41]. A study of Fourier analysis of the generated waveforms in overmodulation region is presented in [42].

4.5 Optimization Parameters of SVM

Space-vector modulation provides certain degrees of freedom in the controlling the switches of a converter. These degrees of freedom are as follows:

1. Decomposition of the reference vector;

2. Sequence of active space-vectors;

3. Placement and share of zero space-vectors; and

4. Selection of the sampling frequency.

These feature of SVM can be exploited to achieve certain performance characteristics such as harmonic performance. Chapter 6 investigates two factors (sequence of active space-vector and placement of zero space-vectors) to find an optimal solution for the proposed harmonic behavior.

4.6 Naturally-Sampled SVM

Readily formulated for digital implementation, space-vector modulation is generally realized using digital processors. Digital implementation of SVM involves sampling at discrete instants of time. This could prevent application of exact switching times. While in computer simulation this can be accounted for by using interpolation-enabled simulation engines [43], this cannot be done in real-time systems. This implies that any implementation of SVM is an approximation. (The same is true about other methods with predetermined switching times such as SHE.)

It has been shown in [44] that the conventional SVM scheme, in which the active space-vectors are centered within the sampling period (with three switchings in a cycle), can be implemented in an analog modulator by adding a zero-sequence voltage to the set of three-phase voltages. The mathematical derivation for the required common-mode voltage is presented in [45] and is found to be half of the

amplitude of envelope of the reference voltages, which is

$$V_{cm} = \frac{\max\{v_a, v_b, v_c\} - \min\{v_a, v_b, v_c\}}{2} \tag{4.14}$$

The resulting waveform is passed to a conventional carrier-based modulator.

One major advantage of this naturally-sampled, analog implementation is that the switching frequency is only limited by the switches themselves, and not the computational ability of the microprocessor or DSP.

4.7 Multilevel Space-Vector Modulation

The first multilevel converter appeared in a patent filed in 1975, in which cascaded converters were suggested [46]. In recent years, multilevel converters are becoming popular in high-power, medium-voltage[2] applications. These applications include pumps, fans, conveyors, mills, laminators, blowers, and compressors. This is due to their ability to meet the increasing demand of power rating. Moreover, they are able to reduce the harmonic content of output voltage and current for a certain switching frequency, and also to reduce the voltage rating of power semiconductor devices.

By synthesizing the ac output voltage using several voltage levels, staircase waveforms are produced, which approximate a sinusoidal waveform with lower harmonic distortion than two-level methods. In addition, cancellation of low frequency harmonics implies reduced filtering requirement. Also, such multilevel converters have a lower rate of voltage change dV/dt across their switches and other power electronic devices. For example, in a three-level VSC, the switches are needed to withstand half of the blocking voltage of a two-level VSC. This reduces the stress on the power

[2]Voltage ratings of 2.3, 3.3, 4.16, and 6.9 kV.

electronic devices. Due to these attractive characteristics, several control algorithms for multilevel converters have been proposed [4], [6], [47].

The conventional space-vector modulation, which is tailored for a three-phase, two-level VSC, can also be adopted for multilevel converters. The number of converter states drastically increases with the number of available voltage levels; i.e., from 8 in a two-level VSC to n^3 levels for an n-level converter, of which some are redundant states and correspond to identical space vectors. The number of distinctive space vectors in an n-level converter is

$$\begin{aligned} N_{\text{vectors}} &= 1 + 6\sum_{i=1}^{n-1} i \\ &= 1 + 3n(n-1) \end{aligned} \tag{4.15}$$

Moreover, while finding the appropriate space vectors for decomposing of any reference vector is straightforward in two-level SVM, it is relatively harder for multilevel SVM. Difficulty in determining the sector in which the reference vector lies, calculation of ON-times, and choosing the proper switching states also contribute to the complexity of multilevel SVM.

Space vectors in three-level SVM can be selected by translating the problem back to the two-level case [48]. Higher-level SVM, for example five-level, can be realized using two phase-shifted three-level converters. The next section discusses the method used to implement three-level SVM in this work.

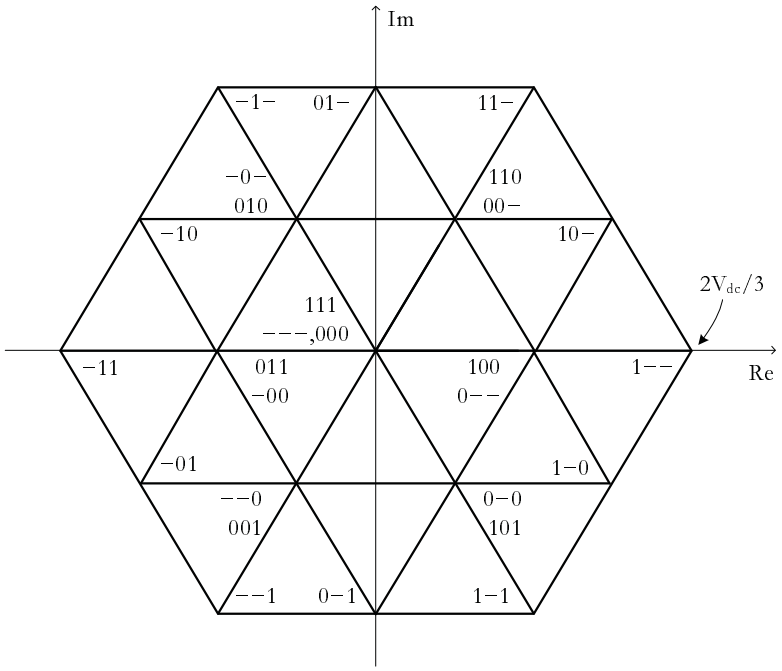

Fig. 4.10. Arrangement of vectors for three-level SVM.

4.8 SVM for Three-level Converters

As mentioned earlier, one reason for complexity of three-level SVM compared to two-level SVM is that there are additional redundancies available in the three-level SVM, than just zero vectors ($\mathbf{Z}_0$ and $\mathbf{Z}_7$) as is the case for two-level SVM.

The goal in three-level SVM is to find proper sequences of vectors that ensure synchronization and existence of relevant symmetries [23]. Another major concern is that the dc bus voltage must remain balanced. That is, the vector sequences should be applied in such a way that the current drawn from the upper capacitor is the same as the current drawn from the lower capacitor over one period.

The number of states in a three-level converter is 27, of which only 19 states are unique. The computational effort for finding suitable vectors to be used in a switching period becomes more intense as the number of converter levels increases. Therefore, it necessitates development of effective approaches to find the most ap-

propriate space vectors. For a dc bus voltage of V_{dc}, one leg can assume states of (ON, ON) for $V_{\text{dc}}/2$, (OFF, OFF) for $-V_{\text{dc}}/2$, and (OFF, ON) for 0.

Following the previously-mentioned method for numbering the states, while for a two-level VSC states are numbered from 000 to 111, in three-level VSC the states are numbered from $---$ (short for $-1\,-1\,-1$) to 111. Each digit in this identifier shows the level of voltage to which the respective leg is switched (c, b, and a, from left to right). That is, -1 for a leg means that it is switched to $-V_{\text{dc}}/2$, 0 means it is switched to 0, and 1 means it is switched to $+V_{\text{dc}}/2$. Note that there are three zero space-vectors in three-level SVM: $---$, 000, and 111. On the dq-plane, the new extended modulator can be pictured as in Fig. 4.10, which shows a large hexagon comprising of a number of smaller ones.

As a method outlined in [24] suggests, each sector of the outer hexagon of three-level SVM can be divided into four smaller triangles, indexed as shown in Fig. 4.11. Each of these smaller triangles are then considered as one sector of a two-level hexagon, with the same redundancy at the origin. Note that the small triangles in a three-level SVM can have their base either at the bottom (type one, $\triangle$) or at the top (type two, $\triangledown$). The first type of triangles ($\triangle_0$, $\triangle_1$, and $\triangle_3$) is similar to the first sector of a two-level hexagon. The second type ($\triangle_2$) is treated in the same as way as the fourth sector in two-level SVM.

In this method, the triangle that bounds the reference vector is found based on coordinates of the tip of the reference vector. The origin $(0, 0)$ is then moved to the origin-vertex of the corresponding triangle. Fig. 4.12 shows the flowchart of this method.

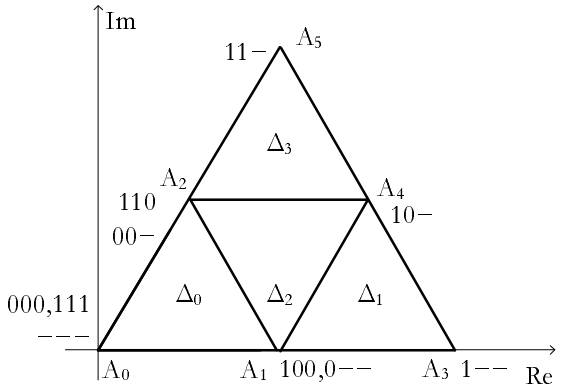

Fig. 4.11. Division of each sector of the hexagon in three-level SVM to four triangles.

TABLE 4.2
RELATIONSHIP BETWEEN k_1, k_2, AND $\triangle$

k_2 \ k_1	0	1
0	0	1, 2
1	n/a	3

The triangle is determined by first calculating auxiliary parameters k_1 and k_2 (Fig. 4.13), which are defined as

$$k_1 = \lfloor V_\alpha + \frac{V_\beta}{\sqrt{3}} \rfloor \tag{4.16}$$

$$k_2 = \lfloor \frac{V_\beta}{\sqrt{3}/2} \rfloor \tag{4.17}$$

where $\lfloor\ \rfloor$ denotes the function `floor()`, and V_α and V_β are the coordinates of the tip of the space vector, as shown in Fig. 4.14. k_1 determines whether the small triangle is in the right-hand side of the sector ($k_1 = 1$) or in the left-hand side ($k_1 = 0$). k_2 determines if it is in the upper half ($k_2 = 1$) or in the lower half ($k_2 = 0$).

The reference vector is shifted to the new set of axes that intersect at the main vertex (or origin) of the triangle. Assuming a type one triangle, the coordinates of the tip of the shifted reference vector $\overline{\mathrm{A}_i\mathrm{P}}$ (Fig. 4.14), where $\mathrm{P} = (V_\alpha, V_\beta)$ is the tip

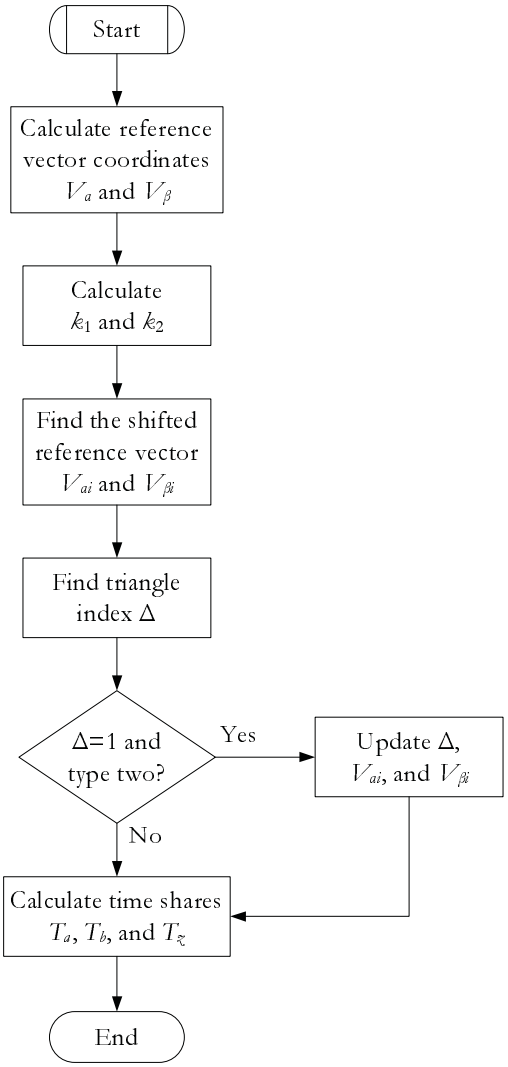

Fig. 4.12. Flowchart for determination of time shares in three-level SVM.

of the original space vector and A_i is the origin of the triangle, are found as follows.

$$V_{\alpha i} = V_\alpha - k_1 + \frac{1}{2}k_2 \tag{4.18a}$$

$$V_{\beta i} = V_\beta - \frac{\sqrt{3}}{2}k_2 \tag{4.18b}$$

The triangle index is found from

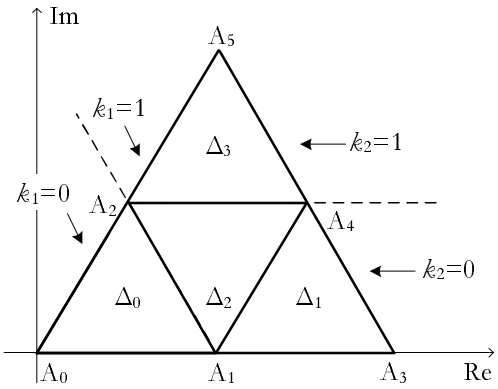

Fig. 4.13. Definition of auxiliary variables k_1 and k_2 to find the triangle index.

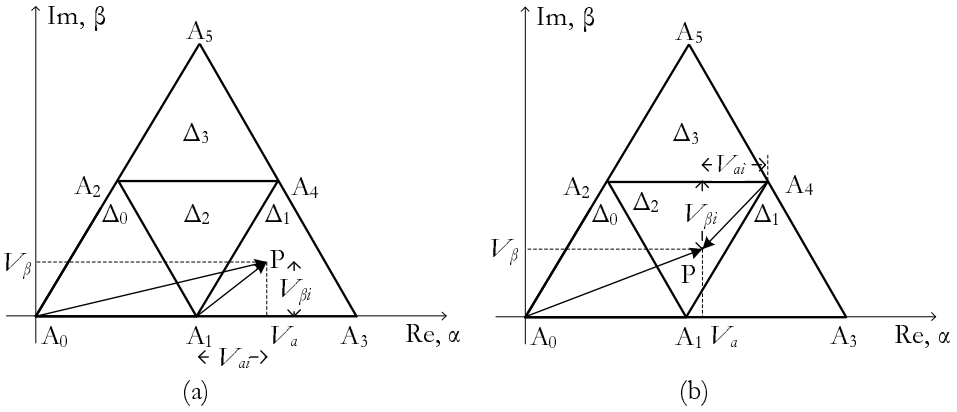

Fig. 4.14. Original and shifted vectors for three-level SVM.

$$\triangle = k_1^2 + 2k_2 \tag{4.19}$$

Table 4.2 summarizes the relationship between k_1, k_2, and $\triangle$. This holds only for a type one triangle. If the triangle is of type two ($\triangle_2$), both $\triangle$ and $(V_{\alpha i}, V_{\beta i})$ need to be updated. This happens only when $k_1 = 1$ and $k_2 = 0$ as they correspond to both $\triangle_1$ and $\triangle_2$; however, (4.19) only gives $\triangle_1$. Therefore, when $\triangle$ is equal to 1, further modification might be necessary.

Inspection of triangles $\triangle_1$ and $\triangle_2$ reveals that for a shifted vector lying in $\triangle_1$, its slope is less than 60°, whereas if it is in $\triangle_2$, its slope is larger than 60°. This observation can be used to distinguish between $\triangle_1$ and $\triangle_2$.

If $V_{\alpha i}$ is negative, the reference vector is always in $\triangle_2$. If it is positive, the slope of the shifted vector is found by calculating $V_{\beta i}/V_{\alpha i}$. If this slope is larger than $\sqrt{3}$, the vector is in $\triangle_2$ and the triangle index calculated in (4.19) should be increased by one, as shown in (4.20).

$$\triangle_{\text{type-two}} = \triangle + 1 \tag{4.20}$$

A further modification is also necessary to change the shifted reference vector accordingly using the previously calculated shifted vector, as shown in (4.21).

$$V_{\alpha i}^{\text{new}} = \frac{1}{2} - V_{\alpha i} \tag{4.21a}$$

$$V_{\beta i}^{\text{new}} = \frac{\sqrt{3}}{2} - V_{\beta i} \tag{4.21b}$$

Once the shifted reference vector is found, time shares are calculated similar to the two-level case. Using shifted coordinates, T_a (duration of the space-vector aligned with the α-axis), T_b (duration of the space-vector at 60° from the α-axis), and T_z (duration of zero space-vectors) can be found from the following.

$$T_a = T_s(V_{\alpha i} - \frac{V_{\beta i}}{\sqrt{3}}) \tag{4.22}$$

$$T_b = T_s(\frac{V_{\beta i}}{\sqrt{3}/2}) \tag{4.23}$$

$$T_z = T_s - T_a - T_b \tag{4.24}$$

The three nearest space vectors are used to synthesize the reference vector. These vectors correspond to the vertices of the bounding triangle. The maximum length of space vectors (for outer space-vectors) is, similar to the two-level SVM, $V_{\text{dc}}/3$, which is obtained by turning both switches of one half-leg ON. If only one switch is turned ON, the resulting voltage vector has a magnitude of $V_{\text{dc}}/6$, which is normalized to 1.

Table 4.3
Space-vectors used in the first sector for three-level SVM

Vector	$\triangle_0$	$\triangle_1$	$\triangle_2$	$\triangle_3$
$\mathbf{Z}_0$	A_0 (000)	A_1 (0 − −)	A_4 (10−)	A_2 (00−)
$\mathbf{A}_1$	A_1 (100)	A_3 (1 − −)	A_2 (00−)	A_4 (10−)
$\mathbf{A}_2$	A_2 (110)	A_4 (10−)	A_1 (0 − −)	A_5 (11−)
$\mathbf{Z}_7$	A'_0 (111)	A'_1 (100)	A'_4 (10−)	A'_2 (110)

Table 4.4
Mapping of switching states between the first sector and other sectors

Sector	c	b	a
1	−b	−a	−c
2	a	c	b
3	−c	−b	−a
4	b	a	c
5	−a	−c	−b
6	c	b	a

As for the square-wave operation (all outer space-vectors with a length of $V_{\text{dc}}/3$), modulation index m is 4/3, the magnitude of the reference vector V_{ref} can be found by normalizing m accordingly, as shown in (4.25).

$$V_{\text{ref}} = \frac{m}{4/3} \times 2 = \frac{m}{2/3} \tag{4.25}$$

The sequence of vectors in the first sector is determined by inspection and is shown in Table 4.3. For other sectors, the states are found from the mapping shown in Table 4.4. The switch states are left unchanged for the first sector, but for other sectors they are changed accordingly so that they use the available space-vectors in other sectors.

For maintaining the balance of capacitor voltages, the space vector sequences

Algorithm 4.2 Summary of implementation of three-level SVM

1. Repeat, for each sample of the reference vector $\mathbf{V}_{\text{ref}}$
    1.1. Find the **sector** in which $\mathbf{V}_{\text{ref}}$ lies.
    1.2. Find the **small triangle** where the tip of $\mathbf{V}_{\text{ref}}$ is.
    1.3. Calculate coordinates of the **shifted** reference vector.
    1.4. Compute **time shares** T_a, T_b, and T_z.
    1.5. **Place** the VSC in the respective states for the calculated time shares.

can be chosen in a way that the available redundancies lead to sharing of current of each leg equally between the respective capacitors.

Algorithm 4.2 summarizes the implementation procedure of the three-level SVM used in this work.

Chapter 5

Developed Model and Case Studies

Contents

Electromagnetic transients simulation programs are standard tools for study of short-term, transient phenomena in power systems. Power electronic circuits embedded in modern power networks extensively use VSCs as their building blocks.

Rapid switchings in these circuits generate harmonics and transients that could be best modeled, simulated, and analyzed using a transient simulation program. As such, it is important to develop models for various firing pulse generation schemes in these programs.

In this chapter, a digital model of an SVM-modulated VSC is presented. As a platform able to handle extensive network studies in power systems, digital implementation and testing of SVM is carried out in the electromagnetic transients simulation program PSCAD/EMTDC [49].

The developed models are able to generate firing pulses for different vector arrangements. The firing commands are generated in such a way that they provide three-phase symmetry (3PS), half-wave symmetry (HWS), and depending on the specific SVM sequence, quarter-wave symmetry (QWS). Moreover, compensation for overmodulation region is implemented and the model provides a smooth transition from linear mode to overmodulation.

The controllable properties of the output waveform are its phase angle, normalized magnitude (modulation index), and sampling frequency. The two- and three-level components in PSCAD and their input and output signals are shown in Fig. 5.1, where G_{ai}, G_{bi}, and G_{ci} are gating signals for phases a, b, and c of the converter, respectively. Fig. 5.2 shows the diode-clamped VSC to be used with the three-level SVM component.

Two case studies are presented in this chapter. The first study investigates the performance parameters of several two-level SVM methods, and compares them with SPWM. The harmonic spectrum and switching losses of the converter are considered for a balanced, star-connected RL load with isolated neutral point.

The second case study considers a three-level, SVM-controlled STATCOM. The output voltage harmonics under no-load conditions, and dynamic response of the

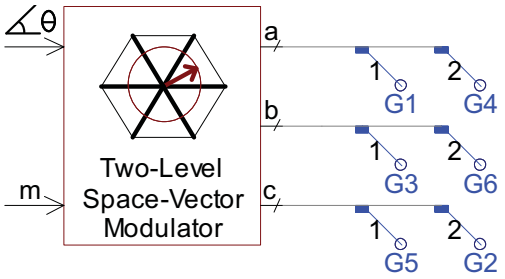

(a) Two-level SVM component

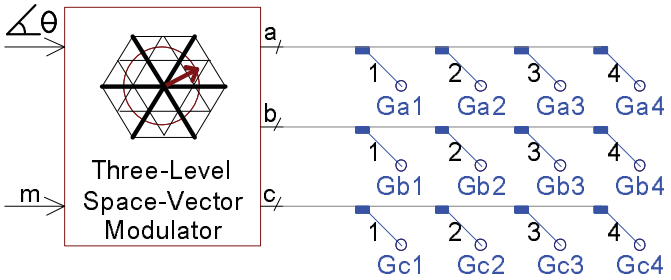

(b) Three-level SVM component

Fig. 5.1. Developed SVM controllers in PSCAD.

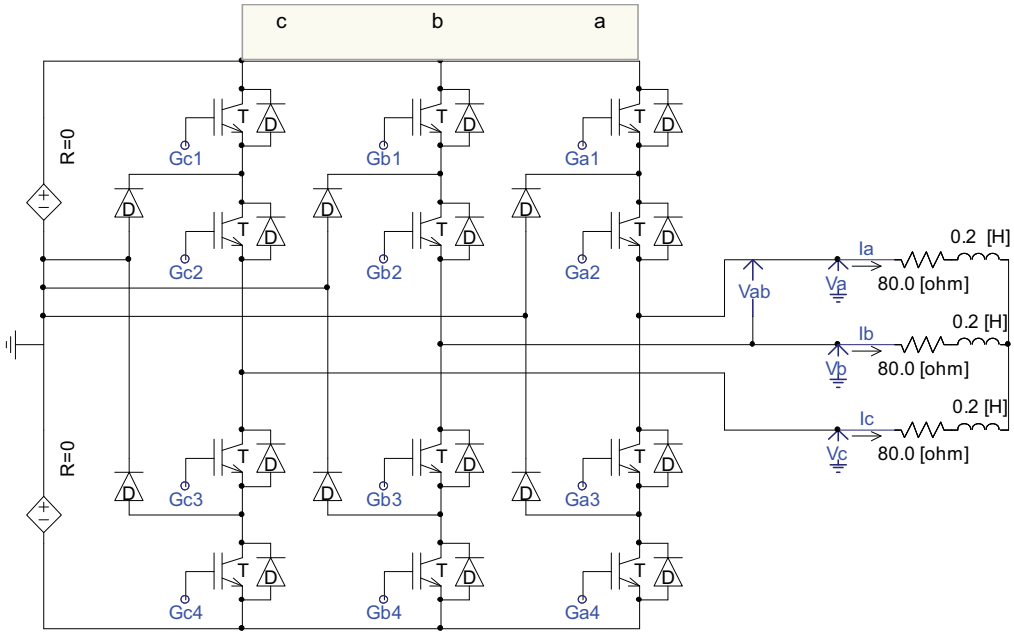

Fig. 5.2. Three-level VSC model in PSCAD.

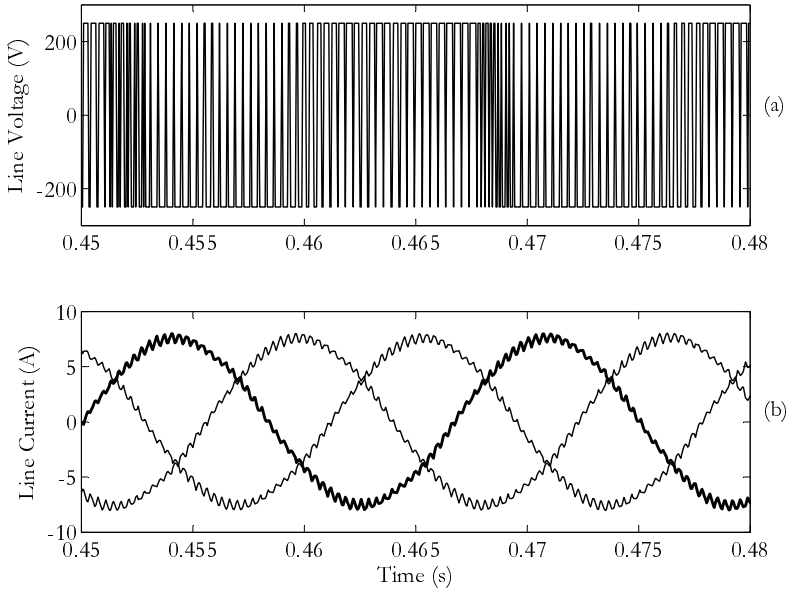

Fig. 5.3. Line voltage and currents of the two-level space-vector modulator.

system to a full load rejection in terms of the injected reactive power and the system voltage are presented.

5.1 Three-Phase Inductive Load

The model is employed in two-level mode to generate firing pulses to control the switches of a VSC for different space-vector placement strategies. It is used to assess the harmonic behavior of the synthesized output voltage by studying the impact of such factors as space-vector arrangement strategy and reference vector sampling rate. Also, modulation losses of the converter are categorized into two groups of switching losses and harmonic losses, and loss performance of SVM methods in comparison with the conventional PWM is investigated [50]. Fig. 5.3 shows typical traces of obtained line voltages and currents.

A balanced, star-connected RL load with isolated neutral is connected to the VSC. The dc bus voltage is provided by two series 250 V dc sources. The load is

TABLE 5.1
CIRCUIT PARAMETERS FOR THE TWO-LEVEL SETUP

V_{dc} (V)	f (Hz)	R (Ω)	L (mH)
2×250	60	25	24.4

26.6 Ω at 60 Hz excitation, with an angle of 20° (pf = 0.94 lagging). Load details are shown in Table 5.1.

5.1.1 Voltage and Current Waveforms

The developed model is used to simulate the operation in both linear and overmodulation regions with $m = 0.8$ and $m = 1.25$, respectively. The sampling frequency for both simulation runs is kept at $F_{sn} = 48$.

Fig. 5.4a shows the generated line voltage for $m = 0.8$. It is evident that the line voltage possesses QWS (and hence, HWS). This efficiently eliminates even-ordered harmonics. Two other graphs, Fig. 5.4b and Fig. 5.4c, show pole and phase voltages, respectively. As shown in Table 4.1, the pole voltage alternates between $-V_{dc}$ and $+V_{dc}$, while the phase voltage can assume values of $\pm 2V_{dc}/3$ and $\pm V_{dc}/3$.

As the load sees only the line voltage, it is worthwhile to study it in more detail. Fig. 5.5 shows the harmonic spectrum of the line voltage for this case. As can be seen, the first group of harmonic components is shifted to cluster around the 48th harmonic. Because of HWS, even harmonics are not present. Due to 3PS, triple-n harmonics are absent from the line voltage. WTHD calculated for the first 50 voltage harmonics is 1.60%.

Fig. 5.6 shows line currents. Because of the inductive nature of the load, higher-order current harmonics are filtered and the current waveform is close to sinusoidal shape.

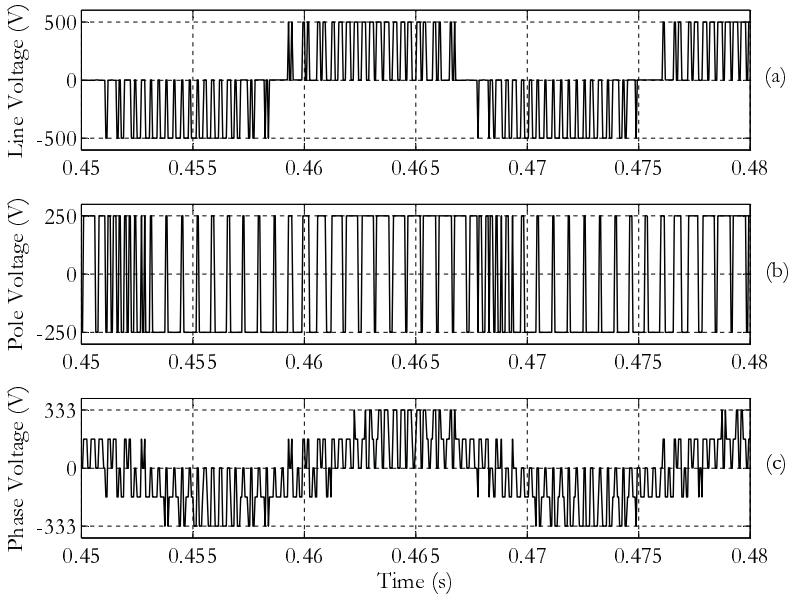

Fig. 5.4. Generated (a) line voltage, (b) pole voltage, and (c) phase voltage, $F_{sn} = 48$ and $m = 0.8$.

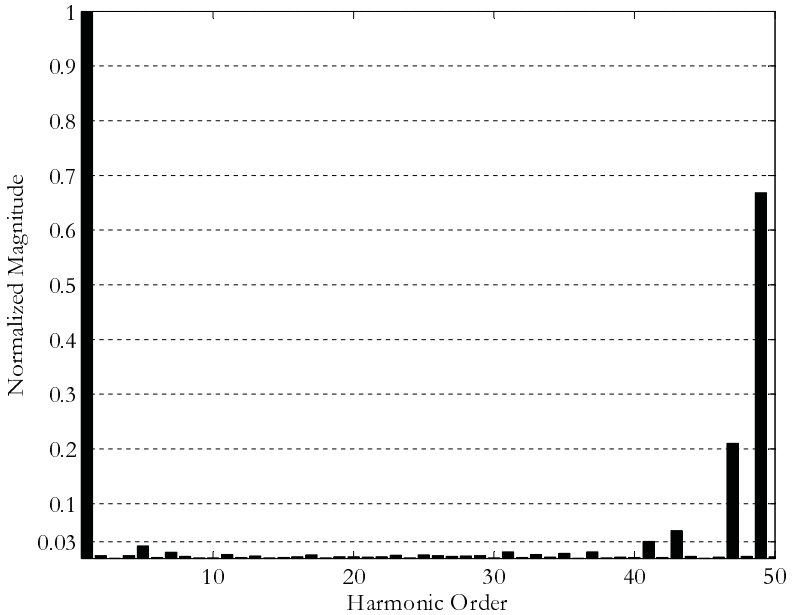

Fig. 5.5. Harmonic components of the line voltage, $F_{sn} = 48$ and $m = 0.8$.

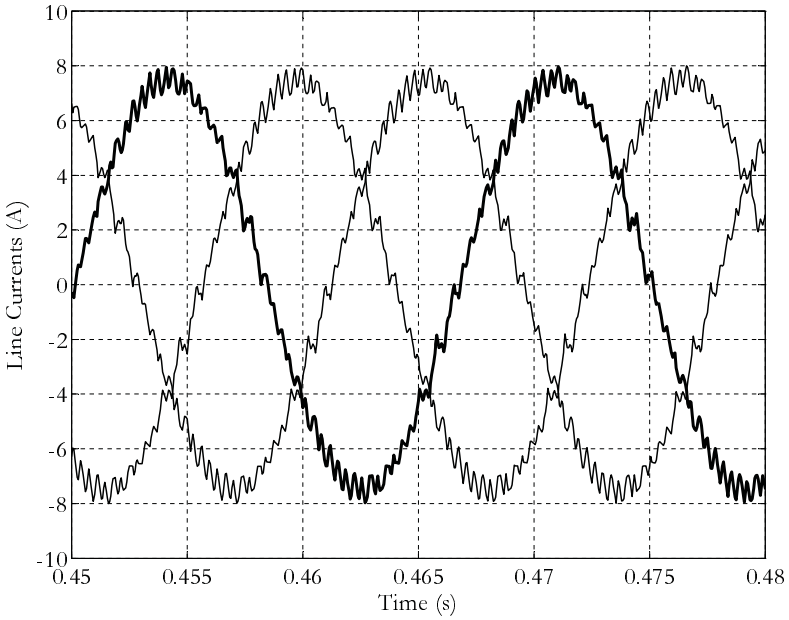

Fig. 5.6. Line currents, $F_{sn} = 48$ and $m = 0.8$.

Results in the case of overmodulation for $m = 1.25$ using the one-zone approach are shown in Fig. 5.7. Fig. 5.7a shows the line voltage, which still possesses QWS. Fig. 5.7b and Fig. 5.7c show pole and phase voltages, respectively.

Harmonic spectrum of the line voltage is shown in Fig. 5.8. Magnitudes of low-order harmonics have been increased. The same as the linear case, even and triple-n harmonics are absent from the harmonic spectrum of the line voltage. Magnitude of the constructed line voltage is 534 V. If the linear mode of operation could have extended to $m = 1.25$, a pole voltage of 541 V was to be obtained. Note that this is a match of over 98%, which is due to compensation in the overmodulation range. Voltage WTHD has been increased to 2.82%.

Fig. 5.9 shows the line currents. The current waveform has deviated from sinusoidal shape, which is expected because the reference voltage is no longer sinusoidal.

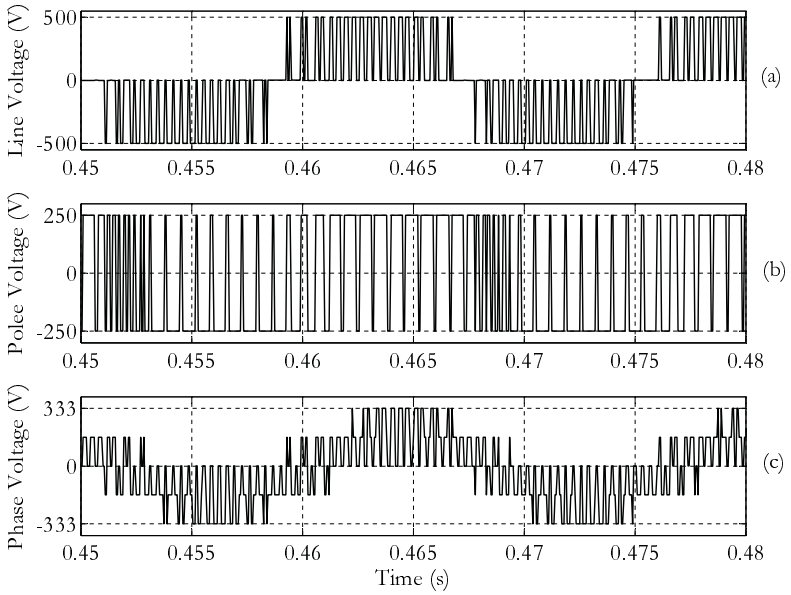

Fig. 5.7. Generated (a) line voltage, (b) pole voltage, and (c) phase voltage, $F_{sn} = 48$ and $m = 1.25$.

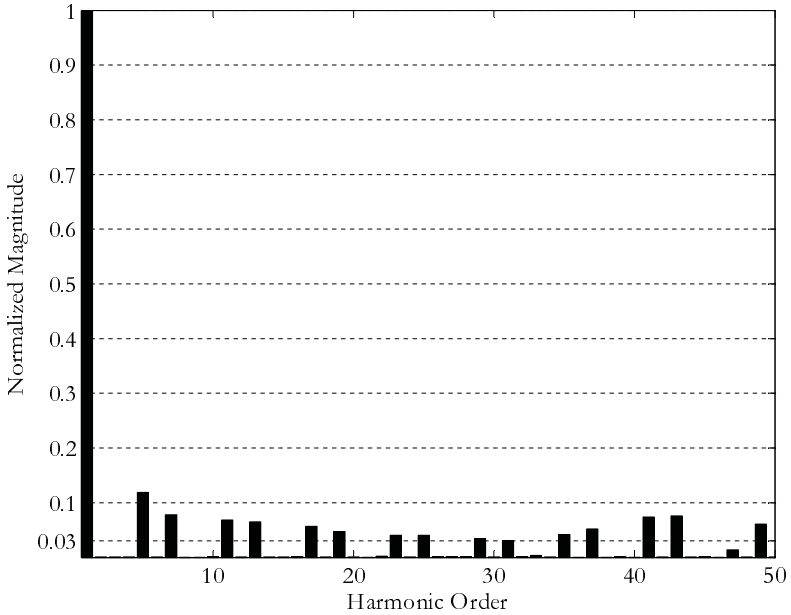

Fig. 5.8. Harmonic components of the line voltage, $F_{sn} = 48$ and $m = 1.25$.

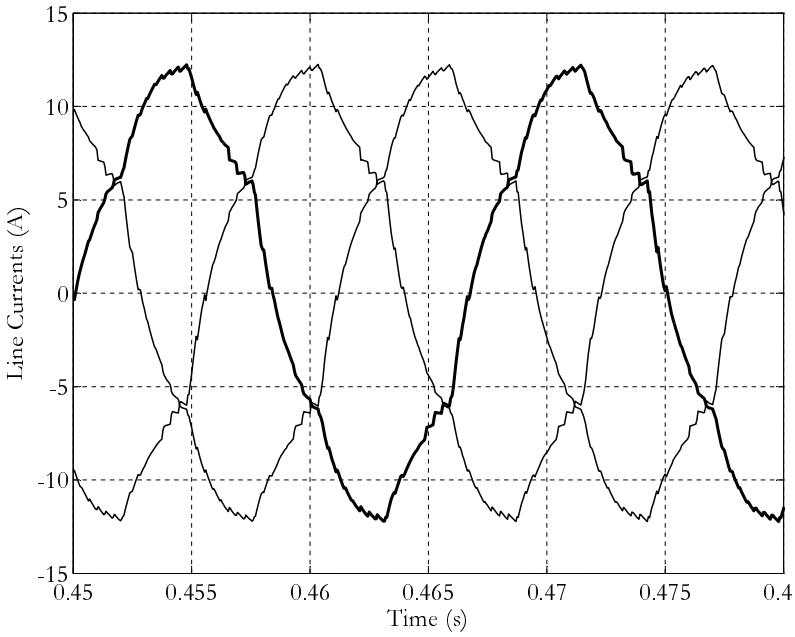

Fig. 5.9. Line currents, $F_{sn} = 48$ and $m = 1.25$.

5.1.2 Harmonic Performance

In conventional power systems, harmonics arise because of nonlinear system elements. In power electronic circuits such as converters, however, nonlinearity is the direct result of turn-ON and turn-OFF action of switches that results in distortion of the waveforms. Harmonics are undesirable as they lead to effects such as excessive heating, taking up the current capacity of the transmission lines, oscillations, and torque pulsation in electric motors. In order to control these effects, study of generated harmonics of the proposed model is of primary importance.

In order to study the harmonic performance of the set of SVM strategies, simulation results for combinations of normalized sampling frequency F_{sn}, modulation index m, and arrangement of space vectors within a sampling period are collected. Of the possible arrangement schemes, conventional ($\mathbf{Z}_0\mathbf{A}_1\mathbf{A}_2\mathbf{Z}_7|\mathbf{Z}_7\mathbf{A}_2\mathbf{A}_1\mathbf{Z}_0$), 120° bus-clamped ($\mathbf{V}_0\mathbf{V}_1\mathbf{V}_2|\mathbf{V}_2\mathbf{V}_1\mathbf{V}_0, \mathbf{V}_0\mathbf{V}_3\mathbf{V}_2|\mathbf{V}_2\mathbf{V}_3\mathbf{V}_0$) [28], and minimum loss SVM ($\mathbf{Z}_0\mathbf{A}_1\mathbf{A}_2|\mathbf{Z}_7\mathbf{A}_2\mathbf{A}_1$) [51] are considered. Note that in this implementation of 120°

bus-clamped SVM, negative side of the dc bus is chosen as the clamp to which each phase is connected for one-third of the fundamental period. This eliminates the $\mathbf{Z}_7$ zero space-vector, leaving $\mathbf{Z}_0$ as the only zero space-vector used. The performance in the case of using the positive side as clamp is similar, but a different sequence from what stated here should be used to keep the number of switchings at its minimum.

As the study is confined to voltage harmonics, no-load conditions are simulated. In a real-world case, this leads to slightly different results as the voltage drop across switches and line impedances as well as time-delays associated with the time constants of the circuit change the performance.

The WTHD values for different normalized sampling frequencies and modulation indices are recorded. Three normalized sampling frequencies of 24 (1440 Hz), 48 (2880 Hz), and 96 (5760 Hz) (which are chosen to be integer multiples of 6 to prevent non-characteristic harmonics) are used.

There is no difference between fundamental harmonic components of the constructed voltage waveforms. This is expected, however, as the fundamental component is directly controlled by time shares of space vectors.

Fig. 5.10 shows the graph of WTHD vs. m for different values of sampling frequency for the conventional, bus-clamped, and minimum-loss arrangements. Except for high values of F_{sn}, where the curve is almost flat (excluding the bus-clamped method for which the first group of harmonics cluster around $F_{sn}/2$), WTHD decreases as m increases. Since increasing the sampling frequency F_{sn} causes the harmonics to move to higher orders (clustering around F_{sn} or $F_{sn}/2$, depending on the strategy), a higher F_{sn} always corresponds to a lower WTHD. This is the main advantage of operating at a higher sampling frequency in PWM switching schemes.

As such, a high modulation index m that remains in the linear region generally corresponds to a lower WTHD. This is particularly true for lower values of F_{sn} where

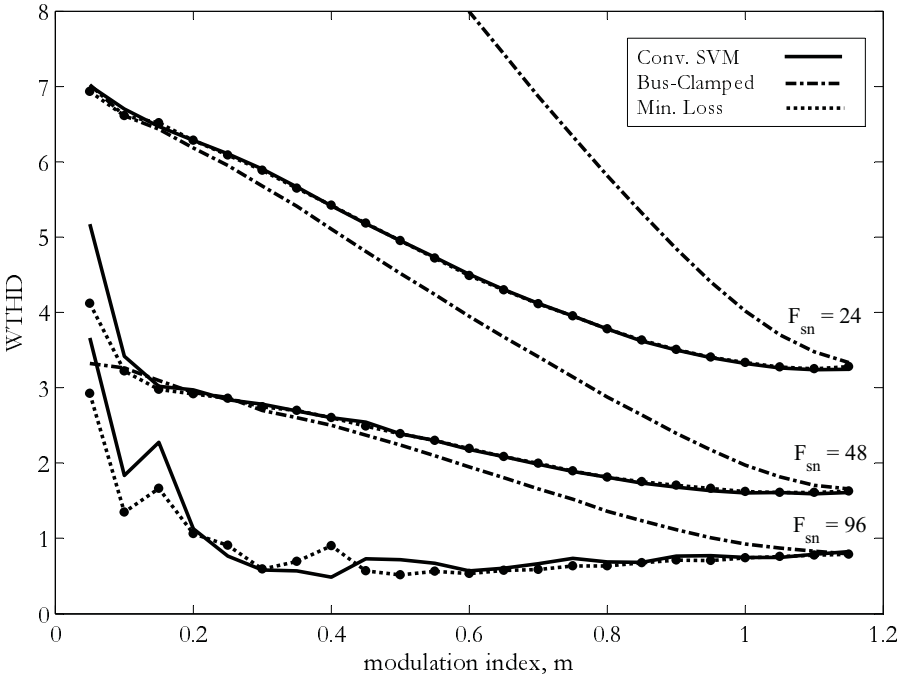

Fig. 5.10. The effect of different normalized sampling frequencies (24, 48, and 96) for three SVM strategies of conventional, 120° bus-clamped, and minimum-loss.

the significant harmonic is of a low order. For a higher F_{sn}, as can be seen for the case of $F_{sn} = 96$, the effect of such harmonics is already small because of the used weights and this general trend is no longer valid.

5.1.3 Switching Loss Behavior

In addition to the harmonic content of generated output waveform, the losses associated with the converter are of fundamental importance. Furthermore, losses result in temperature increase in both switches and the load, which could damage these devices. Therefore, it is important to estimate such losses.

In this section, temperature increase and losses of switches are estimated using the method presented in [52]. In addition to the electrical specifications of the power electronic device, accurate modeling of losses needs values of thermal resistance and capacitance of the semiconductor device and its heat sink. As these parameters are

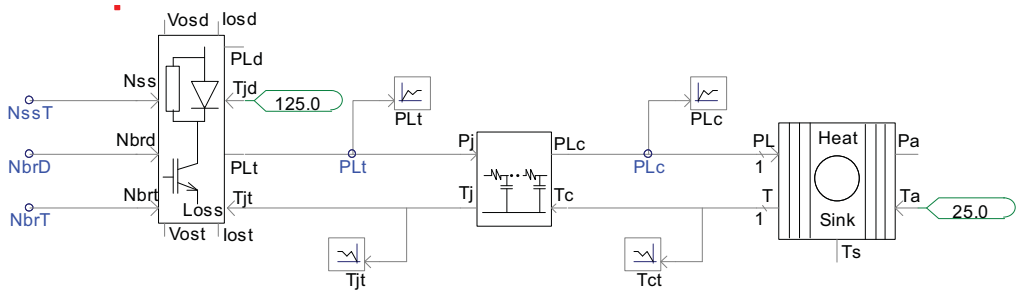

Fig. 5.11. Switching loss calculation blocks in PSCAD.

not always conveniently accessible and an error as high as 20% in temperature calculations is normal and acceptable [53], the results are mainly used as a qualitative measure for comparison of different methods. The PSCAD components used for calculation of the losses are shown in Fig. 5.11. To assess the second category of losses, which occurs in the load supplied by the converter, harmonically-weighted loss factor σ, as defined in (A.6) in Appendix A, is used.

Switching losses and WTHD for the three aforementioned SVM schemes (conventional, 120° bus-clamped, and minimum-loss) as well as sinusoidal PWM are obtained. Thermal parameters of the Toshiba ST1500GXH24 IGBT are used for simulation. The voltage and current ratings of this device are 4500 V and 1500 A, respectively. For all cases, the simulation is performed for $m = 0.8$, which is in the linear region. The sampling frequency is 2880 Hz, 48 times the fundamental frequency of 60 Hz. For each switching scheme, junction temperature of the IGBT T_J, switching losses P_L, WTHD (as a measure of harmonic performance), and loss factor σ are recorded.

Simulation results are summarized in Table 5.2. Although sinusoidal PWM demonstrates moderate converter losses, its WTHD (4.0%) is the highest among the four modulation methods studied. Loss factor of the sinusoidal PWM (1.00) is also higher than other methods, reflecting the non-optimized situation. The conventional SVM has the highest converter losses because of employing four states in

Table 5.2
Comparison of switching losses, temperature, and WTHD of the different modulation schemes

Parameters	SPWM	SVM		
		(a)	(b)	(c)
T_J (increase, °C)	35	45	32	30
P_L (per-unit of SPWM)	1.00	1.33	0.83	0.80
WTHD (%)	4.0	1.8	2.9	1.8
σ (per-unit of SPWM)	1.00	0.28	0.61	0.27

(a) conventional SVM
(b) 120° bus-clamped SVM
(c) minimum-loss SVM

each sampling period. On the other hand, its harmonic performance, as implied by a WTHD of 1.8%, is fairly good. Because of generation of small voltage harmonics, its loss factor is also small (0.28). The WTHD and loss factor of conventional SVM are comparable to the minimum-loss SVM, with the latter showing a modest superiority. Minimum-loss SVM, however, displays the lowest temperate increase and switching losses, hence the name. The 120° bus-clamped SVM strategy features close, but higher, switching losses than the minimum-loss method. Its loss factor (0.61) and WTHD (2.9%) are inferior to those of the conventional and minimum-loss methods.

Although the sampling frequency is kept constant in this study, note that since in the 120° bus-clamped and minimum-loss methods the number of switchings is smaller than the conventional SVM method (they use three states in each sampling period instead of four), they can operate at a higher frequency (33% higher) while not exceeding the thermal capability of switches, provided that the control circuitry is able to operate at higher frequencies.

5.2 Three-Level, SVM-Controlled STATCOM

Power system parameters (e.g., line impedances) and variables (e.g., voltages and currents) limit the power transmission capability of transmission lines. An emerging technology, *flexible ac transmission systems* (FACTS), which employs power electronics in power system applications, improves controllability and enhances power transfer of power systems and enables them to meet the stringent operating conditions of today's heavily-loaded networks. These devices are able to enhance the voltage profile of power system, control the flow of real and reactive power, and improve the dynamic performance and stability of the system. They can control power and current flow by:

1. **Shunt compensation:** To fix the voltage at the midpoint (or sending or receiving ends) of the line and to provide reactive power;

2. **Series compensation:** To apply a voltage in series with the line (in quadrature with current, or at an arbitrary phase angle, depending on the ability of injecting real power) and hence, changing the angle δ; or

3. **Inductance control:** To change the value of line reactance X_L to change the maximum possible power transfer.

A shunt compensator can be a thyristor-controlled reactor (TCR), a thyristor-switched capacitor (TSC), a static VAR compensator (a number of TCRs in parallel with one or more TSCs), or a static compensator (STATCOM). Examples of series compensators include thyristor-switched series capacitor (TSSC), thyristor-controlled series capacitor (TCSC), forced-commutation–controlled series capacitor (FCSC), series static VAR compensator (SSVC), and advanced SSVC. Unified power

flow controller (UPFC) is the combination of an advanced SSVC and a STATCOM that share a common dc link.

A STATCOM is a voltage-sourced converter connected in shunt to the power system through a small reactance (usually the leakage reactance of the connecting transformer) [54], as shown in Fig. 5.12. Since there is no source of real power included in a STATCOM, its generated voltage is kept in phase with the network voltage to eliminate real power transfer and discharging of the capacitor. Flow of reactive power can be manipulated by controlling the magnitude of the STATCOM output voltage, as shown in (5.1) and (5.2).

$$P_{1\to 2} = \frac{V_1\ V_2}{X_L} \sin\delta \tag{5.1}$$

$$Q_{1\to 2} = \frac{V_1\ (V_1 - V_2\cos\delta)}{X_L} \tag{5.2}$$

where $P_{1\to 2}$ and $Q_{1\to 2}$ are real and reactive power, respectively, transferred from point 1 with a voltage of $\mathbf{V}_1 = V_1\angle\delta$ to point 2 with a voltage of $\mathbf{V}_2 = V_2\angle 0°$ and X_L is the reactance between these two nodes.

When the converter voltage is larger than the system voltage, a net reactive current flows from the STATCOM to the system and STATCOM behaves as a capacitor, providing reactive power to the system. On the other hand, when the magnitude of the converter voltage is smaller than that of the system, STATCOM behaves as a reactor and draws reactive power from the system. In either case, operation of the STATCOM provides a negative feedback for the system to return the system voltage to its normal operating conditions. As mentioned earlier, the phase angle of the STATCOM output voltage should be kept in phase with the system voltage; otherwise, the dc bus voltage either increases or decreases and does not remain constant, which is essential for proper operation of the STATCOM.

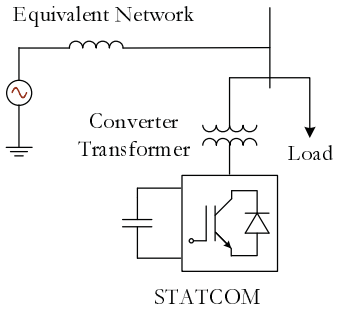

Fig. 5.12. Schematic diagram of the SVM-controlled STATCOM.

TABLE 5.3
STATCOM TEST SYSTEM PARAMETERS

AC Network	115 kV, SCMVA = 500 MVA at 80°
Distribution Transformer	115 kV/20 kV, 30 MVA, $X_L = 8.0\%$
Distribution Line	$0.02 + j0.05$ pu
Series RL Load	20 MVA, pf = 0.9
STATCOM Converter	3.3 kV, 10 MVA, $C = 0.74$ pu
STATCOM Transformer	20 kV/3.3 kV, 10 MVA, $X_L = 14\%$

This case study employs the SVM controller in the context of such a STATCOM. A three-level STATCOM is used to enhance the performance of a simple power system. Several studies are performed using the developed controller and results are compared to those of a three-level sinusoidal PWM controller.

5.2.1 Network Description

A schematic diagram of the sample network used in this study is depicted in Fig. 5.12. The parameters of STATCOM and network are summarized in Table 5.3. The STATCOM generates the output voltage using a three-level voltage-sourced converter.

STATCOM is controlled using a decoupled system as outlined in [55], [56]. Control system parameters are chosen from the optimization results presented in [57]. For the sinusoidal PWM control mode, firing pulses for each leg are generated by

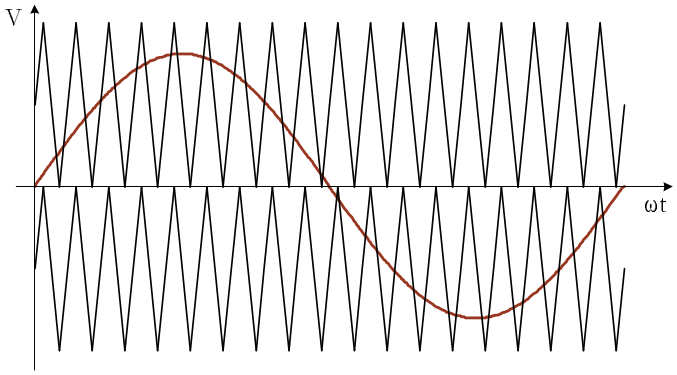

Fig. 5.13. Generation of firing pulses for three-level, sinusoidal PWM control.

comparing a reference sinusoidal waveform with a set of two triangular carrier waveforms as shown in Fig. 5.13 [58].

5.2.2 No-Load Voltage Waveform of the Converter

To study the quality of output waveforms of the SVM-controlled converter regardless of network conditions, this section presents harmonic performance of the generated voltage waveforms.

Fig. 5.14 shows harmonic components of the output voltage for a normalized sampling frequency of 48 and a modulation index of 0.8. As expected, compared with the two-level controller, harmonics have been drastically decreased; e.g., WTHD has been decreased from 2.7% in the two-level case to 0.73% in the three-level case, for the same m and F_{sn}.

Overall waveform quality is quantified using WTHD. Fig. 5.15 shows WTHD as a function of the modulation index m (ranging from 0.1 to 1.15) for normalized sampling frequencies of 24, 36, and 48. Using a higher sampling frequency improves WTHD, as it pushes harmonic components towards higher orders. Also, as the modulation index increases, regardless of the employed sampling frequency, WTHD decreases. This is expected, as with a higher modulation index a larger portion

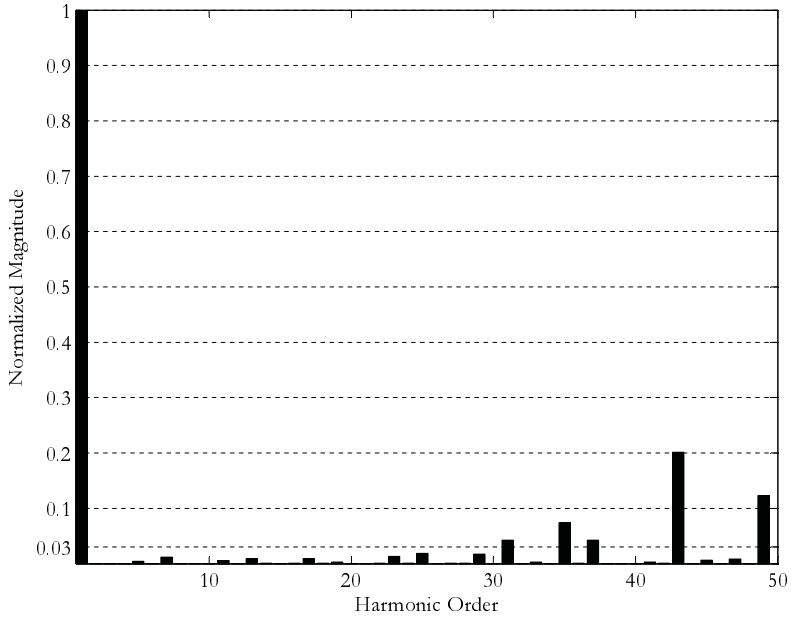

Fig. 5.14. No-load voltage harmonics of the three-level SVM for $F_{sn} = 48$ and $m = 0.8$.

of the energy of waveform constitutes the fundamental component and as a result, unwanted harmonic components decrease.

5.2.3 Network Variables

This section studies the operation of the SVM-controlled STATCOM in a network application scenario. The network shown in Fig. 5.12 operates at steady-state when it experiences a full load rejection $t = 1.0$ s followed by reconnection of the load after 0.5 s.

Fig. 5.16 shows the network voltage for the test period for the two modulation schemes. As the STATCOM controllers use the optimized values for the sinusoidal PWM, the respective waveform (Fig. 5.16a) demonstrates a smoother waveform than the SVM-controlled case. However, the ripple in the voltage under SVM control (Fig. 5.16b) is still small (3%) and is not expected to cause the system to malfunction.

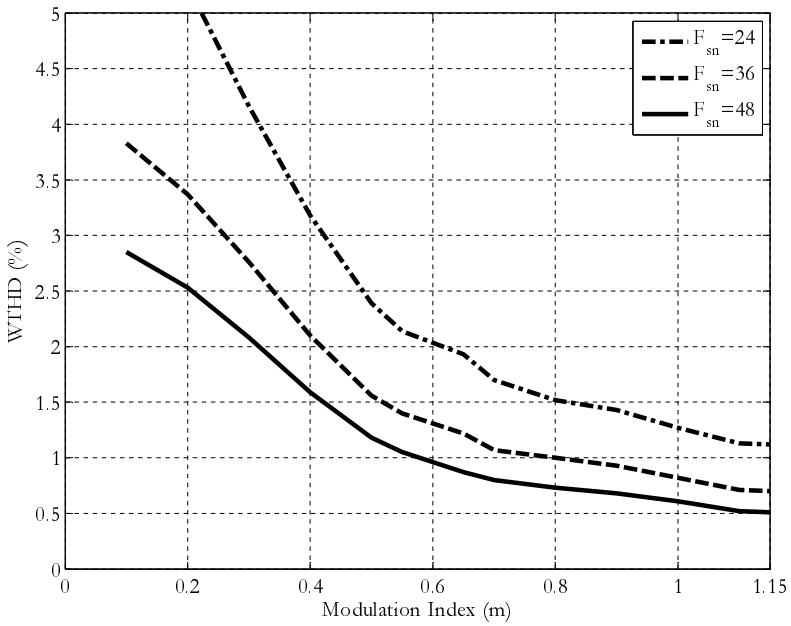

Fig. 5.15. No-load voltage WTHD of the three-level SVM for $F_{sn} = 24$, 36, and 48 and $m = 0.1 \ldots 1.15$.

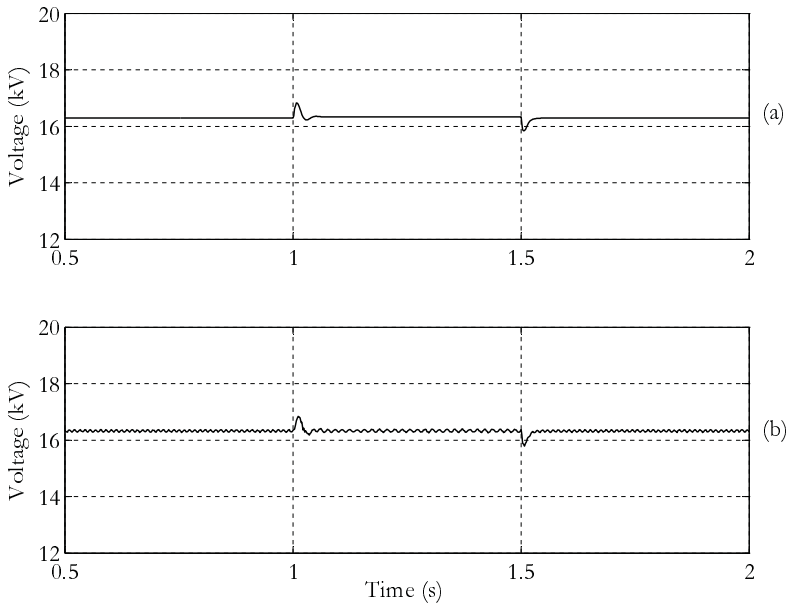

Fig. 5.16. Network voltage for (a) SPWM, and (b) SVM control.

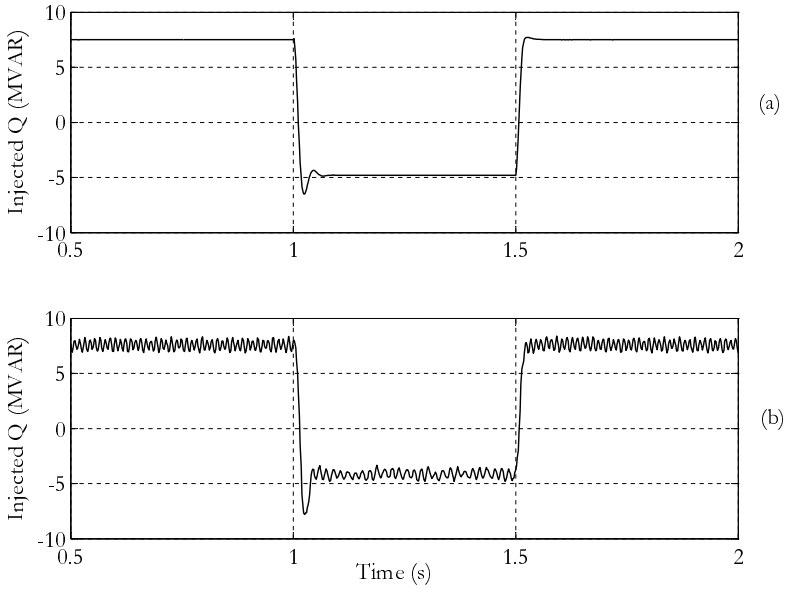

Fig. 5.17. Injected reactive power for (a) SPWM, and (b) SVM control.

Fig. 5.17 shows the injected reactive power Q_{inj} for the same period. The overall shape of resulting waveforms for two modulation methods are the same in steady state and also during the disturbance. Nevertheless, similar to the previous case and because the controller parameters are optimized for the SPWM control mode, the injected reactive power has some ripple (just over 7%).

It should be noted, however, as the SVM scheme is intrinsically capable of generating higher output voltages, the SVM-controlled STATCOM has a larger operating region and can enhance the system performance under severe more system loading conditions.

5.3 Summary of Simulation Results

In this chapter, a digital implementation of space-vector modulation controllers in the PSCAD/EMTDC electromagnetic transients simulation program has been presented. As shown for the second case study of STATCOM, the model can be used

for studying power systems with embedded power electronics. The model also allows detailed simulation of short-term and transient phenomena in power systems. Moreover, harmonic analysis of voltage and current waveforms becomes possible that yields invaluable information about their harmonic spectrum and filtering requirements. In addition, parametric studies can be performed. This capability of the model is used in Chapter 6 to find optimized SVM sequences.

Simulation results reported for the two-level case confirm that the developed model generates waveforms with symmetries in linear and overmodulation regions. The harmonic content, switching losses, and load harmonic losses can be controlled by using proper vector arrangements and sampling frequency. As such, the harmonic performance of generated waveforms of several schemes is studied and compared to others (using WTHD as the figure of merit).

It is found that the conventional and minimum-loss methods provide the least harmonic distortion, with the minimum-loss method, which only uses three space-vectors in each sampling period, producing lower switching losses. The losses in an inductive load are estimated using the loss factor, which in turn depends on the harmonic behavior of the modulation scheme. The loss factors of conventional and minimum-loss SVM methods are almost identical and are the lowest. The downside of the minimum-loss method is that its first significant voltage harmonic is at a smaller order than other methods. Sinusoidal PWM method has intermediate switching losses, but its WTHD is significantly higher.

In the studied network application, the original SPWM-controlled VSC of the STATCOM is replaced with an SVM-controlled VSC. Although the STATCOM control parameters optimized for the sinusoidal PWM are used for both cases, the dynamic performance of the STATCOM with the SVM controller is comparable to that of the sinusoidal PWM.

In practice, there are factors that could contribute to deviation of the actual system variables from their theoretically expected values. These factors include inherent uncertainties in parameter values, fluctuations in dc bus voltage, and numerical round-off errors. The model focuses on generation of switching signals and does not consider secondary effects such as the following.

- **IGBT dead-times:** The switches used in simulation have zero dead-times, while in practice switches have a non-zero dead-time (for example, 2μs) to prevent short circuit in the dc circuit. Other associated device parameters, such as rise and fall time, are not accounted for in the simulation.

- **Stray parameters:** The simulation case represents a simplified model of the actual setup. It does not account for stray losses as well as stray inductances and capacitances.

- **Inductor and capacitor values:** While in the simulation model circuit inductors and capacitors are assumed to remain constant, skin effect and iron-core losses make them frequency-dependent in practice [55].

- **Voltage source:** The three-phase voltage source as well as the dc voltage source used in simulation are ideal sources as they produce perfect sinusoidal waveforms (constant frequency, no harmonics, and constant rms value) and perfect dc voltages, respectively. In practice, the rms voltage may fluctuate arbitrarily as the network conditions change.

These factors can be accounted for in more details for the specific application. However, it is beyond the scope of this thesis.

Chapter 6

Optimization of SVM Sequences

Contents

As mentioned in earlier chapters, SVM can be realized using various switching sequences. These sequences are different in the way they treat zero vectors and arrange space vectors, and also the number of samples they use in each period. The performance characteristics of SVM depend on such sequences. This is in contrast to sinusoidal PWM, which has a relatively robust harmonic spectrum, i.e., the harmonic spectrum of the resulting waveform is tied to the selected sampling frequency. As such, devising proper SVM sequences is the key to achieving desired performance. Definition of the desired performance depends on the specific application. Examples include lowering the magnitude of certain harmonic components, minimizing the WTHD, and minimization of switching losses.

The task of optimizing SVM sequences is a complex issue. Analytical formulation of the problem is not expedient. Even if one manages to derive closed-form expressions for each harmonic component, it is exceedingly difficult to solve the resulting nonlinear equations to achieve the required performance.

This chapter aims to optimize space vector sequences through exploiting the available degrees of freedom. As will be described later, the problem involves both real and integer variables. Therefore, *genetic algorithms* (GAs) [59], [60], which can handle such mixed-integer problems, are used for its optimizations. GAs have been previously applied to find the filter parameters in electrical drives [61] as well as to a two-level SPWM converter to minimize the harmonic content of its output waveform [62].

The objective of optimization is to relieve filtering requirement [63], by distributing the energy of the waveform more uniformly among harmonic components. This

is constrained by limits on individual harmonics and overall quality of the waveform imposed by applicable industry standards.

In this chapter, genetic algorithms are briefly reviewed and methods for presentation of the problem in a GA-ready form are proposed. Finally, optimization results for different values of sampling frequency and modulation index are discussed [64].

6.1 Review of Genetic Algorithms

Genetic algorithms (GAs) belong to a group of evolutionary algorithms that are inspired by natural processes [65]. Such methods seek to maximize the fitness of a population, or as in the common notion, minimize the associated cost (or objective) function. An important feature of genetic algorithms is their ability to deal with real and integer (or binary-coded) optimization variables simultaneously. This proves to be essential in SVM harmonic spectrum optimization, which involves both such parameters (the arrangement of space vectors is specified as an integer variable and the share of zero vectors is a real variable).

In GAs, the solution space is represented by a series of candidate solutions, which are called *chromosomes*. Each chromosome in turn consists of a number of *genes*, representing possible values of optimization parameters. An objective function is calculated based on the *fitness* of each chromosome, i.e., its conformity to the desired objectives, and serves as a quantitative measure of its suitability as a potential solution. In the particular case of SVM optimization, calculation of the objective function for a chromosome in each generation involves (i) construction of a waveform using SVM for the sequence embedded in the chromosome, (ii) calculation of the harmonic spectrum, and (iii) evaluation of the objective function. Akin to what happens in natural process of evolution, such chromosomes evolve and as

good traits tend to pass to next generations, the possibility of survival for unfit chromosomes is low.

A chromosome can be a string of binary genes, real-valued genes, or a combination of both, which is the intended use here. While these two types of genes both represent optimization parameters, they differ in the way their algorithmic procedures are implemented. This is discussed in more detail in the next section.

The optimization usually starts with a randomly-generated population of chromosomes. The larger the size of the initial population, the higher the probability of evenly probing the solution space. Successive generations usually have a lower number of chromosomes than the initial one. That is, if the initial population has N_{ipop} chromosomes, the best N_{pop} performers are kept and $N_{\text{ipop}} - N_{\text{pop}}$ are discarded to prevent them from passing their traits to next generations (Fig. 6.1). The same idea is implemented for successive generations, where the best N_{parents} are kept (which are called *parents*) and the remaining $N_{\text{pop}} - N_{\text{parents}}$ are rejected. In order to keep the number of chromosomes in each generation constant, the rejected chromosomes are replaced with the *offspring* of parents. Therefore, each generation after the initial one consists of a number of best performing chromosomes (parents) copied directly from the previous generation along with their offspring.

Offspring is obtained by means of combining (or *mating*, in GA terminology) parent chromosomes of the preceding generation. Each pair of parent solutions mate and normally generate two offspring that combine the characteristics (or genes, in GA terminology) of parents. The mating of parents means generation of new chromosomes that partly consist of mother's genes with the rest copied from father's genes. The contribution of each parent is determined by a crossover point, which is chosen randomly. This is illustrated in Fig. 6.2.

The parents are chosen randomly in such a way that fitter chromosomes receive a

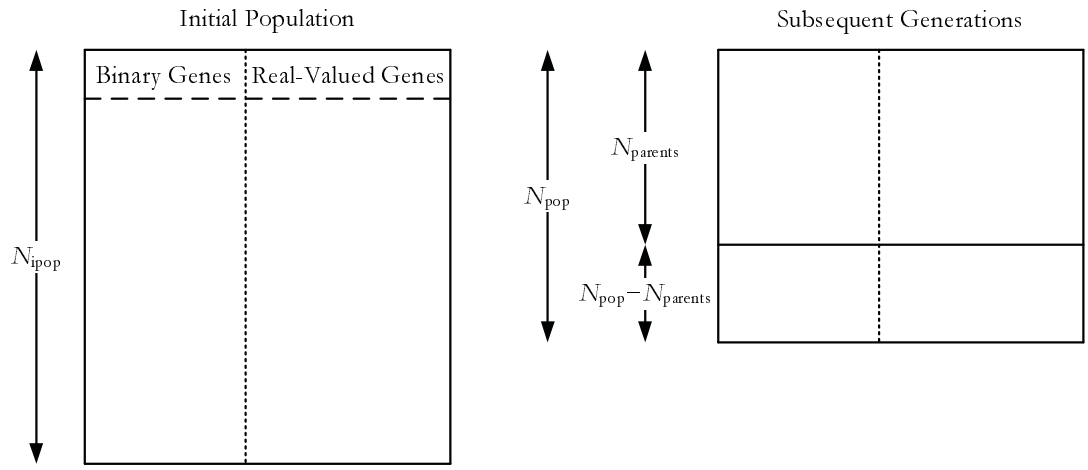

Fig. 6.1. Initial population and subsequent generations.

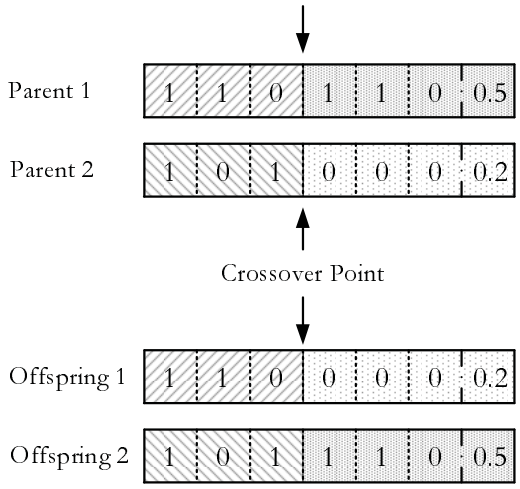

Fig. 6.2. An example of mating by crossover.

higher chance of mating. This selection process, which is called *pairing*, can be done in a number of methods [59]. One approach, called rank-weighting, is to assign a weight to each chromosome based on its rank in the sorted population. This method is used in the implementation of GAs presented in this work.

Mating of good chromosomes is one of the two means to enhance the chromosomes towards a generation that is expected to have a lower average cost function. Another method is *mutation*, which ensures that convergence does not happen prematurely and the algorithm is provided with ample time to explore more of the

solution space. In mutation, a number of genes are randomly selected and their values are randomly changed to new values. This mimics the natural process of mutation, when under certain circumstances genes of a living organism may fortuitously change. These random modifications introduced during reproduction allow new behaviors to be examined and, if they turn out to be advantageous, to spread through the population in later generations.

This general process is repeated until a certain set of conditions are met by a generation. The algorithm may be terminated when a certain number of generations is reached, allocated computation time span is passed, the minimum cost has reached its criteria, or the statistical characteristics of successive generations are the same within the required accuracy.

A summary of how GAs are implemented is shown in Algorithm 6.1.

Algorithm 6.1 Summary of implementation of genetic algorithms

---

1. Create an **initial** random population with size N_{ipop}.
2. Repeat
   - 2.1. Calculate the **fitness** of chromosomes of the current generation.
   - 2.2. **Sort** chromosomes based on their fitness.
   - 2.3. If satisfactory fitness is achieved, **stop**.
   - 2.4. **Keep** the top N_{parents}, and discard the rest.
   - 2.5. **Pair** the parents using the paring strategy.
   - 2.6. **Mate** the paired parents and generate $N_{\text{pop}} - N_{\text{parents}}$ offspring.
   - 2.7. **Mutate** the generation, if applicable.
   - 2.8. Use the current population for the **next** step.
3. **Output** the best performing chromosome (the first one in the sorted list).

6.2 Adaptation of the Problem for Solution with Genetic Algorithms

The first stage in implementing GA is to find a suitable representation of the optimization parameters, and hence the chromosomes. Such a representation seeks to facilitate applying GA operators during mating and mutation operations.

6.2.1 Chromosome Structure

Each chromosome needs to fully describe the SVM sequences, i.e., it should carry information about the order of the space vectors (two adjacent active vectors of $\mathbf{A}_1$ and $\mathbf{A}_2$ and two zero vectors of $\mathbf{Z}_0$ and $\mathbf{Z}_7$), plus the allotment of inactive time between two zero vectors.

In the proposed representation, exactly four distinct vectors are used in each period and hence, only sequences such as $\mathbf{Z}_0\mathbf{A}_1\mathbf{A}_2\mathbf{Z}_7$ are acceptable (although with a $\mathbf{Z_0}$-share of zero it could be effectively reduced to $\mathbf{A}_1\mathbf{A}_2\mathbf{Z}_7$). Note that the shares of active space-vectors are determined by the SVM technique itself, and are not part of the optimization. As mentioned earlier, this leads to a mixture of real and integer variables, which necessitates defining hybrid chromosomes that consist of both real and integer genes.

Moreover, once a sequence format is chosen, it can be applied in two ways: either the same for consecutive sampling periods, or alternatively forward and backward. Therefore, chromosomes determine if adjacent periods switch between forward and backward sequences. For example, if the sequence $\mathbf{Z}_0\mathbf{A}_1\mathbf{A}_2\mathbf{Z}_7$ is chosen, it can be applied as $\mathbf{Z}_0\mathbf{A}_1\mathbf{A}_2\mathbf{Z}_7|\mathbf{Z}_0\mathbf{A}_1\mathbf{A}_2\mathbf{Z}_7$ (only forward sequence) or forward sequence for one sampling period and backwards for the next period, i.e., $\mathbf{Z}_0\mathbf{A}_1\mathbf{A}_2\mathbf{Z}_7|\mathbf{Z}_7\mathbf{A}_2\mathbf{A}_1\mathbf{Z}_0$. One such chromosome is shown in Fig. 6.3.

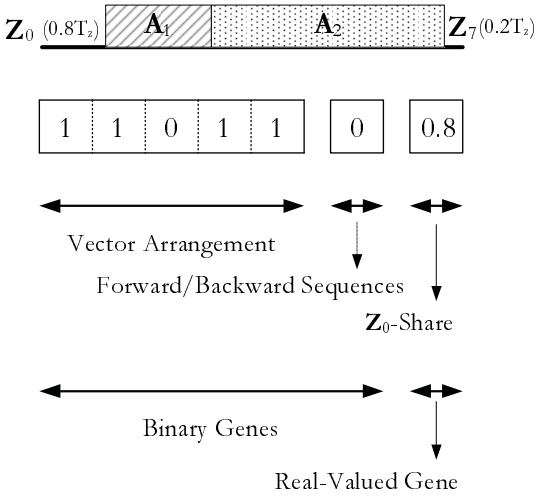

Fig. 6.3. Structure of the hybrid chromosome.

The real part of the chromosome does not need manipulation to become fit for the GA application. A real value ranging between 0 and 1 represents the share of the zero space-vector $\mathbf{Z}_0$ in the inactive part of the sampling period. A $\mathbf{Z}_0$-share of zero means that $\mathbf{Z}_0$ is not used at all and $\mathbf{Z}_7$ is applied for the whole inactive period T_z, leading to a sequence such as $\mathbf{A}_1\mathbf{A}_2\mathbf{Z}_7$. On the other hand, a $\mathbf{Z}_0$-share of 1 means only $\mathbf{Z}_0$ is used, as in $\mathbf{Z}_0\mathbf{A}_1\mathbf{A}_2$.

The part that conveys information about the arrangement of vectors, however, needs to be properly represented in the binary part of the chromosome. Therefore, a method to translate the sequences into a string of binary genes is suggested.

Since the number of valid SVM sequences (taking into account only the order of space vectors) for a two-level converter is $4! = 24$, one simple approach is to number the sequences from 1 to 24 (or 0 to 23), and encode them in binary format. This method, while being easy to implement, introduces some problems. Binary coding of the 24 sequences requires 5 bits; however, the number of possible combinations represented by 5 bits is 32. Since GA operators, i.e., mating and mutation, combine

and alter the bits in a random manner, the resulting binary-coded combinations may correspond to invalid sequences (numbers between 25 and 32).

To remedy these, a method for coding SVM sequences has been developed. The proposed method has the advantage that it defines the position of individual vectors relative to each other. This makes passing the traits of each chromosome from one generation to the next ones more meaningful and hence, is tailored to how GAs work. Besides, this method inherently avoids the problem of getting invalid combinations. Such benefits are not present in the simple numbering method.

In the proposed method, the sequences are defined based on how active and zero vectors are located with respect to each other. Stating the active vectors as $\mathbf{A}_1$ and $\mathbf{A}_2$ and zero vectors as $\mathbf{Z}_0$ and $\mathbf{Z}_7$, one can describe a sequence based on factors such as whether it starts with an active vector ($\mathbf{A}_1$ or $\mathbf{A}_2$) or a zero vector ($\mathbf{Z}_0$ or $\mathbf{Z}_7$), and if $\mathbf{A}_1$ appears before $\mathbf{A}_2$ or vice versa. Such factors are described in more detail in the next subsection.

In short, a valid chromosome for SVM is one that meets the following conditions.

1. Share of T_0 from $T_z = T_0 + T_7$ ($\mathbf{Z}_0$-share) is a real number between 0 and 1;
2. Position of space vectors $\mathbf{A}_1$, $\mathbf{A}_2$, $\mathbf{Z}_0$, and $\mathbf{Z}_7$ within a sampling period is arbitrary;
3. T_1 and T_2 are indeed not arbitrary and instead are specified by the SVM method;
4. $T_0 + T_7$ is also determined by the SVM method; and
5. Each chromosome has both $\mathbf{A}_1$ and $\mathbf{A}_2$.

6.2.2 Proposed Coding Approach

The arrangement of vectors shows the order in which they appear in each sampling period. Examples of possible arrangements are $\mathbf{Z}_0\mathbf{A}_1\mathbf{A}_2\mathbf{Z}_7$, $\mathbf{A}_1\mathbf{Z}_0\mathbf{A}_2\mathbf{Z}_7$, and $\mathbf{A}_2\mathbf{Z}_7\mathbf{A}_1\mathbf{Z}_0$. In the proposed method, each arrangement is described by a finite string of binary digits.

An algorithm has been excogitated to enable translation between these two representations. In the proposed method, there are five binary genes that represent answers to five YES/NO questions, which in turn translate to a series of 1/0s in the binary domain, respectively. These five questions are as follows:

1. Does $\mathbf{A}_1$ appear before $\mathbf{A}_2$ in the sequence?
2. Does $\mathbf{Z}_0$ appear before $\mathbf{Z}_7$ in the sequence?
3. Is the first vector in the sequence an active one?
4. Is the second vector in the sequence an active one?
5. Is the third vector in the sequence an active one?

To demonstrate how sequences are encoded, consider the sequence $\mathbf{Z}_0\mathbf{A}_1\mathbf{A}_2\mathbf{Z}_7$, which is conventionally used in SVM. Encoding results in a string of 1 ($\mathbf{A}_1$ is before $\mathbf{A}_2$), 1 ($\mathbf{Z}_0$ is before $\mathbf{Z}_7$), 0 (the first vector in the sequence is a zero vector), 1 (the second vector is an active one), and 1 (the third vector is an active one), or in the condensed form: 11011. Other sequences are also encoded in a similar way.

Decoding is done similarly by deciphering the answers into a valid sequence. For example, a string of 10101 is decoded as $\mathbf{A}_1\mathbf{Z}_7\mathbf{A}_2\mathbf{Z}_0$. In some cases, decoding does not need answers to all five questions, which is the reason why this 5-bit representation decodes into only 24 vector arrangements rather than the original

32. This, however, does not cause any problem for the algorithm, as (i) the GA optimizer uses the encoded sequences (of 5 bits), and (ii) decoding from the 5-bit representation to the actual vector arrangement is always unique.

An important feature of the proposed encoding/decoding procedure is that any 5-digit combination of 1/0s will result in a valid SVM sequence (unlike the simple numbering method). As such, GA operators of mating and mutation can be directly used to manipulate chromosomes without any further adjustments.

6.3 SVM Optimization Setup

As shown earlier, space-vector modulation provides a number of degrees of freedom in controlling the switches of a converter. This feature of SVM can be exploited to enhance certain performance characteristics such as its harmonic spectrum.

6.3.1 Potential for Optimization

Flexibility of SVM comes from the seemingly unlimited number of implementation methods, which is due to the degrees of freedom inherent to the SVM method, and can be used as parameters for optimizing the modulation [66]. These parameters are as follows.

6.3.1.1 Decomposition of the reference voltage

A reference vector can be decomposed using virtually any subset of the eight space vectors. Nonetheless, decomposition is done typically using only the two adjacent active vectors [67]. For example, if the reference vector is in the fourth sector, it is decomposed onto $\mathbf{V}_4$ and $\mathbf{V}_5$. This allows for computational simplicity and lower number of switchings per cycle.

6.3.1.2 Sequence of active space-vectors

Once constituent active space vectors for decomposition of the reference vector and their durations are found, they generate the same average output voltage regardless of the *order* in which they are applied within the current sampling period. SVM does not recommend any specific order, and this can be exploited as a degree of freedom for crafting waveforms with given properties. For example, although normally centered active vectors are chosen, to achieve the least possible number of switchings, sequences have been devised that limit the state transitions only between adjacent states (with only one switching state difference) [28], [29].

6.3.1.3 Placement and share of zero space-vectors

Space-vector modulation also offers flexibility with zero vectors. Not only can they be used in any order within the sampling period and relative to active vectors, but one also can divide the total share of zero vectors determined by the SVM algorithm in any proportion between them. In the extreme case, one may use only one of the two available vectors; i.e., exclusively one of $\mathbf{Z}_0$ or $\mathbf{Z}_7$ and not the other.

A simple example will clarify the point why zero-vector placement is important. Considering the waveforms for voltage and current in Fig. 6.4, it is clear that while both currents have an average of zero, in the second case that active vectors are placed back to back, the current has a much higher ripple. Furthermore, the ripple has a lower frequency—a condition that exacerbates the harmonic spectrum. From this simple example it can be inferred that the closer active vectors to the center of switching period are, the lower amplitude of harmonics will be. Moreover, the harmonics will occur at higher frequencies.

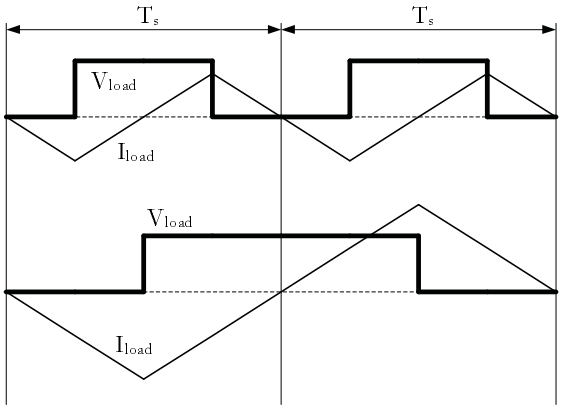

Fig. 6.4. Impact of zero vector placement on the magnitude and frequency of current ripple.

6.3.1.4 Selection of sampling frequency

Selection of sampling frequency is a compromise between harmonic content and switching losses. An excessively high sampling frequency results in significant losses in the power electronic elements. Even in the absence of switching losses, the sampling frequency cannot be deliberately increased because of the limitations imposed by the physics of semiconductor switches as well as regulations regarding electromagnetic compatibility [68]. On the other hand, a low sampling frequency, while allowing more time for calculations and enabling performing more complex schemes, results in poor sampling of the reference waveform, which further exacerbates the harmonic performance. Since the first group of significant harmonics clusters around the sampling frequency, care should be exercised in choosing the frequency to achieve an acceptable trade-off between switching losses and harmonic spectrum.

6.3.2 Posing as an Optimization Problem

By exploiting the aforementioned degrees of freedom inbuilt to SVM, appropriate switching sequences can be devised to obtain the desired waveform quality [69]-[71], through definition of an apposite *objective function* (OF).

The available degrees of freedom have been previously used to devise sequences that feature lower switchings and losses, or lower harmonic contents [69]. Although this chapter focuses on two-level SVM, the developed method can be extended to multilevel schemes by devising proper formulation.

Definition of the objective function depends on the specific application of interest. For example, if it is desired to lower the harmonic content of the output current, one can use weighted THD (WTHD) as the objective function. WTHD, defined in Appendix A and repeated here for convenience, is calculated in the same way as THD, but each harmonic component is divided by its order so that higher-order harmonics receive lower weight and contribute less in this figure of merit. An upper limit of $n = 50$ is often recommended for the calculation of WTHD [8].

$$\text{WTHD} = \frac{\sqrt{\sum_{h=2}^{n} \left(\frac{V_h}{h}\right)^2}}{V_1} \tag{6.1}$$

A more insightful objective function can be devised by considering the industry standards concerning the harmonic content of voltage and current waveforms. The IEEE Standard 519 [8] provides guidelines for harmonic control in electrical power systems and is used as the reference here. It limits the magnitude of individual harmonic components of a system operating below 69 kV to 3% of the fundamental.

As can be seen in the harmonic spectrum of the conventional SVM shown in Fig. 6.5 for a normalized sampling frequency of 36, harmonic components 35 and 37 are the largest ones and hence, they determine the parameters of the required filter. The goal in this study is to reduce these two adjacent harmonic components grouped around the sampling frequency to relieve the filtering requirement of the VSC. However, this is possible only at the expense of increasing other harmonics, which are

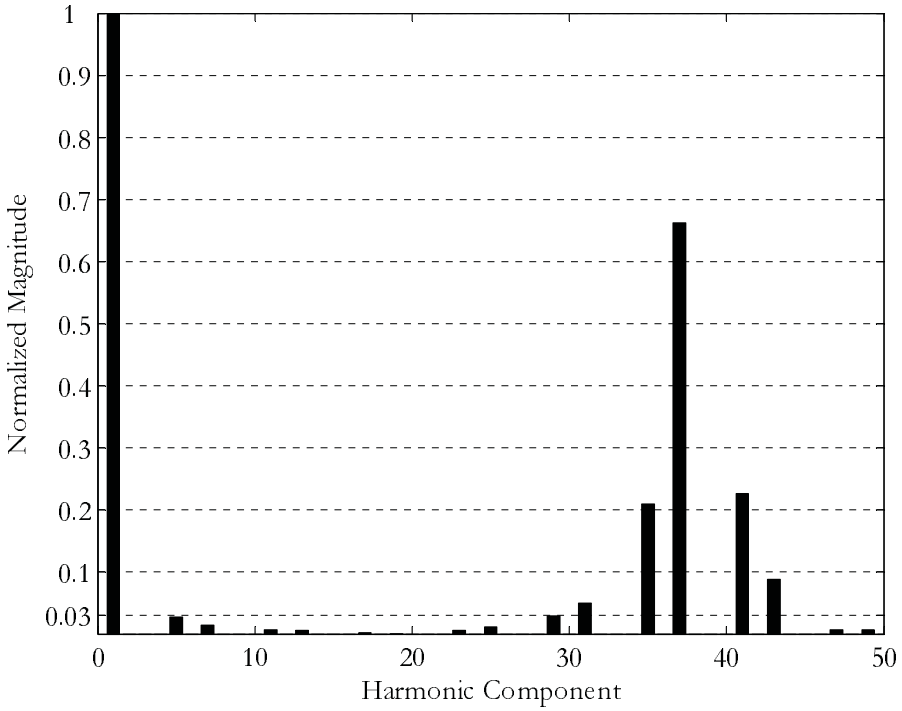

Fig. 6.5. Harmonic spectrum of the conventional SVM, $F_{sn} = 36$, $m = 0.8$.

tolerable as long as they are below the 3% limit imposed by the IEEE Standard 519. Therefore, the compromise is between lowering the high-order harmonics to relieve filtering, and keeping the low-order harmonics within their maximum permissible values. At the same time, the overall quality of the waveform indicated by its WTHD should not exceed its maximum allowable value of 5% according to the IEEE Standard 519.

6.3.3 Development of an Objective Function

The *objective function* (OF) needs to embed the above requirements and also reflect the allowable harmonic magnitude. The following conditions must be considered in the objective function:

1. The two harmonic components adjacent to the sampling frequency are minimized;

2. Individual harmonic components do not exceed their 3% limit; and

3. The waveform WTHD is below 5%.

This constrained optimization problem can be posed mathematically as shown in (6.2). This is shown for a normalized sampling frequency of 36; for other frequencies, the two adjacent harmonic components are adjusted accordingly.

$$\begin{aligned} &\text{Minimize} \\ &\qquad \text{OF}(\text{seq}, \mathbf{Z}_0\text{-share}) = v_{35} + v_{37} \\ &\text{Subject to} \\ &\qquad v_i \leq 3\%, \quad i \leq 50, i \neq 35, 37 \\ &\qquad \text{WTHD} \leq 5\% \end{aligned} \tag{6.2}$$

where *seq* and $\mathbf{Z}_0$-share are SVM sequences of vectors and share of the zero-vector $\mathbf{Z}_0$, respectively, and v_i is the magnitude of the ith harmonic.

It is often easier to optimize an unconstrained objective function than one with constraints as in (6.2). Optimization theory suggests use of techniques commonly referred to as transformation methods to remove constraints by augmenting them onto the original objective function [72], [73]. The augmented OF developed to eliminate constraints in (6.2) is given in (6.3).

$$\begin{aligned} \text{OF}(\text{seq}, \mathbf{Z}_0\text{-share}) = \alpha_1 &\left[\left(\frac{\text{WTHD}}{0.05}\right)^p + v_{35} + v_{37}\right] \\ &+ \alpha_2 \left(\frac{v_5}{0.03}\right)^{p^*} + \alpha_3 \sum_{\substack{i=7,11,13,\\ 17,19,23,25}} \left(\frac{v_i}{0.03}\right)^p + \alpha_4 \left(\frac{v_{29}}{0.03}\right)^p \\ &+ \alpha_5 \left(\frac{v_{31}}{0.03}\right)^p + \alpha_6 \left[\left(\frac{v_{35}}{0.03}\right)^p + \left(\frac{v_{37}}{0.03}\right)^p\right] \end{aligned} \tag{6.3}$$

Table 6.1
Parameters of the objective function

Parameter	α_1	α_2	α_3	α_4	α_5	α_6	p	p^*
Value	1000	2000	100	400	200	10	8	16

Least pth (see Appendix C) interior point penalty functions (with large, even exponents p and p^*) are used to ensure that the WTHD and individual harmonic components are limited to their permissible ranges of 5% and 3%, respectively. As long as WTHD and harmonics components meet these criteria, their contribution to the objective function is negligibly small; whereas if they exceed these limits, they sharply increase the OF to prompt the optimization algorithm that it has violated a vital condition.

Weighting factors α_i and exponents p and p^* are listed in Table 6.1. These values do affect the optimization process and are normally obtained through preliminary sample runs of the optimization algorithm. Formal procedures, such as Pareto frontiers [72], for determination of weighting factors also exist; however, they have not been used in this study.

A script written in MATLAB determines the harmonic spectrum pertaining to each run. The results are passed to the GA optimizer, which seeks to find the best-performing sequence. The optimization results are presented in the next section.

6.4 Optimal Solution and Discussion of Results

The GA optimizer is run with the aforementioned objective function. Although mutation is implemented in the GA solver as a means to reduce the likelihood of converging to a local minimum, the stochastic nature of genetic algorithms necessi-

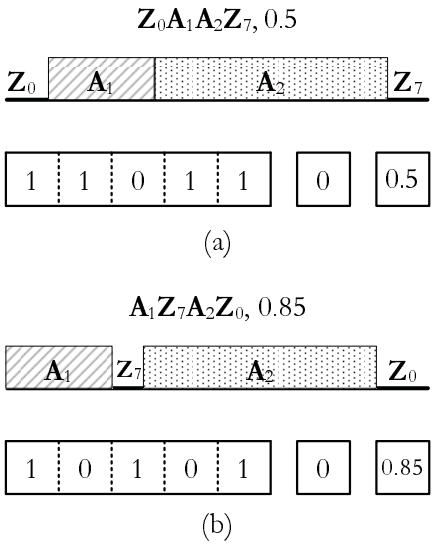

Fig. 6.6. SVM sequences, (a) conventional, and (b) optimized.

tates running the optimizer several times to further reduce this possibility. For each run, the best sequence of vectors as well as the share of $\mathbf{Z}_0$ are recorded.

Fig. 6.6 shows the sequence and share of space vectors for the conventional (Fig. 6.6a) and the optimized (Fig. 6.6b) SVM arrangements. Both sequences are forward; however the optimized sequence positions the vectors in a different order and allots 85% of the inactive time interval to the zero vector $\mathbf{Z}_0$. The sequence of constituent vectors has been changed from $\mathbf{Z}_0\mathbf{A}_1\mathbf{A}_2\mathbf{Z}_7$ (11011) to $\mathbf{A}_1\mathbf{Z}_7\mathbf{A}_2\mathbf{Z}_0$ (10101).

Three studies are done: First, harmonic spectrum of the optimized space-vector technique is studied. Second, sensitivity of the harmonic spectrum to optimization parameters are presented. Finally, dependence of results on SVM parameters (F_{sn} and m) is investigated.

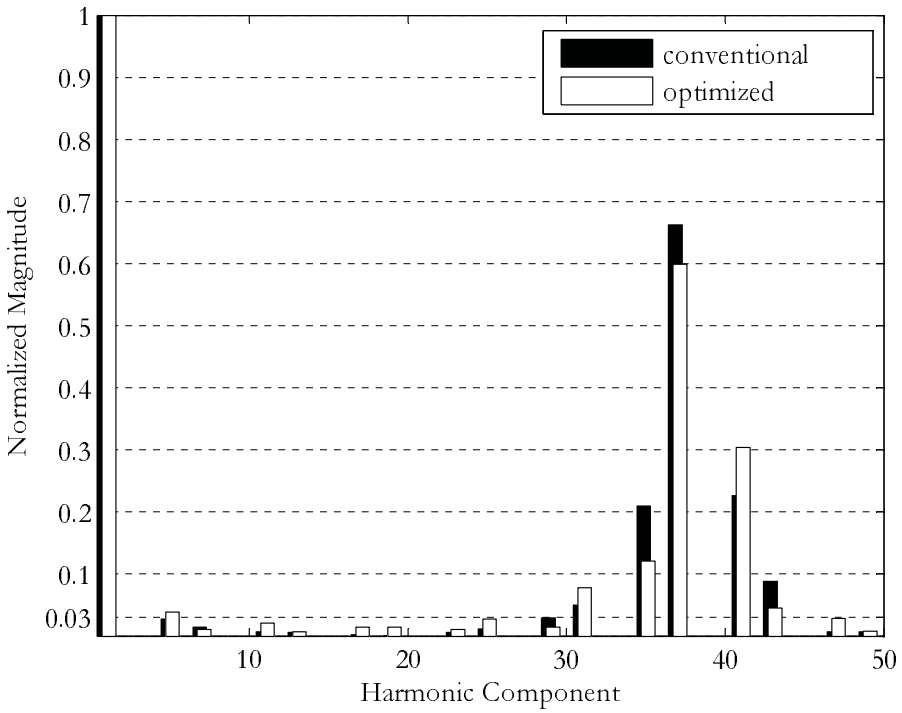

Fig. 6.7. Harmonic spectra of conventional and optimized SVM.

6.4.1 Harmonic Spectrum

Fig. 6.7 shows the harmonic spectrum of the voltage waveform for both conventional and optimized SVM sequences for a modulation index of 0.8 and normalized sampling frequency of 36. For both cases, harmonic components 35 and 37 are the largest contributors to the harmonic distortion. However, optimization has reduced the 35th and 37th harmonics from 21.6% and 65.6% for the conventional SVM sequence to 12.1% and 59.9% for the optimized sequence, respectively. This is a reduction of 44% and 9% for the 35th and 37th harmonics, respectively. Such significant reduction results in smaller harmonic currents in the filter and thus allows use of smaller filters.

As shown in Table 6.2, as a result of lowering harmonics 35 and 37, some of lower order harmonics have been increased slightly; however, the reduction in the two adjacent harmonics has been so significant that the WTHD of the optimized

TABLE 6.2
HARMONIC SPECTRA OF THE TWO SVM METHODS FOR A NORMALIZED SAMPLING FREQUENCY OF 36 AND A MODULATION INDEX OF 0.8

Order	Conventional SVM	Optimized SVM
1	100.00	100.00
5	3.02	3.86
7	1.71	1.06
11	1.29	2.06
13	0.99	0.73
17	1.17	1.46
19	1.17	1.45
23	1.54	1.06
25	1.90	2.79
29	3.75	1.41
31	5.71	7.79
35	21.59	12.10
37	65.58	59.88
41	23.24	30.42
43	9.43	4.57
47	1.04	2.84
49	1.26	0.75
WTHD	**2.10**	**2.01**

waveform (2.01%) is 5% lower than that of the original waveform obtained using the conventional sequence (2.10%).

The 5th harmonic component of the original waveform is 3.02%, which is slightly larger than the recommended 3% limit. The optimized sequence shows a 3.86% value for the 5th harmonic. However, the converter is connected to the power system through a converter transformer with a leakage reactance of 10-15%. The converter transformer acts as a low-pass filter, which further reduces the harmonics. Therefore, a slight increase in the 5th harmonic is not expected to adversely affect the overall performance.

As can be seen, the optimized SVM sequence does not reduce individual harmonic components. Instead, compared to the conventional SVM, it distributes the

waveform energy more evenly among the harmonic components. This has resulted in a smaller WTHD, which helps decrease the current distortion and hence, lowers propagation of harmonics through the network.

6.4.2 Sensitivity to the Optimized Parameters

In practice, it is not always possible to produce the switching signals at the exact instants of time prescribed by the SVM algorithm. This could be due to a number of factors, such as the limited resolution of the digital implementation and numerical round-offs (the number of bits of the microcontroller) and also device delays. Therefore, it is important to study the sensitivity of the results to small changes in optimization parameters. In the following, the impact of the variations of the time share of the zero vector $\mathbf{Z}_0$ on the harmonic performance of the SVM is studied. The analysis is done for a normalized sampling frequency of 36.

The magnitudes of harmonic components of the waveforms generated by the optimized sequence of $\mathbf{A}_1\mathbf{Z}_7\mathbf{A}_2\mathbf{Z}_0$ for $\mathbf{Z}_0$-shares of 0.80, 0.85 (the optimized value), and 0.90 are shown in Table 6.3. While WTHD in all three cases remains practically identical (at just above 2%), harmonic components slightly change with variations in the share of $\mathbf{Z}_0$ space vector. As observed in Fig. 6.8 and shown in Table 6.3, the magnitudes of harmonic components vary as the time share of $\mathbf{Z}_0$ deviates from its optimal value of 0.85. For some mid-order harmonics (e.g., 11 to 25), an increase in the share results in a decrease in the magnitude of respective harmonic components, while some other components (e.g., 29, 35, and 37) see an increase with increasing the $\mathbf{Z}_0$-share value.

This dual behavior results in the WTHD remaining essentially constant, and also maintains the balance between harmonic components. In other words, even with a slight change in $\mathbf{Z}_0$-share, the optimized SVM sequence is capable of distributing

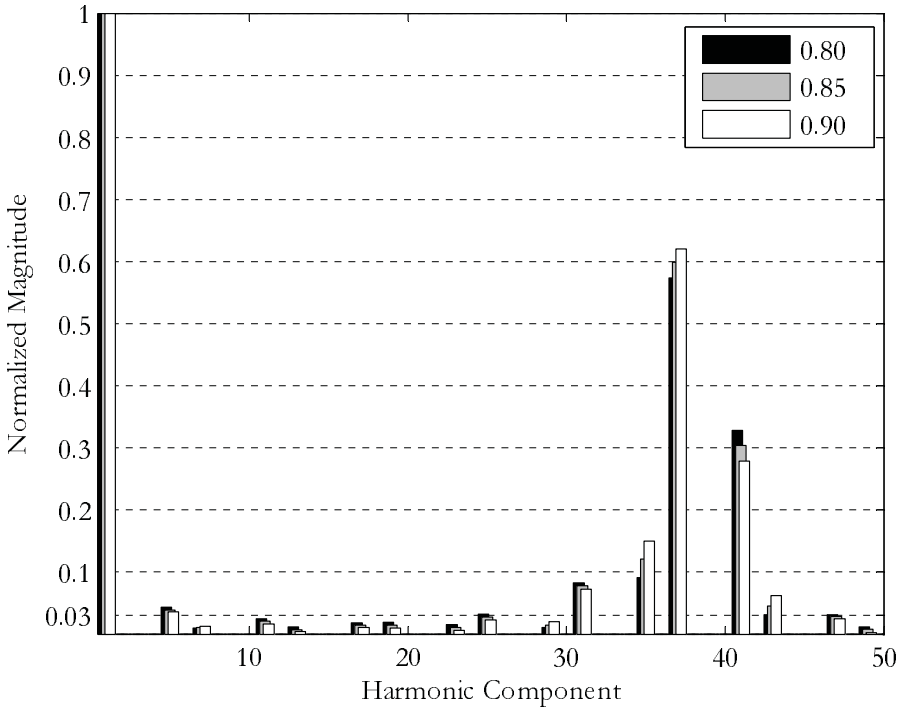

Fig. 6.8. Harmonic spectrum of the optimized SVM for three values of $\mathbf{Z}_0$-share of 0.80, 0.85 (the optimized value), and 0.90.

the waveform energy in such a way that individual changes in harmonic magnitudes cancel each other and result in an essentially constant WTHD. This relieves the implementation requirements of the optimized SVM scheme, as it demonstrates that the harmonics have limited sensitivity to potential variations of the time share that may result from its digital implementation.

6.4.3 Dependence on SVM Parameters m and F_{sn}

The preceding results are reported for the specific case of a normalized sampling frequency F_{sn} of 36 and a modulation index m of 0.8. It is, however, important to determine whether the optimized sequence varies with the modulation index or the sampling frequency. In this section, dependence of results on various modulation indices and sampling frequencies is studied. Normalized sampling frequencies of 24,

TABLE 6.3
HARMONIC COMPONENTS OF THE OPTIMIZED SVM SEQUENCE AS A FUNCTION OF $\mathbf{Z}_0$-SHARE

Order	$\mathbf{Z}_0$-Share		
	0.80	0.85	0.90
1	100.00	100.00	100.00
5	4.30	3.86	3.60
7	0.98	1.06	1.28
11	2.44	2.06	1.67
13	1.18	0.73	0.46
17	1.84	1.46	1.05
19	1.93	1.45	0.96
23	1.58	1.06	0.59
25	3.26	2.79	2.25
29	1.03	1.41	1.96
31	8.27	7.79	7.21
35	9.11	12.10	14.99
37	57.41	59.88	62.02
41	32.80	30.42	27.90
43	3.09	4.57	6.18
47	3.10	2.84	2.44
49	1.15	0.75	0.20
WTHD	**2.01**	**2.01**	**2.03**

36, and 48 are used for the optimization and best-performing switching patterns for modulation indices of 0.5 to 1.1 are recorded.

The optimization results suggest that in all cases the optimized sequences are the same as the base case of $F_{sn} = 36$ and $m = 0.8$; i.e., the sequence $\mathbf{A}_1\mathbf{Z}_7\mathbf{A}_2\mathbf{Z}_0$ yields the optimal harmonic spectrum according to the objective function defined in (6.3). The $\mathbf{Z}_0$-share, however, changes with the change in both sampling frequency and modulation index.

Fig. 6.9 shows the trend of change in the optimized value of the $\mathbf{Z}_0$-share as a function of the modulation index for three values of normalized sampling frequency (F_{sn} = 24, 36, and 48). As shown, the $\mathbf{Z}_0$-share increases almost linearly (with a

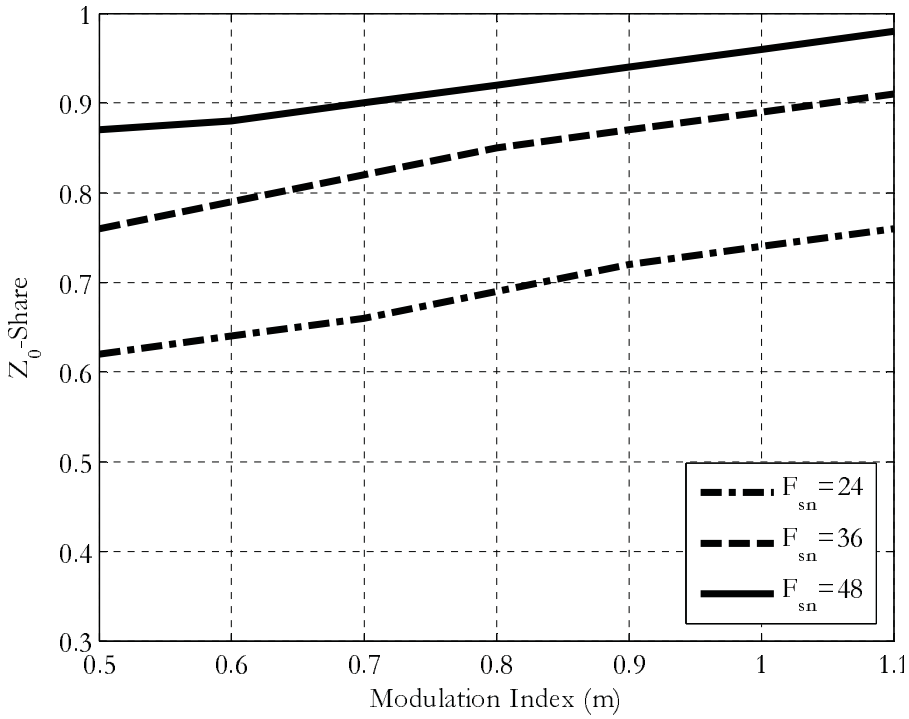

Fig. 6.9. Dependence of $\mathbf{Z}_0$-share on modulation index and normalized sampling frequency.

relatively small slope) with the modulation index. Considering that the optimized SVM sequence is not overly sensitive to small variations in the optimal value of the $\mathbf{Z}_0$-share (as shown in the preceding section for $F_{sn} = 36$ and $m = 0.8$), it is possible to use average values for the $\mathbf{Z}_0$-share for various normalized sampling frequencies as shown in Table 6.4.

6.5 Computational Aspects

The performance of the optimizer depends on the GA parameters. In this optimization study, an initial population of 100 chromosomes is used, which is reduced to 50 after the first round of fitness evaluation. In each generation, top-thirty best-performing chromosomes are kept as parents, which are paired according to rank-weighted method and mated using one crossover point to generate 20 offspring. The

Table 6.4
Optimized $\mathbf{Z}_0$-share values for different modulation indices and sampling frequencies of SVM and the suggested values

m	$\mathbf{Z}_0$-Share		
	$F_{sn} = 24$	$F_{sn} = 36$	$F_{sn} = 48$
0.5	0.62	0.76	0.87
0.6	0.64	0.79	0.88
0.7	0.66	0.82	0.90
0.8	0.69	0.85	0.92
0.9	0.72	0.87	0.94
1.0	0.74	0.89	0.96
1.1	0.76	0.91	0.98
Suggested Value	**0.70**	**0.85**	**0.92**

maximum number of generations is set to 50. Chromosomes are subject to mutation with a probability of 10%, with the exception of the top-two chromosomes that are kept as elite ones. The optimizer is run using MATLAB (version 7.3) on a computer with a 2.41 GHz dual-core processor and 1 GB of RAM. Each run of the optimizer takes between 6 to 10 minutes, depending on the sampling frequency.

6.6 Concluding Remarks

The possibility of applying genetic algorithms for achieving optimized SVM sequences has been investigated in this chapter. The objective function is defined with the goal of minimizing the filtering requirement by lowering most significant harmonics while conforming to available standards for waveform quality.

The conventional SVM sequence is $\mathbf{Z}_0\mathbf{A}_1\mathbf{A}_2\mathbf{Z}_7$ with the zero-vector–time shared equally between $\mathbf{Z}_0$ and $\mathbf{Z}_7$ (resulting a $\mathbf{Z}_0$-share of 0.5); the optimized sequence obtained using GA is $\mathbf{A}_1\mathbf{Z}_7\mathbf{A}_2\mathbf{Z}_0$, for which the share of $\mathbf{Z}_0$ depends on the values of the normalized sampling frequency and modulation index. This sequence distributes the waveform energy more evenly among its harmonic components, resulting in less

current harmonic pollution. For operation at a normalized sampling frequency of 36 and a modulation index of 0.8, the optimizer has resulted in a reduction of 44% for 35th harmonic and 9% for 37th harmonic.

This chapter also demonstrated that the optimized SVM sequence and time share have insignificant sensitivity to variations of the $\mathbf{Z}_0$-share, which simplifies its digital implementation. Optimization has been carried out for three values of the normalized sampling frequency and for a range of modulation index values. It is shown that the same optimized sequence is valid for all sampling frequencies, with the $\mathbf{Z}_0$-share varying slightly with the modulation index, which makes it possible to use an average $\mathbf{Z}_0$-share value.

Chapter 7

Conclusions

Contents

This concluding chapter summarizes contributions of the thesis as well as possible future extension of the work.

7.1 Thesis Contributions

The contributions of the thesis are as follows:

1. This thesis has provided a thorough review of the state-of-the-art of SVM, its degrees of freedom, overmodulation methods, and implementation strategies.

2. In this thesis, an SVM model for two-level VSCs for use in the electromagnetic transients simulation program PSCAD/EMTDC (and also the MATLAB software) has been developed, which can be used in network studies. The model is able to control the VSC in linear as well as overmodulation regions. It is

also capable of generating firing pulses for different SVM switching strategies, including conventional, bus-clamped, and minimum-loss.

3. In addition to the two-level component, another component is developed that is able to control three-level converters, which provide less harmonic content through use of more voltage levels.

4. The two-level SVM component is used for a three-phase inductive load. The harmonic content of the resulting voltage and current waveforms in linear and overmodulation regions is investigated. Moreover, the converter-associated losses (both losses resulting from harmonics in the load, and losses occurring in the power electronic devices) for different SVM approaches are estimated and compared. It is observed that the conventional SVM has the least WTHD, while the minimum-loss method has the lowest switching losses (hence the name). The minimum-loss SVM, together with conventional SVM, has the lowest loss factor.

5. The developed three-level component is used in a three-level VSC application to demonstrate its validity. It is employed in a STATCOM-equipped power network. The dynamic response of the system for a simulated full load rejection is observed and compared to the case of control under conventional SPWM. In the SVM-controlled scheme, waveforms of voltage and reactive power are generally similar to the SPWM case; however, as the STATCOM controller parameters are optimized for SPWM, the waveforms under SVM have more ripple.

6. Several auxiliary PSCAD components to help with assessing the performance of the SVM components are developed. This components include (i) WTHD

calculator, (ii) SHE-scheme firing pulse generator, (iii) loss factor calculator, and (iv) MATLAB interface component.

7. Exploiting the available degrees of freedom in SVM, the thesis has applied genetic algorithms to optimize SVM sequences. The optimization objective was to minimize the most significant harmonic components (e.g., 35 and 37 when a normalized sampling frequency of 36 is used) while meeting the constraints described by the industry standards. The optimizer has found sequences that show significant reduction in the respective harmonic components, as well as the overall harmonic content of the waveform as portrayed by a reduced WTHD. The obtained sequence has minimal sensitivity to modulation parameters, which allows use of average values for $\mathbf{Z}_0$-share.

7.2 Suggestions for Future Work

The work done in this thesis can be expanded in several ways, including:

1. The developed component for three-level SVM uses converter states that keep the number of switchings minimal. However, this does not necessarily maintain the balance of the voltage of capacitors under all conditions. The model can be extended to develop methods to account for voltage balancing by dynamic selection of appropriate converter states.

2. Since higher-level SVM schemes, in addition to the implemented two- and three-level components, are also possible and sometimes used in power system applications, it is advisable to develop such components.

3. SVM can also be used for unbalanced loads where a four-leg VSC is employed. This mode of operation was not considered in this thesis, which could be a possible extension.

4. As mentioned earlier in Section 5.3, secondary effects involved in SVM could cause the simulation results to deviate from experimental results. This is particularly important when the modulator operates at high values of modulation index and the dc bus voltage has some ripple. In this case, the operation swings between linear and overmodulation modes. The performance parameters of SVM in such a case can be investigated. Moreover, studies considering switch dead-times and stray parameters further expand the work.

5. The optimization of SVM sequences has been performed for two-level SVM. Readily, the work can be expanded to multilevel modulators, specifically three-level SVM.

Appendices

Appendix A

Harmonic Indices

The rms harmonic current is a measure of harmonic content of the line current and is defined as (A.1).

$$I_{h(\text{rms})} = \sqrt{\frac{1}{T}\int_T \left(i(t) - i_1(t)\right)^2 \, dt} \tag{A.1}$$

The magnitude of $I_{h(\text{rms})}$, in addition to the employed modulation method, depends on the system impedance. To eliminate this dependence, a new factor, distortion factor d, is defined [1] as (A.2).

$$d = \frac{I_{h(\text{rms})}}{I_{h,\text{rms(square-wave)}}} \tag{A.2}$$

where $I_{h,\text{rms(square-wave)}}$ is the rms harmonic current calculated for square-wave operation.

Total harmonic distortion (THD) is a measure of the energy of the waveform harmonics and is defined as

$$\text{THD} = \frac{\sqrt{\sum_{h=2}^{n} V_h^2}}{V_1} \tag{A.3}$$

where V_1 is the fundamental component of voltage and V_h is the rms value of the hth voltage harmonic.

Normally a maximum number of 50 harmonics is used for calculation of THD ($n = 50$ in (A.3)). Maximum permissible THD for low voltage applications is 5% and maximum permissible individual voltage harmonic is 3% as suggested by IEEE Standard 519 [8].

Presence of inductances in power systems causes higher order harmonics to damp out more quickly. In other words, a high order harmonic is not as severe as a low order one. One problem with THD is that THD disregards this difference and treats all harmonics equally. Moreover, for two-level VSCs, THD is merely a function of the magnitude of the fundamental component and does not change with the pulse-width modulation scheme and sampling frequency. This is because the rms value of the generated waveform is always equal to the dc bus voltage.

Another figure of merit, known as the weighted THD (WTHD), gives a better measure of harmonic pollution by using the order of harmonic components as their weighting factor in the calculation of THD. It is defined for current as (A.4),

$$\text{WTHD} = \frac{\sqrt{\sum_{h=2}^{n}\left(\frac{I_h}{h}\right)^2}}{I_1} \tag{A.4}$$

and for voltage as (A.5).

$$\text{WTHD} = \frac{\sqrt{\sum_{h=2}^{n}\left(\frac{V_h}{h}\right)^2}}{V_1} \tag{A.5}$$

Slight modification to WTHD results in the harmonically-weighted loss factor σ [70]. This index assumes an inductive load connected to the converter (for example,

an electric motor) and provides a measure of the losses that occur in such a load due to harmonics in the voltage waveform. Harmonically-weighted loss factor σ is defined as

$$\sigma = \sum_{h=2}^{n} \frac{V_h^2}{(hf)^{3/2}} \tag{A.6}$$

where f is the fundamental frequency, h is the harmonic order, V_h is the hth voltage harmonic component, and n is the total number of harmonics considered.

Generally, the smaller the loss factor, the less the losses in the load. However, as the loss factor is defined essentially for a motor load, it is biased toward losses in the load itself and does not consider the converter switching losses.

Appendix B

Derivation of Formulae

This appendix summarizes the derivation of a number of expressions used throughout the thesis. They are listed in the same order as they appear in the thesis.

B.1 Third Harmonic Injection Modulation

In the third harmonic injection method, a such zero sequence voltage is added to the originally sinusoidal reference waveforms. The ratio of the magnitude of the third harmonic to that of the original waveform should be so that it causes maximum reduction of the peak of the resulting waveform. This ratio is calculated as follows.

Assume a waveform consisting of a fundamental component aplus a triple frequency term, at a modulation index of m as shown in (B.1).

$$v(\theta) = m\big[\sin(\theta) + a\sin(3\theta)\big] \tag{B.1}$$

The parameter a should be found such that the maximum value of $v(\theta)$ is as small as possible. Note that since the value of m does not affect the calculations, it is dropped in what follows.

The maximum value of $v(\theta)$ is found by first finding its derivative with respect to θ.

$$v'(\theta) = \cos(\theta) + 3a\cos(3\theta) \tag{B.2}$$

Equating $v'(\theta)$ to zero and solving for a gives

$$a = -\frac{\cos(\theta)}{3\cos(3\theta)} \tag{B.3}$$

The maximum value of $v(\theta)$ happens for the value of a as obtained above. Substituting for a from (B.3) in (B.1) gives

$$v(\theta)^{\max} = \sin(\theta) - \frac{\cos(\theta)}{3\cos(3\theta)}\sin(3\theta) \tag{B.4}$$

As this maximum value has to be the smallest possible, its derivative with respect to θ is found and made equal to zero.

$$v'(\theta)^{\max} = \frac{\sin(3\theta)\big[\sin(\theta)\cos(3\theta) - 3\cos(\theta)\sin(3\theta)\big]}{3\cos(3\theta)^2} \tag{B.5}$$

Equating (B.5) to zero gives two θ values. For $\sin(3\theta) = 0$, the solution is $\theta = \pi/3$. For the term inside the bracket equal to zero, the solution is $\theta = 0$, which actually makes $v(\theta)$ minimum (as `tan()` is a monotically increasing function and $3\tan(3\theta)$ remains inside $\tan(\theta)$ for $-\pi < \theta < \pi$). Therefore, the only valid solution is

$$\theta_{\max} = \frac{\pi}{3} \tag{B.6}$$

for which the value of a, that minimizes the peak of $v(\theta)$ is found from (B.3) as follows.

$$a = \frac{1}{6} \tag{B.7}$$

B.2 Time Shares for the Linear Region

The reference vector $\mathbf{V}_{\text{ref}}$ is constructed using the adjacent space vectors. For example, in the first sector, $\mathbf{V}_{\text{ref}}$ is constructed using $\mathbf{V}_1$ and $\mathbf{V}_2$ as shown.

$$\mathbf{V}_{\text{ref}} = \frac{T_1\mathbf{V}_1 + T_2\mathbf{V}_2}{T_s} \tag{B.8}$$

where $\mathbf{V}_{\text{ref}} = V_{\text{ref(max)}}\angle\theta$, $\mathbf{V}_1 = 2V_{\text{dc}}/3\angle 0$, and $\mathbf{V}_2 = 2V_{\text{dc}}/3\angle\dfrac{\pi}{3}$. Expanding (B.8) gives

$$\begin{aligned} T_s V_{\text{ref(max)}}\big[\cos(\theta) + j\sin(\theta)\big] = T_1\frac{2V_{\text{dc}}}{3}\big[\cos(0) + j\sin(0)\big] \\ + T_2\frac{2V_{\text{dc}}}{3}\big[\cos(\pi/3) + j\sin(\pi/3)\big] \end{aligned} \tag{B.9}$$

Solving the above system of equations, expressions for T_1 and T_2 are found as

$$T_1 = T_s\frac{V_{\text{ref(max)}}}{2V_{\text{dc}}/3}\frac{\sin(\pi/3-\theta)}{\sin(\pi/3)} \tag{B.10}$$

$$T_1 = T_s\frac{V_{\text{ref(max)}}}{2V_{\text{dc}}/3}\frac{\sin(\theta)}{\sin(\pi/3)} \tag{B.11}$$

Substituting for $m = V_{\text{ref(max)}}/(V_{\text{dc}}/2)$ and expanding the sine terms, the following expressions are obtained, which are the same as (4.3) and (4.4), respectively.

$$T_1 = \frac{\sqrt{3}}{2} \times T_s m\sin(\pi/3-\theta) \tag{B.12}$$

$$T_2 = \frac{\sqrt{3}}{2} \times T_s m\sin(\theta) \tag{B.13}$$

The time share of zero vectors is

$$T_0 + T_7 = T_s - T_1 - T_2 \tag{B.14}$$

B.3 Maximum Value of m as a Function of θ

The maximum magnitude of $\mathbf{V}_{\text{ref}}$ can be found considering that it is largest when totally constructed from active vectors with T_0 and T_7 equal to zero. This means that T_1 and T_2 should sum up to T_s. That is,

$$\frac{\sqrt{3}}{2} \times T_s m_{\max} \big[\sin(\pi/3 - \theta) + \sin(\theta) \big] = T_s \tag{B.15}$$

Therefore, the maximum value of m as a function of θ is

$$\begin{aligned} m_{\max} &= \frac{2/\sqrt{3}}{\sin(\pi/3 - \theta) + \sin(\theta)} \\ &= \frac{2/\sqrt{3}}{\sin(\theta + \pi/6)} \end{aligned} \tag{B.16}$$

B.4 Time Shares for the Overmodulation Region

The expressions for T_1 and T_2 for the overmodulation region can be found by adjusting the values obtained for the linear region so that they sum up to T_s, while maintaining their ratio. That is,

$$T_1 = \frac{T_1^{\text{old}}}{T_1^{\text{old}} + T_2^{\text{old}}} \tag{B.17}$$

$$T_2 = \frac{T_2^{\text{old}}}{T_1^{\text{old}} + T_2^{\text{old}}} \tag{B.18}$$

Simplifying (B.17) for T_1 gives

$$\begin{aligned} T_1 &= T_s \frac{\frac{\sqrt{3}}{2} T_s m \sin(\pi/3 - \theta)}{\frac{\sqrt{3}}{2} T_s m \big[\sin(\pi/3 - \theta) + \sin(\theta) \big]} \\ &= T_s \frac{\sin(\pi/3 - \theta)}{\sin(\pi/3 - \theta) + \sin(\theta)} \\ &= T_s \frac{\sqrt{3}\cos(\theta) - \sin(\theta)}{\sqrt{3}\cos(\theta) + \sin(\theta)} \end{aligned} \tag{B.19}$$

which is the same expression as (4.7). T_2 is found from the following.

$$\begin{aligned} T_2 &= T_s - T_1 \\ &= T_s \frac{2\sin(\theta)}{\sqrt{3}\cos(\theta) + \sin(\theta)} \end{aligned} \tag{B.20}$$

B.5 Hold Angle θ_h for One-Zone Overmodulation

In the one-zone approach, the hold angle is defined as angle of the ray from the origin to the intersection of the circular locus of reference vector and the boundary of the hexagon. For $m < 2/\sqrt{3} \simeq 1.15$, this angle is zero, which is expected because the inverter is totally in the linear modulation range. The following shows the calculation of θ_h for an m larger than 1.15.

Consider Fig. 4.9. The intersection of the hexagon and circle can be found by first finding their equations. For the sake of simplicity, define the auxiliary variable a as

$$a = \frac{2}{3} V_{\text{dc}} \tag{B.21}$$

With its y-intercept at $a\sqrt{3}$, the equation of the side of the hexagon in the first section expressed in Cartesian coordinates is

$$y = \sqrt{3}a - \sqrt{3}x \tag{B.22}$$

The radius of the circle is

$$r = m \times \frac{V_{\text{dc}}}{2} = \frac{3}{4}m \times a \tag{B.23}$$

So, the equation of the circle is

$$\begin{cases} x = \dfrac{3}{4}m \times a\cos(\theta) \\ y = \dfrac{3}{4}m \times a\sin(\theta) \end{cases} \tag{B.24}$$

The intersection of the hexagon and circle can be found by equating (B.22) and (B.24). This gives

$$\frac{\sqrt{3}}{4}m \times a\sin(\theta_h) = a - \frac{\sqrt{3}}{4}m \times a\cos(\theta_h) \tag{B.25}$$

or

$$\begin{aligned} \sin(\theta_h) + \sqrt{3}\cos(\theta_h) &= \frac{4}{\sqrt{3}}\frac{1}{m} \\ \cos(\pi/6 - \theta_h) &= \frac{2}{\sqrt{3}}\frac{1}{m} \end{aligned} \tag{B.26}$$

Solving for θ_h gives

$$\theta_h = \frac{\pi}{6} - \arccos(\frac{2}{\sqrt{3}m}) \qquad 2/\sqrt{3} \leq m \leq 4/3 \tag{B.27}$$

Appendix C

Least pth Interior Point Penalty Functions

Least pth interior point penalty functions are used to transform optimization problems with inequality constraints to unconstrained problems. This is done by augmenting the original objective function and penalizing the points that do not comply with the constraints.

The general form of a least pth function is $\alpha(x/d)^p$. For optimization purposes, even p values are used. The value of such a function is small for $-d < x < d$, and is large otherwise. Therefore, although such a function allows x values larger than d (or less than $-d$), it penalizes them. The exponent p determines the level of penalization of the variable x. Fig. C.1 shows graphs of the function for three values of p. As shown, large p values tend to severely penalize deviations of the variable x outside the range specified by d. Note that for $p = 2$, the least pth interior point penalty function reduces to the well-known least-square method.

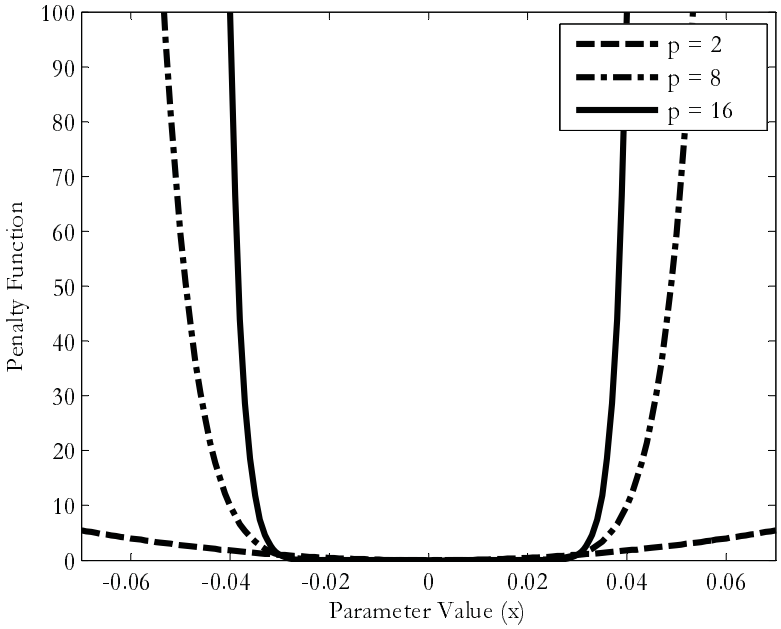

Fig. C.1. Behavior of the penalty function for three exponents of 2, 8, and 16.

References

[1] J. Holtz, "Pulsewidth modulation—a survey," *IEEE Trans. Ind. Electron.*, vol. 39, no. 5, pp. 410–420, Oct. 1992.

[2] ——, "Pulsewidth modulation for electronic power conversion," *Proc. IEEE*, vol. 82, no. 8, pp. 1194–1214, Aug. 1994.

[3] S. R. Bowes and D. Holliday, "Optimal regular-sampled PWM inverter control techniques," *IEEE Trans. Ind. Electron.*, vol. 54, no. 3, pp. 1547–1559, Jun. 2007.

[4] J. Rodríguez, J.-S. Lai, and F. Z. Peng, "Multilevel inverters: A survey of topologies, controls, and applications," *IEEE Trans. Ind. Electron.*, vol. 49, no. 4, pp. 724–738, Aug. 2002.

[5] J. Rodríguez, L. Morán, P. Correa, and C. Silva, "A vector control technique for medium-voltage multilevel inverters," *IEEE Trans. Ind. Electron.*, vol. 49, no. 4, pp. 882–888, Aug. 2002.

[6] L. M. Tolbert and T. G. Habetler, "Novel multilevel inverter carrier-based PWM method," *IEEE Trans. Ind. Appl.*, vol. 35, no. 5, pp. 1098–1107, Sep./Oct. 1999.

[7] M. H. Rashid, *Power Electronics: Circuits, Devices, and Applications*. Upper Saddle River, NJ: Prentice Hall, 2003.

[8] *IEEE Recommended Practices and Requirements for Harmonic Control in Electric Power Systems*, IEEE Std. 519, 1992.

[9] G. Narayanan and V. T. Ranganathan, "Synchronized PWM strategies based on space vector approach. Part 1: Principles of waveform generation," *IEE Proc.-Electr. Power Appl.*, vol. 146, no. 3, pp. 267–275, May 1999.

[10] N. S. Choi, J. G. Cho, and G. H. Cho, "A general circuit topology of multilevel inverter," in *Power Electronics Specialists Conf. Rec. (PESC 91)*, Jun. 1991, pp. 96–103.

[11] L. Li, D. Czarkowski, Y. Liu, and P. Pillay, "Multilevel selective harmonic elimination PWM technique in series-connected voltage inverters," *IEEE Trans. Ind. Electron.*, vol. 36, no. 1, pp. 160–170, Jan./Feb. 2000.

[12] D. G. Holmes and T. A. Lipo, *Pulse Width Modulation for Power Converters: Principles and Practice*. Hoboken, NJ: John Wiley, 2003.

[13] K. Taniguchi and H. Irie, "Trapezoidal modulating signal for three-phase PWM inverter," *IEEE Trans. Ind. Electron.*, vol. IE-33, no. 2, pp. 193–200, May 1989.

[14] A. Boglietti, G. Griva, M. Pastorelli, F. Profumo, and T. Adam, "Different PWM modulation technique indexes performance evaluation," in *IEEE Int. Symp. on Industrial Electronics*, Jun. 1999, pp. 193–199.

[15] S. Halasz, G. Csonka, and A. A. M. Hassan, "Sinusoidal PWM techniques with additional zero-sequence harmonics," in *Int. Conf. Industrial Electronics, Control and Instrumentation (IECON 94)*, Sep. 1994, pp. 85–90.

[16] S. Sirisukprasert, J.-S. Lai, and T.-H. Liu, "Optimum harmonic reduction with a wide range of modulation indexes for multilevel converters," *IEEE Trans. Ind. Electron.*, vol. 49, no. 4, pp. 875–881, Aug. 2002.

[17] J. N. Chiassona, L. M. Tolbert, K. J. McKenzie, and Z. Du, "A complete solution to the harmonic elimination problem," *IEEE Trans. Power Electron.*, vol. 19, no. 2, pp. 491–499, Mar. 2004.

[18] J. R. Wells, B. M. Nee, P. L. Chapman, and P. T. Krein, "Selective harmonic control: A general problem formulation and selected solutions," *IEEE Power Electron. Lett.*, vol. 20, no. 6, pp. 1337–1345, Nov. 2005.

[19] C. Domnisoru, "Using MATHCAD in teaching power engineering," *IEEE Trans. Educ.*, vol. 48, no. 1, pp. 157–161, Feb. 2005.

[20] M. Saeedifard, H. Nikkhajoei, and R. Iravani, "A space vector modulated STATCOM based on a three-level neutral point clamped converter," *IEEE Trans. Power Del.*, vol. 22, no. 2, pp. 1029–1039, Apr. 2007.

[21] M. Saeedifard, H. Nikkhajoei, R. Iravani, and A. Bakhshai, "A space vector modulation approach for a multimodule HVDC converter system," *IEEE Trans. Power Del.*, vol. 22, no. 3, pp. 1643–1654, Jul. 2007.

[22] V. T. Somasekhar, K. Gopakumar, M. R. Baiju, K. K. Mohapatra, and L. Umanand, "A multilevel inverter system for an induction motor with open-end windings," *IEEE Trans. Ind. Electron.*, vol. 52, no. 3, pp. 824–836, Jun. 2005.

[23] A. R. Beig, G. Narayanan, and V. T. Ranganathan, "Modified SVPWM algorithm for three level VSI with synchronized and symmetrical waveforms," *IEEE Trans. Ind. Electron.*, vol. 54, no. 1, pp. 486–494, Feb. 2007.

[24] A. K. Gupta and A. M. Khambadkone, "A space vector PWM scheme for multilevel inverters based on two-level space vector PWM," *IEEE Trans. Ind. Electron.*, vol. 53, no. 5, pp. 1631–1639, Oct. 2006.

[25] H. W. van der Broeck, H.-C. Skudelny, and G. V. Stanke, "Analysis and realization of a pulsewidth modulator based on voltage space vectors," *IEEE Trans. Ind. Appl.*, vol. 24, no. 1, pp. 142–150, Jan./Feb. 1988.

[26] A. Mehrizi-Sani and S. Filizadeh, "Digital implementation and transient simulation of space-vector modulated converters," in *IEEE-PES Gen. Meeting 2006*, Montreal, QC, Jun. 2006.

[27] D. G. Holmes, "The general relationship between regular-sampled pulse-width-modulation and space vector modulation for hard switched converters," in *Conf. Rec. IEEE-IAS Annu. Meeting*, Oct. 1992, pp. 1002–1009.

[28] R. Jobing, F. S. van der Merwe, and M. J. Kamper, "Digital implementation of bus clamped space vector modulation," *IEEE Trans. Energy Convers.*, vol. 9, no. 2, pp. 344–348, Jun. 1994.

[29] G. Narayanan and V. T. Ranganathan, "Two novel synchronized bus-clamping PWM strategies based on space vector approach for high power drives," *IEEE Trans. Power Electron.*, vol. 17, no. 1, pp. 84–93, Jan. 2002.

[30] G. Narayanan, H. K. Krishnamurthy, D. Zhao, and R. Ayyanar, "Advanced bus-clamping PWM techniques based on space vector approach," *IEEE Trans. Power Electron.*, vol. 21, no. 4, pp. 974–987, Jul. 2006.

[31] A. M. Trzynadlowski, R. L. Kirlin, and S. F. Legowski, "Space vector PWM technique with minimum switching losses and a variable pulse rate," *IEEE Trans. Ind. Electron.*, vol. 44, no. 2, pp. 173–181, Apr. 1997.

[32] A. R. Bakhshai, G. Joós, P. K. Jain, and H. Jin, "Incorporating the overmodulation range in space vector pattern generators using a classification algorithm," *IEEE Trans. Power Electron.*, vol. 15, no. 1, pp. 83–91, Jan. 2000.

[33] A. M. Hava, R. J. Kerkman, and T. A. Lipo, "Carrier-based PWM-VSI overmodulation strategies: Analysis, comparison, and design," *IEEE Trans. Power Electron.*, vol. 13, no. 40, pp. 674–689, Jul. 1998.

[34] J. Holtz, W. Lotzkat, and A. M. Khambadkone, "On continuous control of PWM inverters in the overmodulation range including the six-step mode," *IEEE Trans. Power Electron.*, vol. 8, no. 4, pp. 546–553, Oct. 1993.

[35] S. Bolognani and M. Zigliotoo, "Novel digital continuous control of SVM inverters in the overmodulation range," *IEEE Trans. Ind. Appl.*, vol. 33, no. 2, pp. 525–530, Mar./Apr. 1997.

[36] G. Narayanan and V. T. Rangathan, "Extension of operation of space vector PWM strategies with low switching frequencies using different overmodulation algorithms," *IEEE Trans. Power Electron.*, vol. 17, no. 5, pp. 788–798, Sep. 2002.

[37] D.-C. Lee and G.-M. Lee, "A novel overmodulation technique for space-vector PWM inverters," *IEEE Trans. Power Electron.*, vol. 13, no. 6, pp. 1144–1151, Nov. 1998.

[38] A. Cataliotti, F. Genduso, and G. R. Galluzzo, "A new over modulation strategy for high-switching frequency space vector PWM voltage source inverters," in *2002 IEEE Int. Symp. Industrial Electronics (ISIE 02)*, vol. 3, May 2002, pp. 778–783.

[39] G. Narayanan and V. T. Ranganathan, "Overmodulation algorithm for space vector modulated inverters and its application to low switching frequency PWM techniques," *IEE Proc.-Electr. Power Appl.*, vol. 148, no. 6, pp. 521–536, Nov. 2001.

[40] R. J. Kerkman, T. M. Rowan, D. Leggate, and B. J. Siebel, "Control of PWM voltage inverters in the pulse dropping region," *IEEE Trans. Power Electron.*, vol. 10, no. 5, pp. 559–565, Sep. 1995.

[41] H.-J. Park and M.-J. Youn, "A new time-domain discontinuous space-vector PWM technique in overmodulation region," *IEEE Trans. Ind. Electron.*, vol. 50, no. 2, pp. 349–355, Apr. 2003.

[42] S. Bolognani and M. Zigliotto, "Space vector Fourier analysis of SVM inverters in the overmodulation range," in *Proc. Int. Conf. Power Electronics, Drive, and Energy Systems for Industrial Growth (PEDES 96)*, Jan. 1996, pp. 319–323.

[43] A. M. Gole, I. T. Fernando, G. D. Irwin, and O. B. Nayak, "Modeling of power electronic apparatus: Additional interpolation issues," in *Int. Conf. Power Systems Transients (IPST 97)*, Seattle, WA, Jun. 1997, pp. 23–28.

[44] D. G. Holmes, "The significance of zero space vector placement for carrier-based PWM schemes," *IEEE Trans. Ind. Appl.*, vol. 32, no. 5, pp. 1122–1129, Sep./Oct. 1996.

[45] G.-M. Lee and D.-C. Lee, "Implementation of naturally sampled space vector modulation eliminating microprocessors," in *Proc. of the 3rd Int. Power Electronics and Motion Control Conf.*, 2000, pp. 803–807.

[46] R. H. Baker and L. H. Bannister, "Electric power converter," U.S. Patent 3,867,643, Feb. 18, 1975.

[47] H. Zhang, A. von Jouanne, S. Dai, A. K. Wallace, and F. Wang, "Multilevel inverter modulation schemes to eliminate common-mode voltages," *IEEE Trans. Ind. Appl.*, vol. 36, no. 6, pp. 1640–1653, Nov./Dec. 2000.

[48] J. H. Seo, C. H. Choi, and D. S. Hyun, "A new simplified space-vector PWM method for three-level inverters," *IEEE Trans. Power Electron.*, vol. 16, no. 4, pp. 545–550, Jul. 2001.

[49] *EMTDC Manual*, Manitoba HVDC Research Centre, Apr. 2004.

[50] A. Mehrizi-Sani, S. Filizadeh, and P. L. Wilson, "Harmonic and loss analysis of space-vector modulated converters," in *Int. Conf. on Power Systems Transients (IPST 07)*, Lyon, France, Jun. 2007.

[51] A. M. Trzynadlowski and S. Legowski, "Minimum-loss vector PWM strategy for three-phase inverters," *IEEE Trans. Power Electron.*, vol. 9, no. 1, pp. 26–34, Jan. 1994.

[52] A. D. Rajapakse, A. M. Gole, and P. L. Wilson, "Electromagnetic transients simulation models for accurate representation of switching losses and thermal performance in power electronic systems," *IEEE Trans. Power Del.*, vol. 20, no. 1, pp. 319–327, Jan. 2005.

[53] J. P. Holman, *Heat Transfer*, 8th ed. New York: McGraw-Hill, 1997.

[54] J. B. Ekanayake and N. Jenkins, "A three-level advanced static VAr compensator," *IEEE Trans. Power Del.*, vol. 11, no. 1, pp. 540–545, Jan. 1996.

[55] C. K. Sao, P. W. Lehn, M. R. Iravani, and J. A. Martinez, "A benchmark system for digital time-domain simulation of a pulse-width-modulated D-STATCOM," *IEEE Trans. Power Del.*, vol. 17, no. 4, pp. 1113–1120, Oct. 2002.

[56] C. Schauder and H. Mehta, "Vector analysis and control of advanced static VAr compensators," *IEE Proc.-Gener. Transm. Distrib.*, vol. 140, no. 4, pp. 299–306, Jul. 1993.

[57] M. Heidari, S. Filizadeh, and A. M. Gole, "Support tools for simulation-based optimal design of power networks with embedded power electronics," *IEEE Trans. Power Del.*, submitted for publication.

[58] R. W. Menzies and Y. Zhuang, "Advanced static compensation using a multilevel GTO thyristor inverter," *IEEE Trans. Power Del.*, vol. 10, no. 2, pp. 732–738, Apr. 1995.

[59] R. L. Haupt and S. E. Haupt, *Practical Genetic Algorithms.* New York, NY: Wiley, 1998.

[60] C. Z. Janikow and D. S. Clair, "Genetic algorithms: Simulating nature's methods of evolving the best design solution," *IEEE Potentials*, vol. 14, no. 1, pp. 31–35, Feb./Mar. 1995.

[61] M. Liserre, A. Dell'Aquila, and F. Blaabjerg, "Genetic algorithm-based design of the active damping for an LCL-filter three-phase active rectifier," *IEEE Trans. Power Electron.*, vol. 19, no. 1, pp. 76–86, Jan. 2004.

[62] K. L. Shi and H. Li, "Optimized PWM strategy based on genetic algorithms," *IEEE Trans. Ind. Electron.*, vol. 52, no. 5, pp. 1458–1461, Oct. 2005.

[63] L. Michels, R. F. de Camargo, F. Botterón, H. A. Grüdling, and H. Pinheiro, "Generalised design methodology of second-order filters for voltage-source inverters with space-vector modulation," *IEE Proc.-Electr. Power Appl.*, vol. 153, no. 2, pp. 219–226, Mar. 2006.

[64] A. Mehrizi-Sani and S. Filizadeh, "An optimized space-vector modulation sequence for improved harmonic performance," *IEEE Trans. Ind. Electron.*, submitted for publication.

[65] J. H. Holland, *Adaptation in Natural and Artificial Systems: An Introductory Analysis with Applications to Biology, Control, and Artificial Intelligence.* Ann Arbor: University of Michigan Press, 1975.

[66] F. Jenni and D. Wueest, "The optimization parameters of space vector modulation," in *Fifth European Conf. on Power Electronics and Applications*, Sep. 13-16, 1993, pp. 376–381.

[67] K. Zhou and D. Wang, "Relationship between space-vector modulation and three-phase carrier-based PWM: A comprehensive analysis," *IEEE Trans. Ind. Electron.*, vol. 49, no. 1, pp. 186–196, Feb. 2002.

[68] *American National Standard Recommended Practice for Electromagnetic Compatibility Limits*, American National Standards Institute Std. ANSI C63.12-1999, 2000.

[69] P. N. Enjeti, P. D. Ziogas, and J. F. Lindsay, "Programmed PWM techniques to eliminate harmonics: A critical evaluation," *IEEE Trans. Ind. Appl.*, vol. 26, no. 2, pp. 302–316, Mar./Apr. 1990.

[70] P. G. Handley and J. T. Boys, "Practical real-time PWM modulators: An assessment," *IEE Proc.-Electr. Power Appl.*, vol. 139, no. 2, pp. 96–102, Mar. 1992.

[71] J. Ye, P. Lin, W. Liqiao, and Z. Zhang, "Development of optimized SVPWM algorithm based on CPLD," in *Int. Power Electronics and Motion Control Conf. (IPEMC 04)*, Aug. 14-16 2004, pp. 1603–1606.

[72] E. Zitzler and L. Thiele, "Multiobjective evolutionary algorithms: A comparative case study and the strength Pareto approach," *IEEE Trans. Evol. Comput.*, vol. 3, no. 4, pp. 257–271, Nov. 1999.

[73] A. Ravindran, K. M. Ragsdell, and G. V. Reklaitis, *Engineering Optimization: Methods and Applications*. Hoboken, NJ: John Wiley & Sons, 2006.